A CENTRALISED MULTI-OBJECTIVE MODEL PREDICTIVE CONTROL FOR BIVENTRICULAR ASSIST DEVICES

VIVIAN KOH CI AI

FACULTY OF ENGINEERING
UNIVERSITY OF MALAYA
KUALA LUMPUR

2020

A CENTRALISED MULTI-OBJECTIVE MODEL PREDICTIVE CONTROL FOR BIVENTRICULAR ASSIST DEVICES

VIVIAN KOH CI AI

THESIS SUBMITTED IN FULFILMENT OF THE REQUIREMENTS FOR THE DEGREE OF DOCTOR OF PHILOSOPHY

FACULTY OF ENGINEERING
UNIVERSITY OF MALAYA
KUALA LUMPUR

2020

UNIVERSITY OF MALAYA

ORIGINAL LITERARY WORK DECLARATION

Name of Candidate: *Vivian Koh Ci Ai*

Matric No: *HHS150003*

Name of Degree: *Doctor of Philosophy*

Title of Project Paper/Research Report/Dissertation/Thesis ("this Work"):

A Centralised Multi-Objective Model Predictive Control for Biventricular Assist Devices

Field of Study: *Biomedical Engineering*

I do solemnly and sincerely declare that:

(1) I am the sole author/writer of this Work;
(2) This Work is original;
(3) Any use of any work in which copyright exists was done by way of fair dealing and for permitted purposes and any excerpt or extract from, or reference to or reproduction of any copyright work has been disclosed expressly and sufficiently and the title of the Work and its authorship have been acknowledged in this Work;
(4) I do not have any actual knowledge nor do I ought reasonably to know that the making of this work constitutes an infringement of any copyright work;
(5) I hereby assign all and every rights in the copyright to this Work to the University of Malaya ("UM"), who henceforth shall be owner of the copyright in this Work and that any reproduction or use in any form or by any means whatsoever is prohibited without the written consent of UM having been first had and obtained;
(6) I am fully aware that if in the course of making this Work I have infringed any copyright whether intentionally or otherwise, I may be subject to legal action or any other action as may be determined by UM.

Candidate's Signature Date: 30/9/2020

Subscribed and solemnly declared before,

Witness's Signature Date: 2/10/2020

Name:

Designation:

A CENTRALISED MULTI-OBJECTIVE MODEL PREDICTIVE CONTROL FOR BIVENTRICULAR ASSIST DEVICES

ABSTRACT

Heart failure is defined as failure of heart to deliver adequate blood flow rate to support tissue perfusion. Heart failure can be treated by implantation of a left ventricular assist device (LVAD) for left heart failure patients, or a biventricular assist device (BiVAD) for bi-heart failure patients. Since left heart failure predominates right heart failure, all commercial ventricular assist devices are LVADs. Therefore, two LVADs are frequently used as BiVAD for bi-heart failure patients. Clinically, the constant speed (CS) control of BiVAD fails to adapt pump flow rate according to physiological changes, thus putting patients at risk of ventricular suction and pulmonary congestion. Speed regulation of a BiVAD may be complicated by process interactions in a cardiovascular-biventricular assist device (CVS-BiVAD) environment. Therefore, in this thesis, a centralised model predictive control (MPC) that could handle process interactions in a multivariable control problem was proposed. Three objectives were proposed in this thesis. Firstly, a simple state-space model of the CVS-BiVAD system was required prior to the development of an MPC algorithm. For this purpose, a complex CVS-BiVAD model was simplified by reducing the number of state variables. New model parameters were optimised using a least squares function and manual tuning approach. The simplified state-space model consists of state and time-varying factors. Therefore, the second objective was to modify a conventional centralised MPC algorithm to cater for the state and time-varying factors of the CVS-BiVAD system. Multiple control objectives were included in the MPC algorithm to: a) adapt pump flow rate according to the Frank-Starling (FS) mechanism, b) avoid ventricular suction, and c) avoid vascular congestion. This modified MPC is called the centralised multi-objective model predictive control (CMO-MPC). The CMO-

MPC was benchmarked against two non-centralised control schemes: CS control and FS-like-proportional-integral (PI-FS) control under two patient scenarios: exercise and postural change, *in silico*, as the first stage evaluation. In exercise, CMO-MPC and PI-FS control increased cardiac output from 5.1 L/min to 7.1 L/min and 6.9 L/min, respectively. CMO-MPC avoided suction and congestion in both patient scenarios as compared to CS control and PI-FS control, based on the assumptions made on risks of suction (mean atrial pressure below 3 mmHg) and congestion events (mean atrial pressure above 18 mmHg). The assumptions only served as a proposed idea and can be changed by clinical experts. The third objective was to evaluate this CMO-MPC *in-vitro* using a mock circulation loop. In the *in vitro* study, CMO-MPC avoided pulmonary congestion in the exercise test while PI-FS control and CS control failed to. In the transient region of postural change test, CMO-MPC (2.0 mmHg) had a higher minimum right ventricular end diastolic pressure than PI-FS control (1.2 mmHg), suggesting that CMO-MPC had lower risks of right ventricular suction as compared with PI-FS control. It is therefore proposed that the CMO-MPC should be a safe physiological controller for BiVAD in the future when reliable pressure and flow sensors become clinically available. *In vivo* validation is also required to increase the confidence of use of CMO-MPC in the future.

Keywords: Frank-Starling mechanism, physiological control, vascular congestion, ventricular suction.

A CENTRALISED MULTI-OBJECTIVE MODEL PREDICTIVE CONTROL FOR BIVENTRICULAR ASSIST DEVICES

ABSTRAK

Kegagalan jantung diertikan sebagai kegagalan jantung untuk menyampaikan aliran darah yang mencukupi untuk menyokong tisu perfusi. Kegagalan jantung boleh dirawat dengan implantasi alat pembantu ventrikle kiri (LVAD) untuk merawat pesakit yang mengalami kegagalan ventrikle kiri, atau alat pembantu dua ventrikle (BiVAD) bagi pesakit yang mengalami kegagalan dua ventrikle. Di klinic, BiVAD yang beroperasi dalam halaju tetap (CS) gagal mengawal aliran darah dengan tepat menurut perubahan fisiogi. Oleh hal demikian, sedutan ventrikle dan kesesakan vascular akan terjadi. Proses interaksi yang terada dalam sistem kardiovaskular-BiVAD (CVS-BiVAD) menyusahkan pengawalan halaju BiVAD. Untuk menangani masalah proses interaksi, sebuah sistem kawalan berpusat yang bernama CMO-MPC sudah direka bentuk. Tiga objektif telah dicadangkan dalam tesis ini. Pertama, sebuah model ruang keadaan yang berasaskan sistem CVS-BiVAD telah diringkaskan untuk reka bentuk CMO-MPC kemudian. Parameters model baru telah dipilih dengan fungsi kuasa dua terkecil dan pilihan secara manual. Model ruang keadaan mempunyai pemboleh ubah yang berubah dengan masa dan keadaan. Kedua, sebuah CMO-MPC yang berasaskan model ruang keadaan tersebut telah direka bentuk. Tujuan utama CMO-MPC adalah untuk mengawal halaju supaya BiVAD boleh mengeluarkan aliran darah yang menepati perubahan fisiologi. Sementara itu, CMO-MPC juga perlu mengelakkan sedutan ventrikle dan kesesakan vascular. Prestasi kawalan CMO-MPC telah dibandingkan dengan CS dan kawalan kamiran berkadaran yang berasaskan prinsip Frank-Starling (PI-FS) dalam dua scenario, iaitu senaman dan perubahan postur dari lentang ke tegak. Penilaian tahap satu melibatkan simulasi dalam model yang telah disah dengan data experimen. CMO-MPC telah berjaya

meningkatkan aliran darah daripada 5.1 L/min ke 7.1 L/min manakala PI-FS meningkatkan aliran darah daripada 5.1 L/min ke 6.9 L/min. Dalam kedua-dua ujian penilaian, hanya CMO-MPC mengelakan sedutan ventrikle dan kesesakan vaskular berdasarkan andaian risiko sedutatan ventrikle (< 3 mmHg) dan kesesakan vaskular (> 18 mmHg). Andaian tersebut adalah sebagai cadangan dalam tesis ini, ia boleh diubah suai oleh pakar doktor mengikut kesesuaian pesakit. Ketiga, CMO-MPC telah dinilaikan dengan experimen in vitro untuk mengesahkan kegunaannya. Keputusan ujian in vitro menunjukkan hanya CMO-MPC berjaya mengelakkan kesesakan vaskular tetapi PI-FS dan CS gagal mengelakkan kesesakan vaskular. Walaupun sedutan ventrikle tidak terjadi semasa semua ujian yang dilangsungkan, nilai tekanan akhir diastolik ventrikle kanan adalah lebih tinggi dengan CMO-MPC (2.0 mmHg) berbanding dengan PI-FS (1.2 mmHg). Oleh itu, CMO-MPC adalah lebih selamat digunakan sebagai sistem kawalan untuk BiVAD berbanding dengan PI-FS dan CS kerana ia mampu meninggikan aliran darah semasa senaman dan mempunyai risiko yang paling rendah untuk sedutan ventrikle dan kesesakan vaskular. Pada masa hadapan, sensor tekanan dan sensor aliran darah perlu ditambah baik supaya CMO-MPC boleh direalisasikan. Ujian in vivo juga boleh dilakukan untuk meninggikan pengetahuan interaksi CMO-MPC dengan sistem CVS-BiVAD.

Kata kunci: Frank-Starling, kesesakan vaskular, sistem kawalan fisiologi, sedutan ventrikle.

ACKNOWLEDGEMENTS

"*Soli Deo Gloria*!" Praise and thanks to my Lord Jesus for His grace for me. He has given me wisdom, knowledge, strength, tenacity, and all resources I required throughout the journey leading up to the completion of the work.

I am grateful to have supervisors at University of Malaya (UM), University of New South Wales (UNSW), and Monash University Malaysia who patiently guided and shared the riches of their experience and knowledge with me throughout the journey of this work. Assoc. Prof. Dr. Lim Einly (UM), Dr. Michael Stevens (UNSW), Dr. Joseph Ho (Monash University Malaysia), and Prof. Nigel Lovell (UNSW) are more than just being my supervisors, they are also my mentor and my dear friends.

I am thankful for Dr. Jo Philipp Pauls and Mr. Eric Wu who supervised me during my research attachment in the Innovative Cardiovascular Engineering and Technology (ICET) lab in Brisbane. They have taught me to use a Mock Circulation Loop for control evaluation.

I am also thankful for a few experts in different fields of study who had reviewed and contributed their valuable insights regarding the work. They are Adj. Clin. Assoc. Prof. Robert Salamonsen who is very experienced in ventricular assist device related work and Dr. Ng Boon Chiang whose expertise is advanced control.

I am thankful for the friendships I share with my dear colleagues – the fellow PhD students, Master students, and interns who work at Asian Cardiac lab in UM, the postgraduate student office in UNSW, and ICET lab. Although each of us had different projects to work on, we encouraged and motivated each other to work toward the success of our respective projects.

I am thankful for my dear family members in Christ (including my biological family) in Malaysia and Australia for all prayers and supports. They have demonstrated the love of Christ for me by providing me transport, accommodation, food, and encouragements when I travelled to-and-fro Malaysia, Sydney, and Brisbane. Their care for my basic needs enabled me to concentrate toward the completion of this work.

TABLE OF CONTENTS

LIST OF FIGURES

LIST OF TABLES

LIST OF SYMBOLS AND ABBREVIATIONS

$\boldsymbol{\Omega}$	:	Matrix associated with linear inequalities
$\boldsymbol{\Theta}$	:	Step response matrix
$\hat{\boldsymbol{Y}}$	:	Vector of predicted output
$\Delta\hat{\boldsymbol{U}}$	:	Vector of predicted slew rate
$\boldsymbol{A}$	:	State matrix
a_{HVAD}	:	Coefficient of HVAD flow rate
$\boldsymbol{B}$	:	Input matrix
b_{HVAD}	:	Coefficient of squared of HVAD flow rate
BiVAD	:	Biventricular assist device
C	:	Compliance
$\boldsymbol{C}$	:	Output matrix
$C(t)$	:	Time varying compliance
c_{HVAD}	:	Coefficient of squared of HVAD speed
C_{la}	:	Left atrial compliance
$C_{lv}(t)$	:	Time varying left ventricular compliance
CMO-MPC	:	Centralised multi-objective model predictive control
CO	:	Cardiac output
C_{pa}	:	Pulmonary arterial compliance
C_{ra}	:	Right atrial compliance
$C_{rv}(t)$	:	Time varying right ventricular compliance
CS	:	Constant speed
C_{sa}	:	Systemic arterial compliance
$C_{vascular}$	:	Vascular compliance
CVS	:	Cardiovascular system

CVS-BiVAD	:	Cardiovascular-biventricular assist device
DI-AP	:	Dual independent atrial pressure
DI-FS	:	Dual independent frank-starling
DI-IP	:	Dual independent inlet pressure
dP	:	Differential pump pressure
dRPM	:	Differential rotation per minute
EDP	:	End diastolic pressure
EDV	:	End diastolic volume
E_{max}	:	Slope of end systolic pressure volume relationship
E_{min}	:	Slope of end diastolic pressure volume relationship
$E_n(t)$	:	Normalised time varying elastance function
F	:	Objective function
FDA	:	Food and drug administration
FS	:	Frank-starling
H	:	Pressure head of pump
HM	:	HeartMate
H_p	:	Prediction horizon
HQ	:	Pressure head-flow
HR	:	Heart rate
HSI	:	Harmonic suction index
H_u	:	Control horizon
HVAD	:	HeartWare ventricular assist device
IAE	:	Integral of absolute error
IMC	:	Internal model control
J	:	Cost function

k	:	Time step
K_1	:	Upper limit of FS curve used in the controller
K_2	:	Scaling factor of FS curve in the controller
K_3	:	Shifting factor of FS curve in the controller
K_i	:	Integral gain
K_p	:	Proportional gain
L	:	Inductance
LAP	:	Left atrial pressure
L_{lvad}	:	LVAD inductance
L_{rvad}	:	RVAD inductance
LTI	:	Linear time-invariant
LVAD	:	Left ventricular assist device
LVEDP	:	Left ventricular end diastolic pressure
LVV	:	Left ventricular volume
M/S	:	Master/Slave
MCL	:	Mock circulation loop
MON-MPC	:	Multi-objective neural-network based model predictive control
MPC	:	Model predictive control
OR	:	Operating region
P	:	Pressure
PAP	:	Pulmonary arterial pressure
P_d	:	Downstream pressure
PID	:	Proportional-integral-derivative
PID-FS	:	Frank-starling-like-proportional-integral-derivative
PI-FS	:	Frank-starling-like-proportional-integral

PIP	:	Pump inlet pressure
P_{la}	:	Left atrial pressure
P_{lv}	:	Left ventricular pressure
P_{pa}	:	Pulmonary arterial pressure
PP_{des}	:	Desired pump power
P_{ra}	:	Right atrial pressure
P_{rv}	:	Right ventricular pressure
P_{sa}	:	Systemic arterial pressure
$P_{suc\_threshold}$	:	Suction threshold pressure
P_{u}	:	Upstream pressure
$P_{vascular}$	:	Vascular pressure
PVC	:	Polyvinyl chloride
PVR	:	Pulmonary vascular resistance
$\boldsymbol{Q}$	:	Output weight matrix
Q	:	Flow rate
q_{cong}	:	Gain for congestion avoidance objective
$Q_{L/RVAD,ref}$	:	Reference LVAD and RVAD flow rate
Q_{lvad}	:	LVAD flow rate
Q_{p}	:	Pump flow rate
QP	:	Quadratic programming
Q_{rvad}	:	RVAD flow rate
q_{suc}	:	Gain for suction avoidance objective
Q_{valve}	:	Valve flow rate
$Q_{vascular}$	:	Vascular flow rate
$\boldsymbol{R}$	:	Move suppression weight matrix

R	:	Resistance
RAP	:	Right atrial pressure
R_{av}	:	Aortic valve resistance
$R_{banding}$	:	Banding resistance
RC	:	Resistance-compliance
R_{can}	:	Cannula resistance
RGA	:	Relative gain array
R_{la}	:	Left atrial resistance
R_{mt}	:	Mitral valve resistance
R_p	:	Pulmonary vascular resistance
R_{pa}	:	Pulmonary arterial resistance
R_{pv}	:	Pulmonary valve resistance
R_{ra}	:	Right atrial resistance
R_s	:	Systemic vascular resistance
R_{sa}	:	Systemic arterial resistance
R_{suc}	:	Suction resistance
R_{tv}	:	Tricuspid valve resistance
$R_{vascular}$	:	Vascular flow rate
RVEDP	:	Right ventricular end diastolic pressure
SAP	:	Systemic arterial pressure
SP	:	Systolic pressure
SPP	:	Suction prevention physiological
SVR	:	Systemic vascular resistance
t	:	Time
TITO	:	Two-input-two-output

t_n	:	Normalised time
$\boldsymbol{u}$	:	Input vector
$\boldsymbol{u_{max}}$	:	Vector of maximum input
$\boldsymbol{u_{min}}$	:	Vector of minimum input
VAD	:	Ventricular assist device
V_{lv}	:	Left ventricular volume
VRI	:	Venous return index
V_{rv}	:	Right ventricular volume
$V_{sv,0}$	:	Systemic venous unstressed volume
$V_{vascular}$	:	Vascular volume
$\boldsymbol{x}$	:	State vector
$\boldsymbol{y}$	:	Output vector
$\boldsymbol{y_{max}}$	:	Vector of maximum output
$\boldsymbol{y_{min}}$	:	Vector of minimum output
ZN	:	Zieger-Nicholls
ΔP	:	Differential pressure
$\boldsymbol{\Delta u_{max}}$	:	Vector of slew rate
$\boldsymbol{\Delta u_{min}}$	:	Vector of slew rate
θ	:	State coefficient with respect to valve opening and closing
λ	:	Degree process interaction
$\boldsymbol{\Lambda}$	:	Matrix of λ
ω	:	Pump speed

LIST OF APPENDICES

CHAPTER 1: INTRODUCTION

1.1 Research background

Heart failure is defined as failure of heart to deliver adequate blood flow rate to meet the need of the body (Guyton & Hall, 2006). Prolonged heart failure, if left untreated, may lead to cardiogenic shock, and subsequently, mortality. The gold standard treatment for heart failure is heart transplantation. However, heart transplantation is limited by several factors such as age, biocompatibility issues, and fitness level. In addition to that, the shortage of donor hearts also limits the number of patients eligible for a heart transplant.

An alternative treatment to heart transplantation was established when the two commercially available rotary left ventricular assist devices (LVADs), namely the HeartMate II (Abbott, Thoratec, Pleasanton, CA, USA) and the HeartWare HVAD (Medtronic, HeartWare International, Inc., Framingham, MA) acquired the Food and Drug Administration (FDA) approval for clinical implantation as a destination therapy in 2010 and 2012, respectively. The 2-year survival rate among heart failure patients supported with an implantable LVAD is 70% (Kirklin et al., 2017). Although patients receiving the implantable LVAD predominantly have isolated left ventricular failure, 5 to 50 % of LVAD patients also experienced right ventricular failure (Drakos et al., 2010; Lee et al., 2010; Potapov et al., 2008). Since there is no commercially available long-term implantable right ventricular assist device (RVAD), a second LVAD is implanted to support the right ventricle of these patients. This configuration of dual left ventricular assist devices is a form of biventricular assist device (BiVAD).

Clinically, all LVAD and BiVAD are operated at a constant-speed (CS) setting (Slaughter et al., 2010). An optimal pump speed is specified by clinicians with the aid of

echocardiography and invasive cardiovascular measurements. The speed will then remain constant thereafter unless inadequate flow rates or a high incidence of ventricular suction are detected during routine follow-up. The CS setting is non-physiological (Salamonsen et al., 2011), insofar that it cannot respond adequately to changes in haemodynamic requirements. Therefore, an automatic physiological control mechanism that adjusts the pump speed to adapt to these changes is highly desirable. This can be achieved by using the Frank-Starling (FS) like control: a strategy that mimics the FS mechanism in the native heart (Gaddum et al., 2014; Gaddum et al., 2012; Stephens et al., 2017; Stevens et al., 2014). The FS mechanism adapts and balances flow rate by matching cardiac output with venous return (preload) (Guyton & Hall, 2006).

Most physiological control strategies imitate the concept of FS mechanism for pump speed regulation. Among those control strategies, direct measurement of preload (i.e. ventricular pressure (Petrou et al., 2016), and ventricular volume (Ochsner et al., 2014)) and indirect measurement of preload using flow pulsatility index (Andreas Arndt et al., 2008), are employed as determinants for reference of pump flow rate. Apart from the FS approach, Giridharan et al. proposed a constant differential pressure head control, that allows autoregulation of cardiac output according to changes in vascular resistance level (Giridharan & Skliar, 2003). The FS control and the constant differential pressure control methods are also employed in the control of BiVAD (Gaddum et al., 2012; Ng et al., 2018; Stephens et al., 2017; Stevens et al., 2014; Wang et al., 2018a; Wang et al., 2018b).

Several studies have reported BiVAD control (Gaddum et al., 2012; Stephens et al., 2017; Stevens et al., 2014) based on fixed FS control relationship in the control scheme. This poses risks of ventricular suction and vascular congestion because the FS curve of native heart changes with preload, afterload, and cardiac contractility (Guyton & Hall, 2006). To avoid risks of ventricular suction and vascular congestion, an adaptive FS

control system (Ng et al., 2016), and multi-objective control systems (Gwak et al., 2005b; Ng et al., 2018; Vollkron et al., 2005), have been proposed.

Another challenge of BiVAD control involves controlling a multi-input-multi-output system, in which interactions may exist between the left and right control loops. For example, changes in LVAD speed affects preloads and pump flow rate on the left and right sides of heart. In such cases, the control system must ensure balanced left and right flow rates, as failing to do so might lead to a high risk of pulmonary and systemic venous congestion or even ventricular suction. Many investigators have implemented simplistic dual proportional–integral–derivative (PID) control for BiVAD to balance the systemic and pulmonary flows (Gaddum et al., 2012; Gregory et al., 2016; Ng et al., 2018; Stephens et al., 2017; Stevens et al., 2014). The dual PID controllers were non-centralised; they failed to consider process interactions in the control algorithm, which may lead to poor control performance. When coupled with inappropriate tuning of the PID controllers (Gaddum et al., 2012), the control stability may also be compromised.

The various shortcomings of the existing control schemes call for the development of a control scheme for BiVAD that can: a) consider process interactions in control optimisation, b) flexibly consider multiple control objectives (i.e. flow adaptation according to the metabolic demand, suction avoidance, and congestion avoidance), and c) predict and provide pre-emptive measures before adverse events (i.e. ventricular suction and vascular congestion) occur. To tackle all the above, model predictive control (MPC), a control strategy that employs a multivariable internal model for prediction over a finite-time horizon and produces a closed loop control law based on minimisation of a performance cost function, is an appropriate base choice. In this work, MPC will be deployed for the centralised control of a BiVAD. The conventional MPC framework that employs a linear time-invariant (LTI) model will be modified to include a time-varying

state-space model that captures the essential dynamics of the cardiovascular-biventricular assist device (CVS-BiVAD) system. This is important to ensure minimal computational cost while not sacrificing the salient features necessary for achieving good control. In addition, safety features that prevent ventricular suction and vascular congestion will be added in the MPC control objectives. This enhanced MPC will be referred to herein as the centralised multi-objective model predictive control (CMO-MPC) scheme.

1.2 Research objective

To achieve the aim of the study, which is to develop the CMO-MPC for a BiVAD to regulate flow balancing between the systemic and pulmonary circulations, several objectives are defined as follows:

1. To develop a simplified state-space model of a CVS-BiVAD system that has comparable mean haemodynamic responses to a wide range of pump operating points as well as pulmonary vascular resistance (PVR) and systemic vascular resistance (SVR) levels.

2. To develop a CMO-MPC algorithm from the simplified state-space model of the CVS-BiVAD system and to benchmark the control performance of the CMO-MPC against a PI-FS controller and CS controller for in different patient scenarios using a validated numerical model.

3. To benchmark the control performance of the CMO-MPC of a BiVAD against the CS and PI-FS controllers for different patient scenarios in a mock circulation loop (MCL).

1.3 Research scope and limitation

The present research includes the development and evaluation of a simplified state-space model of CVS-BiVAD interaction, the development of a CMO-MPC for biventricular assist devices, and the evaluation of the CMO-MPC in silico and in vitro. Animal studies are not included in the scope of thesis.

1.4 Thesis outline

The remaining six chapters are briefly described as follows:

Chapter 2 presents the general literature review for the present study. A basic understanding of the ventricular assist device (VAD), types of controllers, the intrinsic regulatory mechanism of the native heart, a description of the physiologic control strategies that have been proposed for both LVADs and BiVADs, the evaluation platform, the simulation protocol, and the performance indices used for the evaluation of the physiological control of LVADs and BiVADs are included.

Chapter 3 fulfils the first objective of the thesis. The model simplification method and parameter optimisation method used to design the state-space model of a CVS-BiVAD system are described. The model-simulated results for various pump operating regions as well as for various PVR and SVR levels are compared with published experimental results.

Chapter 4 documents the work for the second objective of the thesis. A relative gain array (RGA) analysis of process interactions between the feedback control loop for pump flow rates and preloads in a numerical model and the design of the CMO-MPC for a BiVAD are presented. The control performance of the CMO-MPC are benchmarked

against the PI-FS and the CS controllers for exercise and postural change scenarios in a validated numerical model.

Chapter 5 accomplishes the third objective of the thesis. Exercise and postural change scenarios are designed in the MCL. The tuning parameters of the controllers and the FS control strategy are optimised for MCL testing. The control performance of the CMO-MPC is benchmarked against the PI-FS and the CS controllers in the MCL.

Chapter 6 summarises the key findings, states the limitations of the studies, and recommends future work that can be extended from the present study.

CHAPTER 2: LITERATURE REVIEW

This chapter presents a comprehensive background of the VAD, the types of controller, and the intrinsic regulation mechanisms of the native heart, and a comprehensive review of the control strategies proposed for the physiological control of LVADs and BiVADs, the simulation platform, the simulation protocol, and the performance index used for the evaluation of physiological control of LVADs and BiVADs. At the end of this chapter, a summary of the literature review is provided to help readers to understand the motivation behind the thesis topic.

2.1 Ventricular assist device (VAD)

VADs have been used as bridge to transplantation (Bull et al., 2010; Holley et al., 2014; Klotz et al., 2006; Reineke & Mohacsi, 2017; Wieselthaler et al., 2000), bridge to recovery (Drakos et al., 2012; George et al., 2013; Jakovljevic et al., 2017), and destination therapy (Fukunaga & Rao, 2018; Lietz et al., 2007; Perri et al., 2017) for heart failure patients. There are two major different flow types of VADs: 1) pulsatile flow VADs and 2) continuous flow VADs.

Pulsatile flow VADs are often known as a volume displacement VADs. They are the first-generation of VADs. They have many mechanical components such as valves, pusher plates, membranes, and bearings. They work like the native heart, in that they have the diastolic and systolic phases defined by the systole-diastole ratio (in time phase) based on the heart rate. Second- and third-generation cardiac assist devices are continuous flow blood pumps. They are miniature because they only employ a single rotating element: an impeller. Second- and third-generation blood pumps are classified by the bearing design. Second-generation pumps employ a mechanical bearing support system whereas third-generation pumps employ a contactless bearing support system (e.g. hydrodynamic

bearing, electromagnetic bearing, and permanent magnet bearing). The emergence of the contactless bearing system has increased the durability of the cardiac assist devices by eliminating the risks of mechanical wear and tear. Figure 2.1-Figure 2.3 depict the structural differences between the pulsatile flow blood pump and continuous flow blood pump.

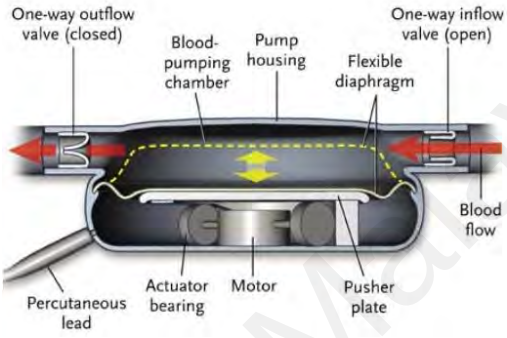

Figure 2.1: Pulsatile flow HeartMate (HM) XVE (Abbott, Thoratec, Pleasanton, CA, USA) (Slaughter, Rogers, et al., 2009).

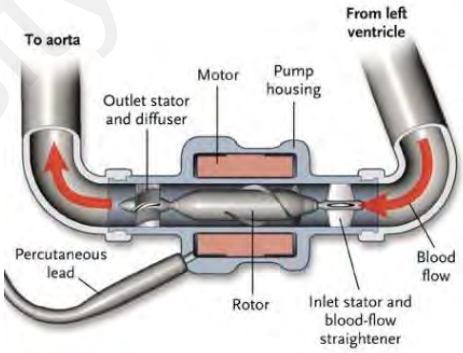

Figure 2.2: Continuous flow (axial flow) HeartMate II (Abbott, Thoratec, Pleasanton, CA, USA) (Slaughter, Rogers, et al., 2009).

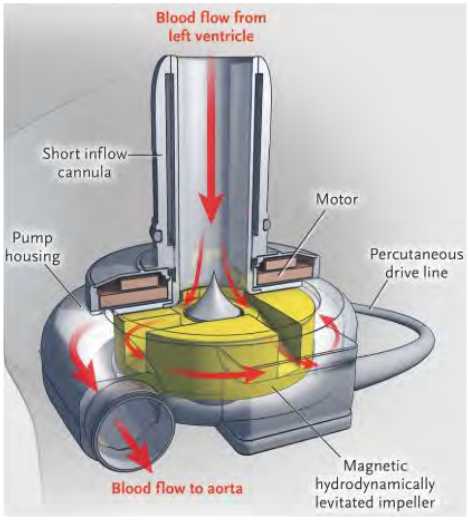

Figure 2.3: Continuous flow (centrifugal flow) HVAD pump (Medtronic, HeartWare International Inc, Framington, MA) (Rogers et al., 2017)

Continuous flow blood pumps are divided into axial flow and centrifugal flow pumps. The axial flow pump has a flow straightener that directs the axial flow of blood in the same direction between the inlet and the outlet. The centrifugal pump has a wide diameter impeller vane. Blood is drawn into the inlet cannula and exits tangentially through the outlet cannula.

The differences between the hydrodynamic performances of axial flow pumps and centrifugal flow pumps are depicted in Figure 2.4. The slope of the pressure head-flow (HQ) curve of the axial flow pump is steep whereas the slope of the HQ curve of the centrifugal pump is flat. Based on the differences between the HQ relationships of the centrifugal flow and axial flow pumps, it can be deduced that the axial flow pump is more susceptible to inlet cannula suction as compared with the centrifugal flow pump in hypovolaemia, hypertension, and right heart failure scenarios. In order to change the pump flow rate, large differential pressure is required in axial flow pumps. When preload decreases, the pump flow rate is insensitive to changes in preload and does not decrease

accordingly to changes in preload, leading to higher risks of ventricular suction (Pagani, 2008).

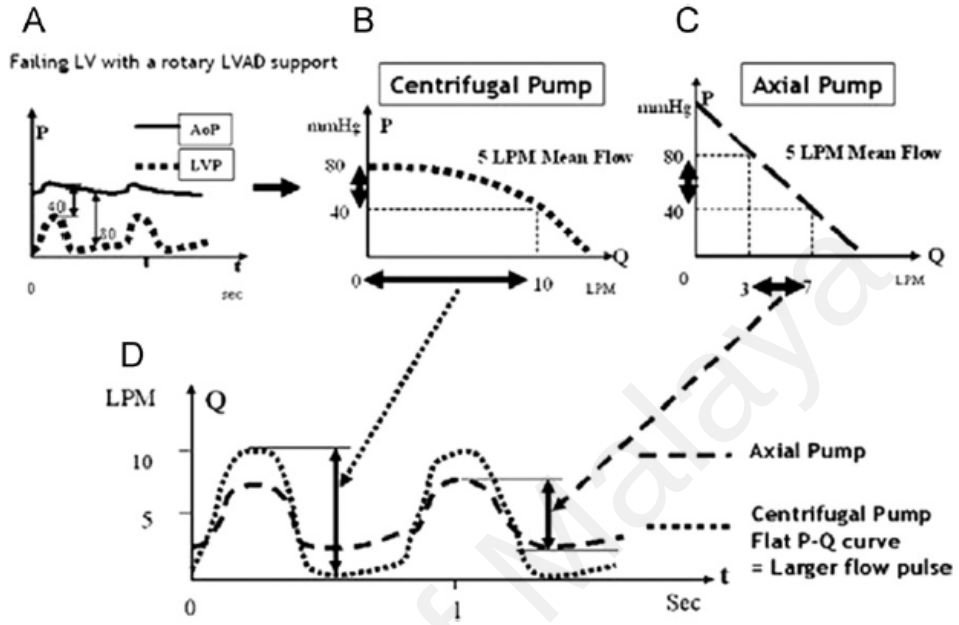

Figure 2.4: A. Aortic pressure and left ventricular pressure of a failing LV supported by a rotary LVAD. B. HQ relationship of a centrifugal flow pump. C. HQ relationship of a axial flow pump. D. Flow pulsatility of centrifugal flow pump and axial flow pump (Pagani, 2008). LV, left ventricle; LVAD, left ventricular assist device; HQ, pressure head-flow.

The performance of a physiological control system relies on the accuracy of feedback variables. Estimation of flow variables in centrifugal flow pumps (e.g. HVAD pumps) is more reliable than the axial flow pumps (e.g. HeartMate II pumps) because the current-to-flow relationship of the centrifugal flow pump is linear across the operating range (Moazami et al., 2013). On the other hand, the current-to-flow relationship of the axial flow pump is not linear across the operating range; it is only enough to provide a trend of the pump flow rate (Slaughter, Bartoli, et al., 2009). Besides pump current, blood viscosity is also required for an accurate estimation of the pump flow rate. Patient's haematocrit level is often used as an indication of the blood viscosity level. The flow estimation algorithm in the HVAD pump (HeartWare International Inc. MA) considers

the haematocrit level of patients, the pump power and the pump speed in the computation of pump flow rate. Since the estimation of pump flow rate is more reliable in HVAD pumps, the development of a reliable sensorless physiological control system for HVAD pumps may be more feasible as compared to the HMII pumps.

Dual HVAD pumps are commonly used to treat biventricular-heart failure patients in clinics because they are miniature and can be well fitted in the human body. Additionally, these pumps are third-generation pumps that have improved haemocompatibility as compared to the first-generation and second-generation pumps due to their contactless bearing . As alluded to earlier, the risk of suction is lower in HVAD pumps as compared with HMII pumps, in addition to the higher estimation accuracy of the pump flow rate of HVAD pumps as compared with HMII pumps, both of which may further encourage the implantation of dual HVAD pumps for bi-heart failure patients.

2.2 Intrinsic regulation of heart pumping

The FS mechanism refers to the intrinsic ability of a native heart in regulating flow balance by pumping the same amount of blood out (i.e. cardiac output) as the total inflow blood volume (i.e. venous return). Venous return is sometimes referred to as preload, although they are technically different terms. Preload means the load on the ventricular muscle before ventricular contraction. When venous return increases, the cardiac muscles stretch and elongate, increasing the opportunity of crosslinking between the actin and myosin within the cardiac muscles, thus greater contractility force is generated. However, this is self-limited by the optimal length of elongation. If the stretching goes beyond the optimal length, the cardiac contractility will not increase further. The plateau region of the FS curve in Figure 2.5 indicates this self-limiting factor.

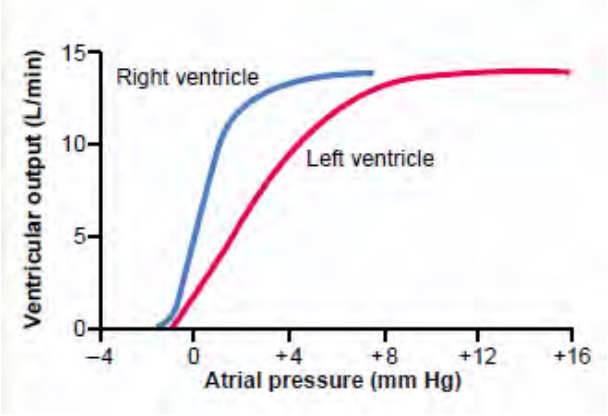

Figure 2.5: Frank-Starling curves of the left ventricle and right ventricle at resting state (Guyton & Hall, 2006).

The FS curves change according to sympathetic and parasympathetic stimulation as shown in Figure 2.6. During activation of sympathetic nerves, the heart rate may be increased up to 200 bpm and the force of cardiac contractility may be doubled, thus the cardiac output can effectively be increased to more than 20 L/min. On the other hand, duirng the activation of parasympathetic nerves, the heart rate may drop to 20-40 bpm and the cardiac contractility may drop by 20-30%.

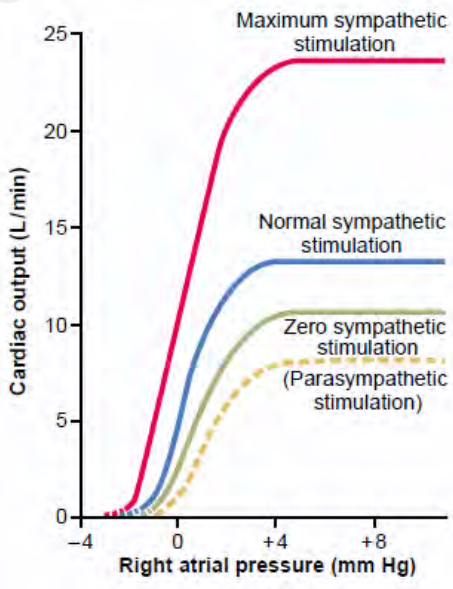

Figure 2.6: Effects of sympathetic and parasympathetic stimulations on the FS curves (Guyton & Hall, 2006).

Characteristic FS curves of heart failure patients are shown in Figure 2.7. A sudden reduction in cardiac output at baseline triggers the activation of the sympathetic nervous system to increase the cardiac output by increasing cardiac contractility and heart rate. However, the maximum stretching limit of the cardiac muscles of heart failure patients plateaus at approximately 5 L/min after the sympathetic stimulation, which limits the exercise capacity and daily life activities of heart failure patients. For this reason, heart failure patients in the category of New York Heart Association Class IV may experience shortness of breath even at rest.

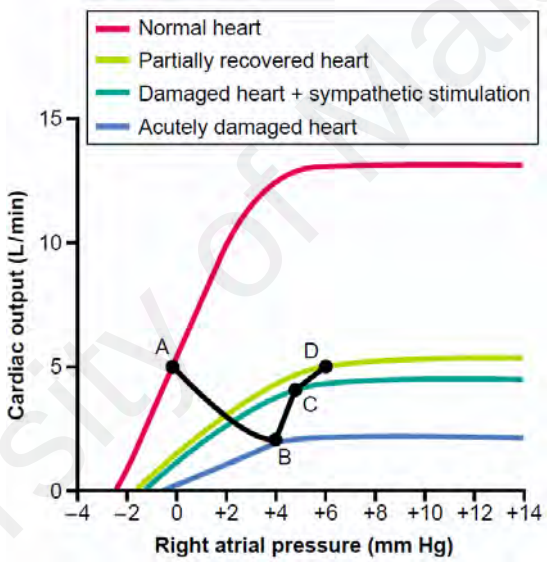

Figure 2.7: Frank-Starling curves of different cardiac conditions. Point A to point D show progressive change of cardiac output and right atrial pressure from normal heart to acutely damaged, damaged heart with sympathetic stimulation, and partially recovery. (Guyton & Hall, 2006).

2.3 Physiological control of LVAD

Design of a physiological control system for a LVAD involves a selection of feedback-controlled variables and a specification of the setpoint values for the feedback-controlled variables. The controlled variables can be either directly measured or estimated from the

pump variables. The controlled variables herein are by default referred to their mean values unless otherwise mentioned as the instantaneous values.

2.3.1 Differential pressure (dP) control

Differential pressure has been used as the controlled variable for LVADs by Waters et al., Giridharan et al., and Wang et al. (Giridharan & Skliar, 2003; Wang et al., 2018a; Waters et al., 1999). Different desired differential pressures (i.e. the difference between aortic pressure and left ventricular pressure) were used by different groups: 75 mmHg (Giridharan & Skliar, 2003) and 110 mmHg (Waters et al., 1999). The control strategy aimed to passively change the cardiac output (i.e. the addition of pump flow rate, Q_p and valve flow rate, Q_{valve}) with changes in vascular resistance, $R_{vascular}$ at different physical activity levels. Assuming blood vessels followed the Hagen-Poiseuille law as described in Eq. (2.1), a decrease in vascular resistance during exercise would raise the cardiac output, if the differential pressure, ΔP was maintained at a constant value.

$$\Delta P = Q_p R_{vascular} \tag{2.1}$$

The control strategy is ideal if the automatic regulatory mechanism (e.g. baroreflex mechanism) responds to the need of cardiac demand of the human body. However, in most end-stage heart failure patients, the automatic regulatory mechanism may become insensitive, thus impacting the flow adaptation strategy.

2.3.2 Aortic pressure control

Aortic pressure has been used as the controlled variable for LVADs control by Wu et al. (Wu et al., 2003). The control strategy aimed to maintain the aortic pressure at a constant desired value of 145 mmHg to match the elevated total peripheral resistance in LVAD patients. Using only the aortic pressure as the controlled variable, risks of suction

were prevalent especially when there were changes in physical activity level. Therefore, the pump differential pressure was introduced as a second controlled variable to help detect any impending ventricular suction event. The desired pump differential pressure was selected at 110 mm Hg, with a ±25-30 mmHg as the marginal boundaries. If the measured pump differential pressure was outside the marginal boundaries of the desired differential pressure, the second control objective would be activated to ensure the differential pressure within the marginal boundaries, while minimising the tracking error of the aortic pressure (Wu et al., 2007). The previous study showed that the control strategy could reverse suction events, however, during the transient phase of suction recovery, left ventricular end diastolic pressure (LVEDP) exceeded 15 mmHg (defined by the authors as the upper limit of LVEDP) for 8 heart beats. The upper limit of LVEDP was used as an indicator for risks of pulmonary congestion.

2.3.3 Frank-Starling (FS) control

Pump flow rate had been used as the controlled variables for all FS like control strategies (Mansouri et al., 2015; Salamonsen et al., 2012; Stevens et al., 2011). Three different types of FS curve have been introduced: 1) a direct interpolated polynomial function of the FS relationship between the pump flow rate and preload (i.e. left atrial pressure, LAP (Stevens et al., 2011) and LVEDP (Mansouri et al., 2017)), 2) a linear FS relationship between the pump flow rate and pump flow pulsatility (Salamonsen et al., 2012), and 3) a general sigmoid function that mimics the FS relationship between the pump flow rate and preload (Ng et al., 2016; Stephens et al., 2017). According to the FS curve, the reference pump flow rate with respect to changes in preload or flow pulsatility would be identified. Flow pulsatility relies on residual ventricular contractility, therefore it is not suitable to be used as the FS control curves in severe heart failure scenarios. Although there was no event of ventricular suction and vascular congestion reported in

the fixed FS control strategy, adaptive control curves had been introduced to ensure the pump operates within the safe operating region (i.e. regions free of ventricular suction and pulmonary congestion) (Gaddum et al., 2014; Stevens et al., 2011).

2.3.4 Left ventricular systolic pressure (SP) control

Left ventricular systolic pressure (SP) had been used as the controlled variable of LVAD control by Petrou et al. (Petrou et al., 2016). The control scheme only required a measurement of pump inlet pressure (PIP). The SP signal was captured as the maximum value of the PIP signal in a cardiac cycle. A fixed proportional gain, k_{sp} of 40 rpm/mmHg was selected in the study. The reference pump speed, N_{ref} was tuned until a baseline cardiac output of 5 L/min was achieved. The corresponding SP at N_{ref} was recorded as the SP_{ref}.

The SP control strategy was robust to a sensor drift of ±15 mmHg and sensor noise. However, the SP control strategy failed to prevent pulmonary congestion in severe heart failure scenario (extreme low cardiac contractility). A decrease in cardiac contractility decreased the SP level and resulted in a decrease in the left pump speed. As a result, the LVEDP elevated to more than 20 mmHg.

2.3.5 Left ventricular volume (LVV) control

Left ventricular volume (LVV) had been used as the controlled variable for LVADs by Oschner et al. (Ochsner et al., 2014). There are three stages in the LVV control strategy: 1) signal processing of the LVV signal to get the heart rate (HR) and end diastolic volume (EDV), 2) calculation of the desired pump power, PP_{des}, and 3) converting the PP_{des} to desired pump speed, N_{des} using a pump power look-up table. Although the LVV control strategy demonstrated similar preload and afterload

sensitivities as the native heart during the preload and afterload variation tests, there are no long-term implantable sensors for volume measurements.

2.3.6 First derivative of minimum pump flow rate to pump speed control

The rate of change of minimum pump flow rate with pump speed, $dQ_{p,min}/d\omega$, decreases with increasing mean pump flow to the systemic circulation – the value further decreases until it becomes negative during the onset of suction (Ferreira et al., 2005). In the past, researchers proposed a control algorithm that aimed to deliver maximum pump flow rate while avoiding suction by setting $dQ_{p,min}/d\omega = 0$ (Ferreira et al., 2005). However, this method does not aim to match the cardiac output with venous return but aim to deliver the maximum possible pump flow rate which may result in high arterial pressure at most scenarios. Other disadvantages of this control strategy include the reliant of an accurate flow probe and the deterioration of control performance when signal-to-noise ratio was 9 dB (i.e. the algorithm was only capable to avoid suction < 50% of the evaluation time).

2.3.7 Pump motor current pulsatility control

Endo et al. designed a control algorithm based on the pump motor current pulsatility (Endo et al., 2002). The pulsatility of pump current is contributed by the cardiac contractility. They proposed an index called the index of current amplitude (ICA) to measure the difference between maximum and minimum of the pump motor current waveform. Similar to the concept of first derivative minimum pump flow rate to pump speed control, they identified an indicator (i.e. ICA = 0.18) for suction and ensure the pump operating range to be maintained below 0.18. This control strategy requires the manual definition of ICA, which is possible to obtain in a mock circulation loop using the profile of ICA versus pump speed but difficult to obtain in real patient body. The target

ICA may vary between patients as well as in patients who are undergoing cardiac recovery.

2.3.8 Multi-objective control of LVAD

A hierarchical control strategy has been proposed for LVADs by Boston, Antaki, & Simaan (Boston et al., 2003), which utilised multiple feedback variables and targets. The highest control level was the multi-objective optimisation control, followed by the heuristic control, and the default control (Figure 2.8). The decision on which level of control was chosen was based on the availability and reliability of the model parameters.

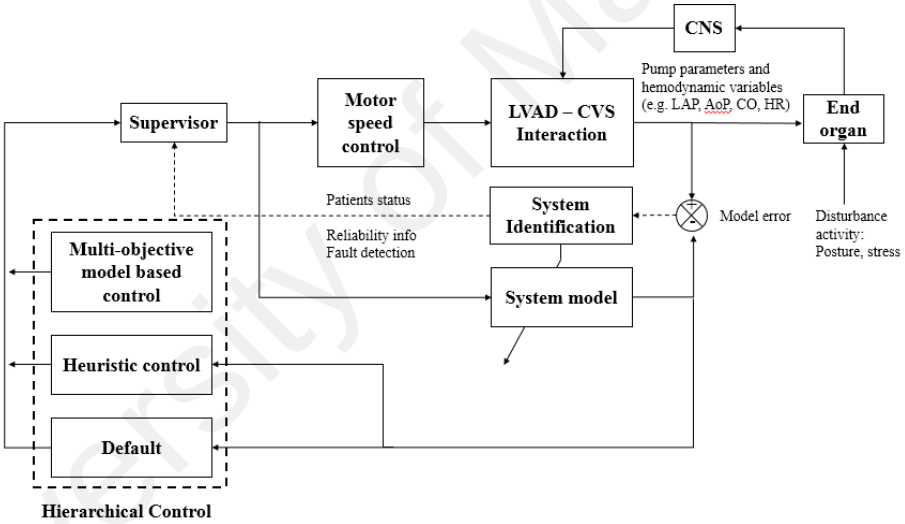

Figure 2.8: Block diagram of the hierarchical control strategy (Boston et al., 2003).

The multi-objective control considered three different feedback variables (each with its own objective):

1. Cardiac output should be greater than the minimum value (value not stated) of patient support
2. Left atrial pressure should be lower than 10–15 mm Hg and greater than 0 mm Hg for avoidance of pulmonary congestion and ventricular suction, respectively

3. Systemic arterial pressure should be maintained between 70–150 mm Hg

Each objective in the cost function was assigned with different scaling weight which ranges from zero to one depending on the relative importance. All three scaling weights should add up to one.

The heuristic algorithm aimed to regulate the pump speed at its maximum level before suction occurred. Several indices were used to detect suction: 1) pulsatility index, 2) diminishing returns index, 3) minimum flow index, and 4) harmonic index. Positive suction detection results that were verified by many different indices increased the confidence level of the presence of suction events.

The default control was the constant speed control that assured minimum acceptable resting perfusion was provided to the patients. If ventricular suction was detected, the default control would be favoured to alleviate suction events.

Another multi-objective control strategy employed two control indices: 1) venous return index (VRI) to control the optimal pump flow rate and 2) harmonic suction index (HSI) to prevent suction (Gwak et al., 2005a). The pump flow rate was the controlled variable. VRI is the derivative of pump flow rate with respect to pump speed whereas the HSI is the ratio of the power of the harmonic components of the flow waveform above the fundamental harmonic to the total power spectra of the flow waveform. The reason for the selection of setpoint was not explicitly stated. The same weighting value was used for both the VRI and the HSI. The preliminary results showed that during a sudden step decrease in preload, the multi-objective control scheme successfully prevented ventricular suction. Events of ventricular suction were reported in the controller that only used VRI as the control index.

Petrou et al. proposed a multi-objective advanced control and monitoring system (Petrou et al., 2017) that aimed to achieve six objectives: 1) to adapt pump flow rate according to physiological requirements of the patients, 2) to increase aortic pulse pressure, 3) to control the opening of the aortic valve for a pre-set period, 4) to extract information of the pre- and after-load conditions of the heart and heart rate, 5) to prevent ventricular suction, and 6) to prevent pulmonary congestion. Three feedback-controlled signals are required: 1) PIP, 2) pump speed, and 3) pump flow for this control strategy.

The most challenging part of the design of multi-objective control scheme is the selection of the number of control objectives and the distribution of the weighting scale for each objective. Although the trade-off between control objectives may complicate the multi-objective control scheme, there is no major conflicting trade-off between the main control objectives of the physiological control of LVADs. Firstly, ventricular suction and vascular congestion do not exist at the same time. Secondly, a list of priority of control objective for the control of LVADs (e.g. ventricular suction or pulmonary congestion shall be prioritised over pump flow rate if the pump flow rate has not reached its minimum limit) is normally applied, giving priority to the safety features that avoid ventricular suction and vascular congestion. Thirdly, there is only one manipulated variable involved in the physiological control of LVADs (i.e. pump speed). If the pump speed has reached its lowest limit (i.e. minimum acceptable flow rate) and yet ventricular suction is not relieved, then clinical intervention (i.e. blood transfusion or drug delivery) is needed to prevent suction so that the minimum acceptable flow rate is maintained.

2.4 Physiological control of a BiVAD

Compared with the physiological control of LVADs, fewer work has been done for the development of physiological control of BiVADs. The previous control strategies of

BiVAD were built mainly on the selection of suitable controlled variables and reference for the controlled variables (constant or adaptive). Most of the control strategies employed PI controllers to achieve its control objectives except one that paired an MPC with a PI controller for BiVAD control. A brief description of each control strategy for a BiVAD and the respective evaluation outcomes are presented in this section.

2.4.1 Dual independent control of a BiVAD

Gaddum et al. investigated the preload sensitivity and control performance of three dual independent control schemes, namely dual independent atrial pressure control (DI-AP), dual independent inlet pressure control (DI-IP), and dual independent Frank-Starling control (DI-FS) in a MCL (Gaddum et al., 2012). Preload sensitivity could be tailored by changing the cannula length and placement of pressure sensors. The preload sensitivity of the DI-AP control was infinite whereas in the DI-IP control and DI-FS control, the preload sensitivities were similar in value, which were 0.3 (L/min)/mm Hg for LVAD and 0.22 (L/min)/mm Hg RVAD, respectively. Instability in a haemodynamic responses were observed in the DI-AP control in the postural change from supine to upright test, possibly attributed to the infinite preload sensitivity of the DI-AP control. To evaluate the controller performance, the systemic venous compliance was reduced so that blood volume was shifted from systemic veins to the right heart. Ripples of oscillation in the pressure and flow waveforms with long settling time were observed during the transient period between the point where the system was perturbed and the point at which a new steady-state was achieved. The authors speculated that process interactions between two control loops and the non-optimal tuning parameters of the PID controllers may be the cause of oscillations and long settling time.

2.4.2 Master/Slave (M/S) control

The dual independent control strategies for BiVAD employed two isolated feedback control loops, that does not account for the flow balancing between the systemic and pulmonary circulations. To balance the systemic and pulmonary circulations, a master/slave control strategy was introduced by Stevens, Wilson, Bradley, Fraser, & Timms (Stevens et al., 2014). The difference between the Master/Slave controller and the DI-FS controller is that the former works in a dependent manner between the master controller and the slave controller whereas the latter works in an independent manner between two controllers Two configurations of master/slave control for BiVAD: left/right master/slave control and right/left master/slave control were examined in the study. The master controller employed a linear FS control method whereas the slave controller employed a linear preload matching approach between the left and right circulations. The two configurations of master/slave controller were evaluated in four patient scenarios: rest, exercise, postural change and Valsalva. The control performance was benchmarked against the CS controller and the DI-FS controller. The left/right master/slave control outperformed the other control strategies for having the least number of recorded suction events and no signs of pulmonary congestion throughout the entire simulation. The linear FS function may not be appropriate because the native heart has a higher preload sensitivity in the lower preload level (i.e. LAP or RAP between 0 mmHg and 3 mmHg). Also, the preload matching strategy may not be physiologically acceptable because this imposes a rigid constraint between the fluid distribution between the systemic and pulmonary circulations (Salamonsen et al., 2011).

2.4.3 Multi-Objective neural-network-based model predictive control (MON-MPC)

Ng et al. proposed a multi-objective neural-network-based MPC (MON-MPC) and an FS like PID (PID-FS) controller for BiVAD control (Ng et al., 2018). Two configurations of pairing were evaluated with the CS controller as well as the DI-FS controller: 1) MON-MPC_L-PID-FS_R (MON-MPC on the LVAD and PID-FS controller on the RVAD) and 2) MON-MPC_R-PID-FS_L (MON-MPC on the RVAD and PID-FS controller on the LVAD). The control objectives were to: 1) adapt pump flow rate according to the FS relationship, 2) avoid ventricular suction, and 3) avoid vascular congestion. Three feedback variables were used in the MON-MPC: 1) LVEDP, and 2) right ventricular end diastolic pressure (RVEDP), and 3) left or right pump flow rate (depending on the control configuration). In all simulation tests, the pairing of MON-MPC and PID-FS controller outperformed the CS controller and the DI-FS controller. In the evaluation of blood loss scenario, the MON-MPC_R-PID-PFS_L successfully prevented events of ventricular suction from occurring. While in the evaluation of exercise scenario, both configurations prevented pulmonary congestion from happening; higher pump flow rate was achieved by MON-MPC_L-PID-PFS_R. As for the future work suggested by Ng et al., a switchable control strategy among the two control configurations of BiVAD was suggested to gain the advantages of both configurations in avoiding suction and increasing the exercise capacity. It was desirable that the MON-MPC has control objectives that avoids ventricular suction and vascular congestion, however, a potential limitation is the parameterisation of the neural-network model would be too slow for real-time adaptation for different patient scenarios.

2.4.4 Suction-Prevention physiological (SPP) control of BiVAD

Wang et al. proposed the use of a suction-prevention physiological (SPP) control of a BiVAD (Wang et al., 2018a). This SPP control strategy employs a total of four PI controllers: two for LVAD and two for RVAD. In brief, the SPP control strategy aims to fulfil two control objectives: 1) to match the left and right differential pressure with their respective user-defined target differential pressure $\Delta Pr_{L/R}$ (ΔPr_L: 110 mmHg and ΔPr_R: 20 mmHg) and 2) to match the left and right pump slew rate with their respective user-defined target slew rate $\Delta RPMr_{L/R}$ ($\Delta RPMr_L$: 640 rpm and $\Delta RPMr_R$: 540 rpm) for the centrifugal pumps. The SPP control also has a safe mode, which sets the target ΔPr_L and ΔPr_R at 60 mmHg and 17 mmHg when $\Delta RPM_{L/R}$ is close to 0 rpm for more than 5 s. The SPP control, when compared to its predecessor control strategy (Giridharan & Skliar, 2003) which only has one control objective (the dP control), showed that the SPP control could avoid constant (persistent) suction in exercise, elevated PVR, and ventricular fibrillation tests, while the dP control could not.

2.5 Types of controller

The conventional controller, namely the PID controller, has been the most commonly used controller for LVAD physiological control (Gaddum et al., 2014; Ochsner et al., 2014; Petrou et al., 2017; Petrou et al., 2016) and BiVAD control (Stephens et al., 2017; Stevens et al., 2014; Wang et al., 2018b). The MPC, which is well-known for control of multi-input-multi-output system has been more commonly employed for BiVAD control (Ng et al., 2018).

2.5.1 Proportional-Integral-Derivative (PID) controller

A PID controller is the most commonly used controller in industry due to its simplicity. The PID controller has three tuning parameters: the proportional gain, integral gain, and derivative gain as shown in Figure 2.9. The proportional gain sets the magnitude and direction (i.e. positive or negative sign) of the changes on manipulated variables with respect to the control error. The integral action of the PID controller helps eliminate the steady-state offset of the control problem. An anti-windup algorithm is usually added to the PID controller to avoid wind-up of control error due to the saturation of manipulated variables. The derivative action of the PID controller is responsible for the stabilising of the control system. It helps reduce the oscillatory effects that may be caused by the high integral gain of the PID controller. However, the derivative term is sensitive to noisy environments. The control parameters of the PID controller can be tuned using the classical Ziegler-Nichols (ZN) tuning method (Ziegler & Nichols, 1942) or the internal model control (IMC) tuning method (Chien & Fruehauf, 1990). Although the PID controller is easy to implement, it is a linear controller that may yield poor performance in control problems that are highly nonlinear (Seborg et al., 2010).

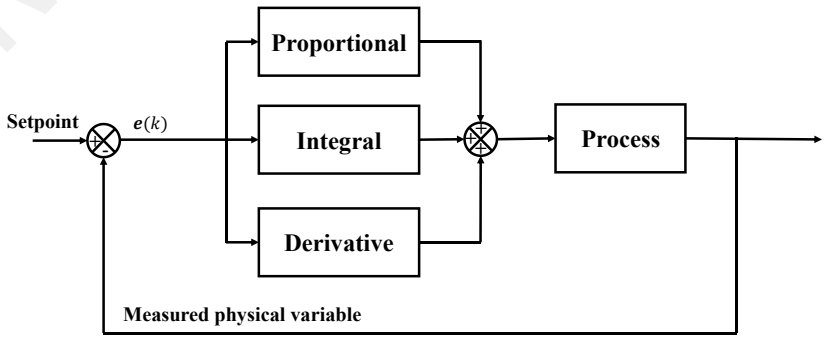

Figure 2.9: Block diagram of a PID controller. $e(k)$ is the tracking error at k^{th} time step.

2.5.2 Model predictive controller (MPC)

A model predictive controller (MPC) (Rossiter, 2003; Seborg et al., 2010) is an advanced control method. MPC has three main components: 1) the internal model, 2) the cost function optimiser block, and 3) the constraints block, as shown in Figure 2.10. The internal model is responsible for the calculation of free response of outputs over a given prediction horizon. The term "free response" refers to the computed predicted state variables using the inputs in one previous time step. The internal model also computes the step response of the outputs over the prediction horizon. Considering the predicted free response outputs, the step response of the outputs, the control objectives, the setpoints, and the constraints of inputs, outputs, and slew rates, the cost function optimiser generates optimal control outputs (also known as manipulated variables) to the process at every time step. The computation of the MPC algorithms takes the receding horizon theory, that moves the prediction window (defined by the prediction horizon) one step ahead at every computational time step, with the updated values of the controlled and manipulated variables.

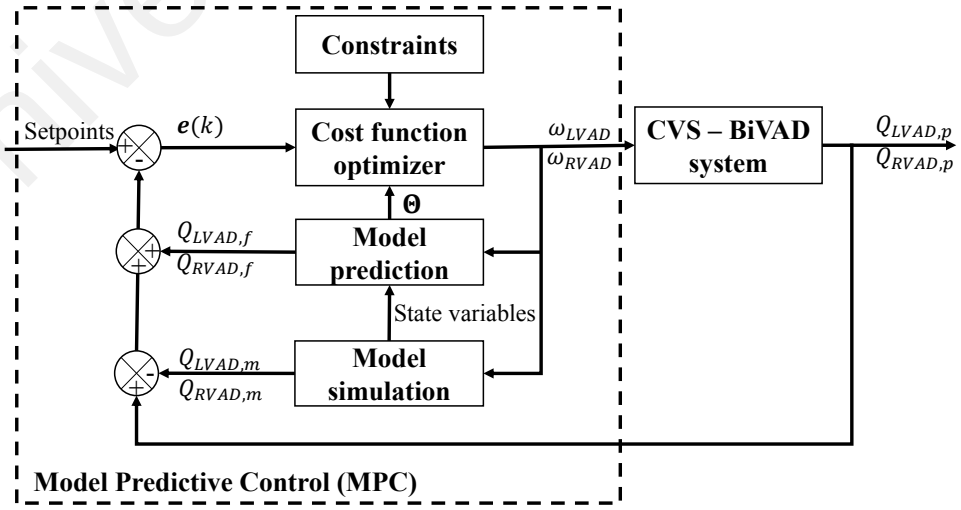

Figure 2.10: Block diagram of an MPC for BiVAD. MPC, model predictive control; CVS-BiVAD, cardiovascular-biventricular assist device; LVAD, left ventricular assist

device; RVAD, right ventricular assist device. $Q_{LVAD,f}$ and $Q_{RVAD,f}$ are the free response LVAD and RVAD flow rate, $Q_{LVAD,m}$ and $Q_{RVAD,m}$ are LVAD and RVAD flow rate generated by the model, and $Q_{LVAD,p}$ and $Q_{RVAD,p}$ are LVAD and RVAD flow rate from the CVS-BiVAD system. ω_{LVAD} and ω_{RVAD} are LVAD and RVAD speeds. $e(k)$ is the tracking error at k^{th} time step.

The advantages of MPC include: 1) able to prevent adverse events from happening based on the prediction outcome of the internal model, 2) better handling of multivariable control problems as compared to other control schemes, 3) considers inequality constraints of inputs, slew rate, and outputs in optimisation of control moves, and 4) it is easy to tune.

2.6 Evaluation platforms for physiological control of LVAD and BiVAD

Physiological control of LVADs and BiVADs can be evaluated in a numerical model (*in silico*), an MCL (*in vitro*), an animal body (*in vivo*), or a patient (*clinical*). The cost of evaluation and the level of validity from the highest to the lowest are as follows: patient, animal, MCL, and numerical model. New control strategies should undergo preliminary evaluations in a valid numerical model or MCL (depending on the availability) before proceeding to evaluation platforms that require higher costs.

2.6.1 Numerical model

An example of a numerical model of CVS-BiVAD interaction is represented by an electric analogue circuit as shown in Figure 2.11. The CVS-BiVAD model was used by Ng et al. for the evaluation of physiological control of a BiVAD (Ng et al., 2018). In the electric analogue circuit, the pressure mimics the voltage, the blood flow rate mimics the electric current, the vessel resistance mimics the resistance, the vessel compliance mimics the capacitance, the flow inertance mimics the inductance, and the diode mimics the heart

valve. The CVS component consists of the four chambers of the heart: 1) left atrium, 2) left ventricle, 3) right atrium, and 4) right ventricle, and the systemic and pulmonary vasculatures. Each elaborated component in the systemic and pulmonary vasculature is outlined in the caption of Figure 2.11. The numerical model is also called as a lumped parameter model because the expanded vessels (i.e. every branch of artery, capillary, and vein) in the pulmonary and systemic circulations are lumped together as systemic peripheral vessels, systemic veins, pulmonary peripheral vessels, and pulmonary veins. The pump models were characterised by three differential equations: motor winding electrical equation, electromagnetic torque transfer function equation, and pump hydraulic equation. The details of other numerical models that were used in the evaluation of physiological control of LVAD and BiVAD can be found in the references (Andreas Arndt et al., 2008; Giridharan et al., 2002; Lim et al., 2015; Nadeem et al., 2015; Schima et al., 1990; Simaan et al., 2009; Wu et al., 2007).

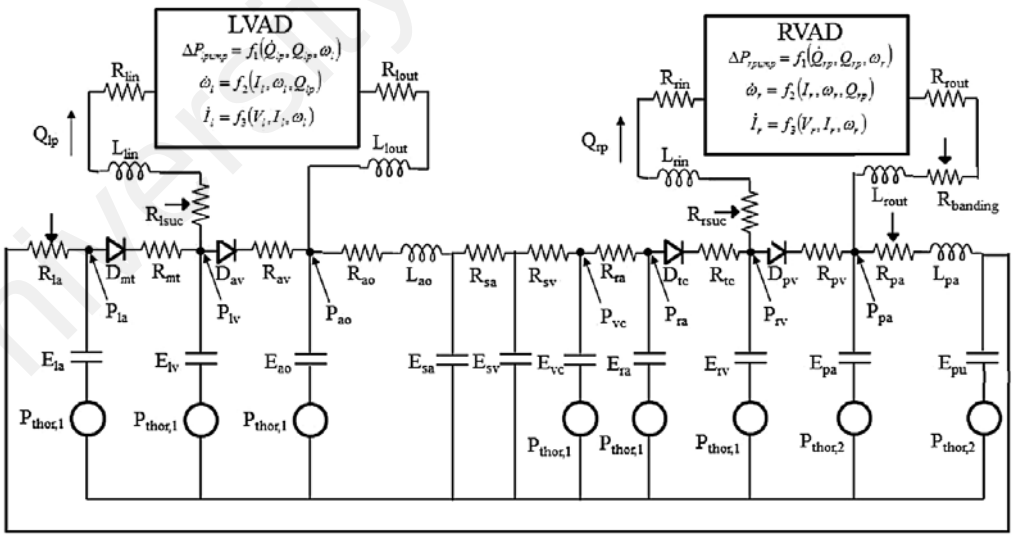

Figure 2.11: An electrical analogue circuit that replicates the CVS-BiVAD interaction model. *P*, pressures; *R*, resistances; *C*, compliances; *E,* elastances (=1/C); *L*, inertances; *D*, diodes. The model consists of three main components: 1) the CVS, which is further divided into ten compartments (*la*, left atrium; *lv*, left ventricle, *ao*, aorta; *sa*, systemic peripheral vessels, including the arteries and capillaries; *sv*, systemic veins, including

small and large veins; *vc*, vena cava; *ra*, right atrium; *rv*, right ventricle; *pa*, pulmonary peripheral vessels, including pulmonary arteries and capillaries; *pu*, pulmonary veins and 2) the heart pumps (the left ventricular assist device (LVAD) and the right ventricular assist device (RVAD)), and 3) the cannula ($R_{l/rin}$ and $R_{l/rout}$, inlet and outlet cannulae resistances; $L_{l/rin}$ and $L_{l/rout}$, inlet and outlet cannulae inertances; $R_{l/ruc}$, suction resistance; $R_{banding}$, banding resistance). The intrathoracic pressure, $P_{thor,1}$ and $P_{thor,2}$ were assigned the same values (–4 mmHg) during closed-chest simulated conditions (Nadeem et al., 2015).

2.6.2 MCL (*in vitro* platform)

A mock circulation loop (MCL) is a benchtop artificial circulatory system that is made up of polyvinyl chloride (PVC) tubes, as shown in Figure 2.12. A water/glycerol mixture (60/40% by mass) that replicates the viscosity of blood at a room temperature of 22^{o}C is filled in the MCL as the working fluid. The temperature was selected at room temperature for the experiment to be conducted. Cardiac contractility is driven by electropneumatic regulators. The resistance, compliance, and inductance are characterised by the dimension of the pipes (i.e. length and diameter). The MCL can be used to simulated different patient scenarios by changing the peripheral resistance, compliance, HR, and cardiac contractility. For more details on the elaborated description of the MCL components, please refer to (Timms et al., 2011). Other MCL designs that have also been used for the evaluation of physiological control of LVAD and BiVAD can be found in references (Ochsner et al., 2013; Pantalos et al., 2004).

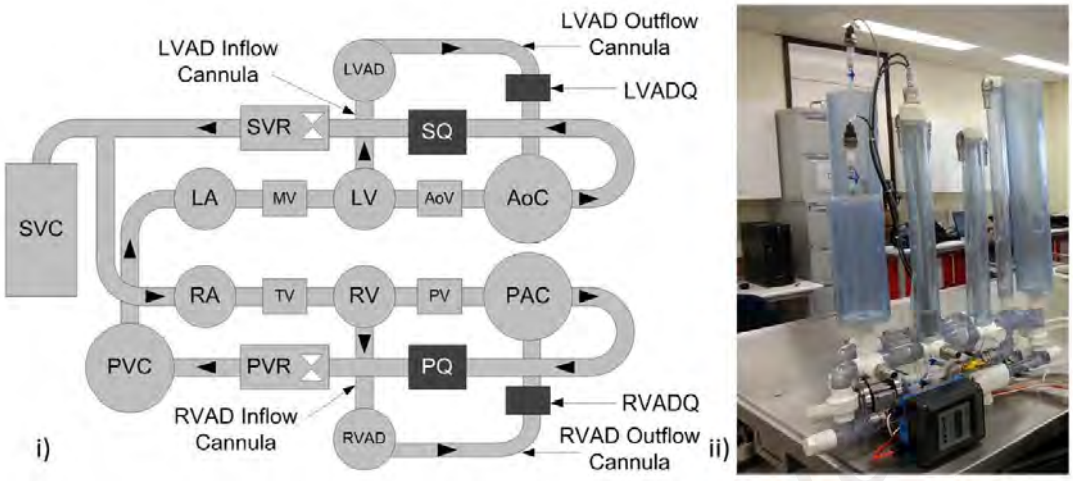

Figure 2.12: i) Schematic diagram of MCL. LA, left atrium; MV, mitral valve; LV, left ventricle; AoV, aortic valve; AoC, aortic compliance chamber; SQ, systemic flow meter; SVR, systemic vascular resistance valve; SVC, systemic venous compliance chamber; RA, right atrium; TV, tricuspid valve; RV, right ventricle; PV, pulmonary valve; PAC, pulmonary arterial compliance chamber; PQ, pulmonary flow meter; PVR, pulmonary vascular resistance valve; PVC, pulmonary venous compliance chamber; LVAD, left ventricular assist device; LVADQ, left ventricular assist device flowmeter; RVAD, right ventricular assist device; RVADQ, right ventricular assist device flowmeter. ii) A photo of MCL (J. P. Pauls, Stevens, Schummy, et al., 2016).

Like the numerical model, the advantage of using the MCL as a control evaluation platform is that the patient scenarios are repeatable for a fair comparison between different control strategies. The MCL provides a more realistic environment (i.e. it is filled with working fluid that replicates the blood viscosity and the electrical and the mechanical aspects of the pumps) when compared with the numerical model. However, the design of simulation protocol in the MCL is limited to the hardware limitations (e.g. the maximum heart rate that can be achieved in this MCL is 120 bpm). Furthermore, the compliance is also difficult to vary in the MCL. Like the numerical model, the MCL also fails to provide the full biological characterisation (i.e. the accurate characterisation of suction (i.e. the collapse of ventricular wall), thrombosis, haemolysis, tissue remodelling, and blood recirculation) for the evaluation of VAD control.

2.6.3 Animal test (*in vivo* platform)

Sheep (Gregory et al., 2016) and pigs (Ochsner et al., 2017) have been used in the evaluation of the physiological control of LVADs and BiVADs. The greatest advantage of animal testing is that it provides the biological environment that allows us to analyse not only the control performance but also the biological implication (i.e. haemolysis and thrombosis) as a result of speed regulation by different controllers. However, the cost of animal models is very much higher than the MCL and numerical model, and the ethics approval is difficult to acquire. Therefore, evaluation in animal models is advised to be conducted after the control scheme has shown excellent and robust performance in the *in silico* and *in vitro* domains (i.e. good control performance and control stability).

2.6.4 Humans (clinical platform)

The first clinical trial of automatic speed control in patients was performed by Schima et al. (Schima et al., 2006). To date, there are no other physiological control schemes for VADs that have been evaluated in any patient. Trials in humans is the highest risk test as failures of the control system during the evaluation tests may lead to mortality. Therefore, the physiological control must be carefully examined and thoroughly tested using the other three evaluation platforms before human trials are performed.

2.7 Evaluation of physiological control of LVAD and BiVAD

Physiological control systems for LVADs and BiVADs are commonly evaluated by benchmarking against the CS control, which is the control scheme that is currently used in clinics, using a range of different performance indices. In this section, the simulation protocol and the performance indices that were used for the evaluation of physiological control performance of LVADs and BiVADs in the previous numerical and MCL studies

are reviewed. The simulation protocol and performance indices used in the previous animal and patient studies are not included because they are not in the scope of the thesis.

2.7.1 Simulation protocol

The simulation protocol used in the evaluation of physiological control of LVADs and BiVADs should reflect the possible daily life activities that the patients may go through. For example, exercise (Giridharan & Skliar, 2003), postural change from supine to upright position (Gaddum et al., 2012), coughing, straining in defecation, Valsalva Maneuvre (Stevens et al., 2014), blood loss (Ng et al., 2018), and potential cardiac recovery (Wu, 2009) had been tested in the previous studies. In several other studies, extreme changes (unrealistic changes in the human body) in preload and afterload (Jo P. Pauls, Stevens, et al., 2016b) had been evaluated to challenge the capability of the physiological control to respond in such circumstances.

2.7.2 Performance index

Physiological control systems have always been evaluated based on three main criteria: 1) to increase exercise capacity by increasing the pump flow rate, 2) to avoid ventricular suction, and 3) to avoid vascular congestion. The exercise capacity is indicated by the maximum cardiac output achieved by the control strategies. In several exercise evaluation studies, the control strategies were benchmarked according to their capability to unload the ventricles (this is normally indicated by ventricular stroke work) .The events of ventricular suction were identified by the numbers of cardiac cycles that the minimum ventricular volume fell below 0 mL (J. P. Pauls, Stevens, Schummy, et al., 2016; Stephens et al., 2017) or when the end diastolic pressure (EDP) fell below 0 mmHg (Petrou et al., 2018). The events of vascular congestion were identified when mean atrial pressure exceeded between 15-25 mmHg (Ng et al., 2018). Preload sensitivity and afterload

sensitivity of the control strategies were also compared with the ones of the native heart (J. P. Pauls, Stevens, et al., 2016a; Salamonsen et al., 2011).

2.7.3 Comparison between different control strategies of LVAD

In 2015, Lim et al. evaluated the control performance of various physiological control strategies of LVAD in exercise and head-up-tilt (HUT) in a numerical model (Lim et al., 2015). The control strategies include the CS control, the constant flow pulsatility index control, the constant average differential pump pressure control, the constant average differential pressure between the aorta and left atrium, $dP_{ao,la}$ control , the linear Starling like control, and the constant atrial pressure control. The constant $dP_{ao,la}$ control was shown to be the most robust physiological control of LVADs based on its overall ability to increase pump flow rate in exercise scenario and maintain stability in the head-up-tilt scenario. Although the constant atrial pressure control achieved the highest the pump flow rate in an exercise, it caused a fall in mean arterial pressure in a head-up-tilt test, which may lead to orthostatic hypotension in patients. The constant flow pulsatility index control and the linear Starling control that relies on flow pulsatility demonstrated poor performance in both evaluated tests. This may be due to the lower sensitivity of flow pulsatility in response to venous return.

In 2016, Pauls et al. added the evaluation tests and control strategies for the evaluation of the control performance of various physiological control strategies of LVAD, the study was conducted in an MCL (Jo P. Pauls, Stevens, et al., 2016b). The study aimed to create a standardised evaluation platform and simulation protocol to benchmark the emerging control strategies for LVADs. The evaluated control strategies include constant inlet pressure control (Bullister et al., 2002), constant dP control (Giridharan & Skliar, 2003), constant $dP_{ao,la}$ control (Wu et al., 2004), constant flow control (Casas et al., 2007),

constant afterload impedance control (Moscato et al., 2010), linear FS control , starling pulsatility control (Gaddum et al., 2012), linear FS control (Stevens, Wilson, Bradley, Fraser, & Timms,, 2014), and compliant inflow cannula control (Gregory et al., 2012). It was concluded that constant inlet pressure control, constant afterload impedance control and linear FS control could increase the exercise capacity by increasing pump flow rate and avoid ventricular suction and pulmonary congestion in all evaluated scenarios. The MCL results agreed with the numerical study conducted by Lim et al. (Lim et al., 2015) for the exercise scenario but not for the HUT test. The reason was that the HUT that was simulated in the MCL only involved a removal of 300 mL of fluid but no changes in resistance values were simulated.

In 2018, Petrou et al. compared three latest physiological control designs of LVAD with the three most superior control strategies of LVAD reported in the study of Pauls et al. (Petrou et al., 2018). The three added control strategies were the SPP controller (Wang et al., 2015), the SP controller (Petrou et al., 2016), and the LVV controller (Ochsner et al., 2014). The evaluation tests included variations in preload, afterload, and cardiac contractility. The robustness of the control strategy against pressure and volume sensor drifts was also studied. The study revealed that only the LVV avoided events of suction and congestion even at extremely low cardiac contractility as well as with sensor drift. However, the pressure sensor drifts (i.e. ±5, ±15, and ±25 mmHg) used in the study was far more excessive than the one published in the literature (Troughten et al., 2011). A maximum of 4.7 mmHg of pressure sensor drift was reported after 3 months implantation and the drift was maintained even up to 48 months after implantation (Troughten et al., 2011). As there is no long-term implantable volume sensor, the volume sensor drifts (i.e. ±10, ±25, and ±50mL) were selected according to the inaccuracies in the volume measurements using echocardiography (Jenkins et al., 2008). The maximum volume

inaccuracies reported by Jenkins et al. was 79 mL. The volume sensor drifts that were used in the study by Petrou et al. was lower than the maximum inaccuracy in volume measurements (Petrou et al., 2018). Therefore, it is not reasonable to conclude that the LVV control strategy is more robust to sensor drifts as compared to other control strategies that used pressure as the feedback variables. Excluding the influence of sensor drifts on the controller performance, the LVV control demonstrated superior control performance based on its ability to adjust pump flow rate while ensuring no events of ventricular suction and pulmonary congestion. The control strategy that ranked second after the LVV controller was another FS control strategy (Mansouri et al., 2015). Events of pulmonary congestion were only recorded in patients with ejection fraction of 13% in the exercise test. The use of LVV control relies on the volume sensor, which may not be practical to be implanted in the human body. The implantation of a pressure sensor is also more practical than a volume sensor. Therefore, the FS control strategy that relies on pressure and flow sensors may be more feasible as a long-term control strategy in the future.

2.7.4 Comparison between different control strategies of BiVAD

Evaluation of BiVAD control has been performed *in vitro* (J. P. Pauls, Stevens, Schummy, et al., 2016) and *in vivo* (Gregory et al., 2016). The control strategies included compliant inlet cannula control (Gregory et al., 2012), compliant outflow cannula control (Gregory et al., 2015), and M/S control (Stevens et al., 2014). The evaluation tests included gradual changes and step changes in the PVR and SVR, and exercise scenarios. In the *in vitro* study, left ventricular stroke work was the lowest in the M/S control in exercise as compared to other evaluated controllers. All physiological control strategies prevented suction and congestion in the *in vitro* test. In the *in vivo* test, the number of suction and congestion events was reduced but not completely avoided by the M/S control

during step increases in PVR (200-1000 dynes s cm^{-5}) and SVR (1400-2400 dynes s cm^{-5}) levels.

2.8 Summary of literature review

Centrifugal flow VADs are more preload sensitive than axial flow VADs. Preload sensitivity is often used to describe the intrinsic FS characteristic of the native heart to regulate cardiac output according to changes in preload (the amount of blood that fills the heart). In clinics, dual HVAD pumps are commonly implanted as a BiVAD for the bi-heart failure patients. Therefore, dual HVAD pumps were chosen as the BiVAD in the thesis.

Most of the previous BiVAD control strategies incorporated two separate PID controllers. Comparing a PID control to an MPC, a PID control is easy to implement but it is difficult to tune, cannot handle input, output, and slew rate constraints, can only solve linear control problems, and it cannot handle multivariable system. MPC, on the other hand, is better at handling a nonlinear and multivariable control systems, it is easy to tune, and it accounts for input, output, and slew rate constraints in the cost function. Furthermore, MPC can handle process interactions that may exist between the control loops of BiVAD while a conventional as well as an advanced PID controller could not handle process interactions. Therefore, MPC is proposed as the base-choice controller for BiVAD's study.

Several control strategies have been proposed for LVAD and BiVAD control. To benchmark the control strategies, clinically relevant tests (e.g. exercise and postural change) must be designed for the control evaluation *in silico*, *in vitro*, and *in vivo*. Several research groups had compared the control strategies proposed for LVAD control and the FS control strategy was found to adapt pump flow rate according to physiological changes

while minimising events of ventricular suction and vascular congestion. Therefore, in this work, the FS control strategy was chosen as the main control objective with additional safety control objectives that explicitly avoid risks of ventricular suction and vascular congestion, for CMO-MPC. Furthermore, exercise and postural change tests that had been used in the previous studies were also designed for control evaluations in this work.

CHAPTER 3: A SIMPLIFIED STATE-SPACE MODEL CARDIOVASCULAR-BIVENTRICULAR ASSIST DEVICE (CVS-BIVAD) INTERACTION

The aim of the chapter was to simplify a complex numerical model of CVS-BiVAD interaction (Nadeem et al., 2015) to a state-space model that would be used in the development of the CMO-MPC. Several objectives were devised to meet the aim of the study as follows:

- To reduce the number of elements (i.e. resistors and capacitors) involved in the complex cardiovascular system (CVS) model.
- To optimise the model parameter values of the simplified CVS-BiVAD model.

3.1 Introduction

Chapter 2 summarised that all previous physiological control of BiVAD incorporated two separate controllers for BiVAD control. They all faced two major challenges: 1) it was difficult to achieve a balanced flow rate between the systemic and pulmonary circulations and 2) it was difficult to tune two separate controllers as feedback loop interactions may exist. Although some of independent control algorithms have achieved balance without the need to worry of process interactions, it requires an additional step to tune the tuning parameters a priori. Therefore, CMO-MPC was proposed for the study because it could deal with the challenges more effectively than two separate controllers. To reduce the computational effort of the CMO-MPC, a simpler internal model of CVS-BiVAD system would be preferred over the complex model. Therefore, in this chapter, a complex numerical model of CVS-BiVAD system was simplified to a state-space model. New model parameters were assigned using a parameter optimisation method. To check the model accuracy after model simplification, the simplified model was simulated over

a wide range of pump operating region, PVR, and SVR and the simulated results were compared to experimental results.

This chapter presents the first simplified state-space model of the CVS-BiVAD system for use in the physiological control of a BiVAD. The work completed for this chapter has been published as a proceeding: Koh, V. C. A., Lim, E., Ng, B. C., Ho, Y. K., & Lovell, N. H. (2016, August). A simplified state-space model of biventricular assist device-cardiovascular system interaction. In *2016 38th Annual International Conference of the IEEE Engineering in Medicine and Biology Society (EMBC)* (pp. 4317-4320). IEEE. The state equations and the model parameters of the CVS components were directly adopted into this chapter. The hydraulic equation of the HeartMate II pump model that was used in the conference proceeding was replaced by a HeartWare HVAD pump model in the thesis because dual HVAD pumps are more commonly used as BiVAD as compared to dual HeartMate II pumps in clinics. The methods, results, and discussions have been expanded to provide a clearer comparison between the simplified model and the published results.

3.2 Methods

The methods are subdivided into model description, the parameter estimation approach, and the simulation protocol for model evaluation.

3.2.1 Model description

The simplified state-space model of CVS-BiVAD system consists of four heart chambers, systemic and pulmonary circulations and two linear hydraulic equations, as shown in Figure 3.1.

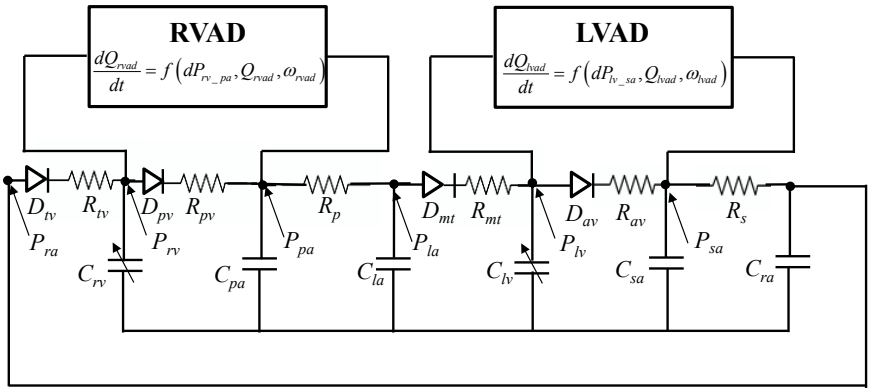

Figure 3.1: A simplified electric analogue circuit of the cardiovascular-biventricular assist device (CVS-BiVAD). *P*, pressure; *R*, resistance; *D*, a diode; *E*, elastance; *L*, inductance. The cardiovascular system model comprises of four major compartments: 1) the left heart (*la*, left atrium; *mt*, mitral valve; *lv*, left ventricle; *av*, aortic valve) 2) the right heart (*ra*, right atria; *tv*, tricuspid valve; *rv*, right ventricle, *pv*, pulmonary valve) 3) the systemic circulation (R_s, lumped resistance of the systemic artery, the systemic capillaries, and the systemic veins; C_{ra}, lumped capacitance of the systemic capillaries, the systemic veins, and the right atrium) and 4) the pulmonary circulation (R_p, lumped resistance of the pulmonary artery, the pulmonary capillaries, and the pulmonary veins; C_{la}, lumped capacitance of the pulmonary capillaries, the pulmonary veins, and the left atrium). *H,* pump differential pressure; LVAD, left ventricular assist device; RVAD, right ventricular assist device; R_{can}, lumped resistance of the inlet and outlet cannula; R_{suc}, suction resistance; L_{can}, lumped flow inertances at the inlet and outlet cannula.

The CVS model is a simplified version of a more complex model (Nadeem et al., 2015). The original numerical model has already been presented in section 2.6.1. The simplified model is not a direct derivative of the original model, thus there is no direct mathematical derivation from the original model. The idea of model simplification method (i.e. the design of a new and simpler electric circuit analogue diagram) is adapted from (Simaan et al., 2009). The output of model simplification is shown in Figure 3.1 corresponding with Eqs. (3.1)-(3.10). The simplification method involves lumping the expanded resistance-compliance (RC) components of arteries, capillaries, and veins of systemic and pulmonary circulations into an equivalent RC element for the systemic and

pulmonary circulations, because the haemodynamic properties of the extended vasculature are not the points of interest in the design of CMO-MPC. The left and right ventricular pressures are modelled as functions of the time varying compliance function, *C(t)*, which was the reciprocal of the time varying elastance function, *E(t)*, as given in (Simaan et al., 2009) and written in Eqs. (3.1-3.4). The terms *t* and *HR* refer to time and heart rate, respectively. The subscripts *n* and *l/rv* refer to the normalised function and left or right ventricle, respectively. E_{max} is the slope of the end systolic pressure volume relationship whereas E_{min} was the slope of the end diastolic pressure volume relationship.

$$t_n = \frac{t}{\left(0.2 + 0.15 * \left(\frac{60}{HR}\right)\right)} \tag{3.1}$$

$$E_n\left(t_n\right) = 1.55 * \left[\frac{\left(\frac{t_n}{0.7}\right)^{1.9}}{1+\left(\frac{t_n}{0.7}\right)^{1.9}}\right] * \left[\frac{1}{1+\left(\frac{t_n}{1.17}\right)^{21.9}}\right] \tag{3.2}$$

$$E_{l/rv}\left(t\right) = \left(E_{\max} - E_{\min}\right) E_n\left(t_n\right) + E_{\min} \tag{3.3}$$

$$C_{l/rv}\left(t\right) = \frac{1}{E_{l/rv}\left(t\right)} \tag{3.4}$$

The pressure-volume relationships of atria and vasculatures are modelled based on the assumption of fixed vascular compliance, $C_{vascular}$, as follows:

$$P_{vascular} = \frac{V_{vascular}}{C_{vascular}} \tag{3.5}$$

where $P_{vascular}$ was vascular blood pressure and $V_{vascular}$ was vascular blood volume.

The valve flow rates, Q_{valve}, were regulated by the opening and closing of the valves as shown in Eq. (3.6). Heart valves were opened when the upstream pressure, P_u was

greater than the downstream pressure, P_d; heart valves were closed in the opposite scenario. For example, in the left heart, the mitral valve was opened when left atrial pressure was greater than left ventricular pressure, and the aortic valve was opened when left ventricular pressure was greater than aortic pressure. In the right heart, the tricuspid valve was opened when right atrial pressure was greater than right ventricular pressure, and the pulmonary artery valve was opened when right ventricular pressure was greater than pulmonary arterial pressure.

$$Q_{valve} = \begin{cases} \dfrac{(P_u - P_d)}{R_{valve}} & \text{if } P_u > P_d \\ 0 & \text{else} \end{cases} \quad \textbf{(3.6)}$$

where R_{valve} was valve resistance.

Since dual HVAD pumps have been widely used as BiVADs in the clinic, it was selected as the pump model in the present study. The model parameters of the hydraulic equation (Eq. 3.7) of the HVAD pump was fitted with experimental results using the least square function. The fitting outcomes was compared with the published hydraulic relationship of HVAD pumps (Moazami et al., 2013).

$$H = a_{HVAD} Q_p + b_{HVAD} Q_p{}^2 + c_{HVAD} \omega^2 + L_{HVAD} \frac{dQ_p}{dt} \quad \textbf{(3.7)}$$

where H, Q_p, ω, and L_{HVAD} were pump differential pressure, pump flow rate, pump speed, and pump inertance, respectively. The fitted model parameters are a_{HVAD}, b_{HVAD}, and c_{HVAD}.

The cannula model describes the resistance of cannula, R_{can}, and the inertance of cannula, L_{can}, as constant parameters, whereas the characteristic of ventricular suction is

modelled as a variable suction resistance, R_{suc}, in Eq. (3.8). The suction resistance is only activated if the suction threshold of pressure, P_{suc_thres}, is violated.

$$R_{suc} = \begin{cases} 0 \text{ if } P_{l/rv} > P_{suc\_thres} \\ -3.5 * \left(P_{l/rv} - P_{suc\_thres} \right) \text{ if } P_{l/rv} < P_{suc\_thres} \end{cases} \quad \textbf{(3.8)}$$

An equivalent 5 mm banding resistance that is derived from the experimental results provided by (Krabatsch et al., 2012) is as follows:

$$R_{banding} \text{ (dynes s cm}^{-5}) = \begin{cases} 636.1 \text{ if } Q_{l/rvad} \le 3.44 \text{ L/min} \\ \left(241.5 * Q_{l/rvad} - 194.7 \right) \text{ if } Q_{l/rvad} > 3.44 \text{ L/min} \end{cases} \quad \textbf{(3.9)}$$

where *l/rvad* refer to the LVAD or RVAD.

There are eight state variables in the CVS-BiVAD model (listed in Table 3.1). The linearised state equations of the simplified CVS-BiVAD model are listed in Eqs. (3.10-3.17). The subscripts used in Eqs. (3.10-3.17) were described as: *lv*, left ventricle; *la*, left atrium; *mt*, mitral valve; *av*, aortic valve; *sa*, systemic artery; *lvad*, left ventricular assist device; *pa*, pulmonary artery; *p*, vasculatures in pulmonary circulation; *ra*, right atrium; *rv*, right ventricle; *s*, vasculatures in systemic circulation; *av*, aortic valve; *tv*, tricuspid valve; *pv*, pulmonary valve; *rvad*, right ventricular assist device; *HVAD,L*, HVAD pump on the left heart; and *HVAD,R*, HVAD on the right heart.

$$\frac{dV_{lv}}{dt} = \frac{P_{la}}{R_{mt}} - \frac{V_{lv}}{C_{lv}(t) R_{mt}} - \frac{V_{lv}}{C_{lv}(t) R_{av}} + \frac{P_{sa}}{R_{av}} - Q_{lvad} \quad \textbf{(3.10)}$$

$$\frac{dP_{la}}{dt} = -\frac{P_{la}}{C_{la} R_{p}} + \frac{P_{pa}}{C_{la} R_{p}} - \frac{P_{la}}{C_{la} R_{mt}} + \frac{V_{lv}}{C_{la} C_{lv}(t) R_{mt}} \quad \textbf{(3.11)}$$

$$\frac{dP_{sa}}{dt} = -\frac{P_{sa}}{C_{sa} R_{s}} + \frac{P_{ra}}{C_{sa} R_{s}} + \frac{Q_{lvad}}{C_{sa}} + \frac{V_{lv}}{C_{sa} C_{lv}(t) R_{av}} - \frac{P_{sa}}{C_{sa} R_{av}} \quad \textbf{(3.12)}$$

$$\frac{dP_{ra}}{dt} = \frac{P_{sa}}{C_{ra} R_{s}} - \frac{P_{ra}}{C_{ra} R_{s}} - \frac{P_{ra}}{C_{ra} R_{tv}} + \frac{V_{rv}}{C_{ra} C_{rv}(t) R_{tv}} \quad \textbf{(3.13)}$$

$$\frac{dV_{rv}}{dt} = \frac{P_{ra}}{R_{tv}} - \frac{V_{rv}}{C_{ra}C_{rv}(t)R_{tv}} - \frac{V_{rv}}{C_{rv}(t)R_{pv}} + \frac{P_{pa}}{R_{pv}} - Q_{rvad} \tag{3.14}$$

$$\frac{dP_{pa}}{dt} = \frac{P_{la}}{C_{pa}R_p} - \frac{P_{pa}}{C_{pa}R_p} + \frac{Q_{rvad}}{C_{pa}} + \frac{V_{rv}}{C_{pa}C_{rv}(t)R_{pv}} - \frac{P_{pa}}{C_{pa}R_{pv}} \tag{3.15}$$

$$\frac{dQ_{lvad}}{dt} = \frac{V_{lv}}{L_{lvad}C_{lv}(t)} - \frac{P_{sa}}{L_{lvad}} - \frac{R_{HVAD,L}Q_{lvad}}{L_{lvad}} - \frac{b_{HVAD}Q_{lvad}^{\ 2}}{L_{lvad}} + \frac{c_{HVAD}\omega_{lvad}^{\ 2}}{L_{lvad}} \tag{3.16}$$

$$\frac{dQ_{rvad}}{dt} = \frac{V_{rv}}{L_{rvad}C_{rv}(t)} - \frac{P_{pa}}{L_{rvad}} - \frac{R_{HVAD,R}Q_{rvad}}{L_{rvad}} - \frac{b_{HVAD}Q_{rvad}^{\ 2}}{L_{rvad}} + \frac{c_{HVAD}\omega_{rvad}^{\ 2}}{L_{rvad}} \tag{3.17}$$

where $R_{HVAD,L} = R_{can} + R_{suc} + a_{HVAD}$, $R_{HVAD,R} = R_{can} + R_{suc} + R_{banding} + a_{HVAD}$

The state equations were linearised and expressed in the general linear state-space equation as shown in Eqs. (3.18) and (3.19):

$$\begin{aligned}
\frac{dx_1}{dt} &= (\theta_{11} - \theta_{13})x_1 + \theta_{12}x_2 + \theta_{14}x_3 - x_7 \\
&\approx f(x_{1,0}, x_{2,0}, x_{3,0}, x_{7,0}) + (\theta_{11} - \theta_{13})(x_1 - x_{1,0}) + \theta_{12}(x_2 - x_{2,0}) + \theta_{14}(x_3 - x_{3,0}) - (x_7 - x_{7,0}) \\
&\approx (\theta_{11} - \theta_{13})x_1 + \theta_{12}x_2 + \theta_{14}x_3 - x_7 \\
\frac{dx_2}{dt} &= \theta_{21}x_1 - \left(\frac{1}{C_{la}R_p} + \theta_{22}\right)x_2 + \frac{1}{C_{la}R_p}x_6 \\
\frac{dx_3}{dt} &\approx \theta_{31}x_1 - \left(\frac{1}{C_{sa}R_s} + \theta_{32}\right)x_3 + \frac{1}{C_{sa}R_s}x_4 + \frac{1}{C_{sa}}x_7 \\
\frac{dx_4}{dt} &\approx \frac{1}{C_{ra}R_s}x_3 - \left(\frac{1}{C_{ra}R_s} + \theta_{41}\right)x_4 + \theta_{42}x_5 \\
\frac{dx_5}{dt} &\approx \theta_{51}x_4 + (\theta_{52} - \theta_{53})x_5 + \theta_{54}x_6 - x_8 \\
\frac{dx_6}{dt} &\approx \frac{1}{C_{pa}R_p}x_2 + \theta_{61}x_5 - \left(\frac{1}{C_{pa}R_p} + \theta_{62}\right)x_6 + \frac{1}{C_{pa}}x_8 \\
\frac{dx_7}{dt} &\approx \frac{1}{L_{lvad}C_{lv}}x_1 - \frac{1}{L_{lvad}}x_3 - \left(\frac{R_{HVAD,L}}{L_{lvad}} + \frac{2b_{HVAD}x_{7,0}}{L_{lvad}}\right)x_7 + \left(\frac{2c_{HVAD}\omega_{lvad,0}}{L_{lvad}}\right)\omega_{lvad} - \frac{b_{HVAD}x_{7,0}^{\ 2}}{L_{lvad}} + \frac{c_{HVAD}\omega_{lvad,0}^{\ 2}}{L_{lvad}} \\
\frac{dx_8}{dt} &\approx \frac{1}{L_{rvad}C_{rv}}x_5 - \frac{1}{L_{rvad}}x_6 - \left(\frac{R_{HVAD,R}}{L_{rvad}} + \frac{2b_{HVAD}x_{8,0}}{L_{rvad}}\right)x_8 + \frac{2c_{HVAD}\omega_{rvad,0}}{L_{rvad}}\omega_{rvad} - \frac{b_{HVAD}x_{8,0}^{\ 2}}{L_{rvad}} + \frac{c_{HVAD}\omega_{rvad,0}^{\ 2}}{L_{rvad}}
\end{aligned} \tag{3.18}$$

$$\frac{dx}{dt} = Ax' + Bu'$$

$$y = Cx$$

$$\frac{d}{dt}\begin{bmatrix} x_1 \\ x_2 \\ x_3 \\ x_4 \\ x_5 \\ x_6 \\ x_7 \\ x_8 \\ x_{7,0} \\ x_{8,0} \end{bmatrix} = \begin{bmatrix} \theta_{11}-\theta_{13} & \theta_{12} & \theta_{12} & 0 & 0 & 0 & -1 & 0 & 0 & 0 \\ \theta_{21} & -\frac{1}{C_{la}R_p}-\theta_{22} & \frac{1}{C_{la}R_p}-\theta_{22} & 0 & 0 & \frac{1}{C_{la}R_p} & 0 & 0 & 0 & 0 \\ \theta_{31} & 0 & 0 & \frac{1}{C_{ao}R_s} & 0 & 0 & \frac{1}{C_{ao}} & 0 & 0 & 0 \\ 0 & 0 & 0 & -\frac{1}{C_{ra}R_s}-\theta_{41} & \theta_{42} & 0 & 0 & 0 & 0 & 0 \\ 0 & 0 & 0 & \theta_{51} & \theta_{52}-\theta_{53} & \theta_{54} & 0 & -1 & 0 & 0 \\ 0 & \frac{1}{C_{pa}R_p} & \frac{1}{C_{pa}R_p} & 0 & \theta_{61} & -\frac{1}{C_{pa}R_p}-\theta_{62} & 0 & \frac{1}{C_{pa}} & 0 & 0 \\ \frac{1}{L_{lvad}C_{lv}} & 0 & -\frac{1}{L_{lvad}} & 0 & 0 & 0 & -\frac{R_{lvad}}{L_{lvad}}-\frac{2b_{HVAD}x_{7,0}}{L_{lvad}} & 0 & \frac{b_{HVAD}x_{7,0}}{L_{lvad}} & 0 \\ 0 & 0 & 0 & 0 & \frac{1}{L_{rvad}C_{rv}} & -\frac{1}{L_{rvad}} & 0 & -\frac{R_{rvad}}{L_{rv}}-\frac{2b_{HVAD}x_{8,0}}{L_{rvad}} & 0 & \frac{b_{HVAD}x_{8,0}}{L_{rvad}} \\ 0 & 0 & 0 & 0 & 0 & 0 & 0 & 0 & 0 & 0 \\ 0 & 0 & 0 & 0 & 0 & 0 & 0 & 0 & 0 & 0 \end{bmatrix}\begin{bmatrix} x_1 \\ x_2 \\ x_3 \\ x_4 \\ x_5 \\ x_6 \\ x_7 \\ x_8 \\ x_{7,0} \\ x_{8,0} \end{bmatrix} + \begin{bmatrix} 0 & 0 & 0 & 0 \\ 0 & 0 & 0 & 0 \\ 0 & 0 & 0 & 0 \\ 0 & 0 & 0 & 0 \\ 0 & 0 & 0 & 0 \\ 0 & 0 & 0 & 0 \\ \frac{2c_{HVAD}u_{lvad,0}}{L_{lvad}} & 0 & -\frac{c_{HVAD}u_{lvad,0}}{L_{lvad}} & 0 \\ 0 & \frac{2c_{HVAD}u_{rvad,0}}{L_{rvad}} & 0 & -\frac{c_{HVAD}u_{rvad,0}}{L_{rvad}} \\ 0 & 0 & 0 & 0 \\ 0 & 0 & 0 & 0 \end{bmatrix}\begin{bmatrix} u_{lvad} \\ u_{rvad} \\ u_{lvad,0} \\ u_{rvad,0} \end{bmatrix}$$

$$\theta_{11}\begin{cases} -\frac{1}{C_{lv}R_{mt}} & \text{if } x_2 > \frac{x_1}{C_{lv}} \\ 0 & \text{else} \end{cases}; \quad \theta_{12}\begin{cases} \frac{1}{R_{mt}} & \text{if } x_2 > \frac{x_1}{C_{lv}} \\ 0 & \text{else} \end{cases}; \quad \theta_{21}\begin{cases} \frac{1}{C_{la}C_{lv}R_{mt}} & \text{if } x_2 > \frac{x_1}{C_{lv}} \\ 0 & \text{else} \end{cases}; \quad \theta_{22}\begin{cases} \frac{1}{C_{la}R_{mt}} & \text{if } x_2 > \frac{x_1}{C_{lv}} \\ 0 & \text{else} \end{cases}$$

$$\theta_{13}\begin{cases} \frac{1}{C_{lv}R_{av}} & \text{if } \frac{x_1}{C_{lv}} > x_3 \\ 0 & \text{else} \end{cases}; \quad \theta_{14}\begin{cases} \frac{1}{R_{av}} & \text{if } \frac{x_1}{C_{lv}} > x_3 \\ 0 & \text{else} \end{cases}; \quad \theta_{31}\begin{cases} \frac{1}{C_{ao}C_{lv}R_{av}} & \text{if } \frac{x_1}{C_{lv}} > x_3 \\ 0 & \text{else} \end{cases}; \quad \theta_{32}\begin{cases} \frac{1}{C_{ao}R_{av}} & \text{if } \frac{x_1}{C_{lv}} > x_3 \\ 0 & \text{else} \end{cases}$$

$$\theta_{41}\begin{cases} \frac{1}{C_{ra}R_{tv}} & \text{if } x_4 > \frac{x_5}{C_{rv}} \\ 0 & \text{else} \end{cases}; \quad \theta_{42}\begin{cases} \frac{1}{C_{ra}C_{rv}R_{tv}} & \text{if } x_4 > \frac{x_5}{C_{rv}} \\ 0 & \text{else} \end{cases}; \quad \theta_{21}\begin{cases} \frac{1}{R_{tv}} & \text{if } x_4 > \frac{x_5}{C_{rv}} \\ 0 & \text{else} \end{cases}; \quad \theta_{22}\begin{cases} -\frac{1}{C_{rv}R_{tv}} & \text{if } x_4 > \frac{x_5}{C_{rv}} \\ 0 & \text{else} \end{cases}$$

$$\theta_{11}\begin{cases} \frac{1}{C_{rv}R_{pv}} & \text{if } \frac{x_5}{C_{rv}} > x_6 \\ 0 & \text{else} \end{cases}; \quad \theta_{12}\begin{cases} \frac{1}{R_{pv}} & \text{if } \frac{x_5}{C_{rv}} > x_6 \\ 0 & \text{else} \end{cases}; \quad \theta_{21}\begin{cases} \frac{1}{C_{pa}C_{rv}R_{pv}} & \text{if } \frac{x_5}{C_{rv}} > x_6 \\ 0 & \text{else} \end{cases}; \quad \theta_{22}\begin{cases} \frac{1}{C_{ps}R_{pv}} & \text{if } \frac{x_5}{C_{rv}} > x_6 \\ 0 & \text{else} \end{cases}$$

(3.19)

where x, u, and y were vector of state variables, vector of input variables, and vector of output variables, respectively. The input vector contains left and right pump speeds, ω_{lvad} and ω_{rvad}. A, B, and C were the state matrix, input matrix, and output matrix, respectively. θ is state coefficient that is dependent on valve opening and closing.

Table 3.1: State variables of the simplified state-space model of CVS-BiVAD system.

State variables	Descriptions	Symbols
x_1	Left ventricular volume	V_{lv}
x_2	Left atrial pressure	P_{la}
x_3	Systemic arterial pressure	P_{sa}
x_4	Right atrial pressure	P_{ra}
x_5	Right ventricular volume	V_{rv}
x_6	Pulmonary arterial pressure	P_{pa}
x_7	LVAD flow rate	Q_{lvad}
x_8	RVAD flow rate	Q_{rvad}

3.2.2 Parameter estimation

Initially, all model parameter values were adopted from the literature (Simaan et al., Lim et al., Nadeem et al.). The model parameters used in the thesis are presented in Table A.1 of Appendix A. Sensitivity analysis was performed to investigate the effect of each model parameter on the key haemodynamic variables. The value of each model parameter was doubled one at a time, while other model parameters remained unchanged. From the outcome of the sensitivity analysis, only a few model parameters were selected to be

optimised to obtain the target baseline mean haemodynamic variables based on published literature for the healthy state. The selection of model parameters to be optimised was also based on the understanding of the model. $E_{max,lv}$, $E_{max,rv}$, R_s, R_p, and HR were not optimised for these parameters were expected to change under different clinical scenarios (e.g. healthy, heart failure, and changes in physical activities). Among all model parameters, $E_{min,lv}$, $E_{min,rv}$, C_{la}, and C_{ra} had the greatest influence on mean cardiac output (CO), systemic arterial pressure (SAP), pulmonary arterial pressure (PAP), left atrial pressure (LAP), and right atrial pressure (RAP), thus they were optimised using the nonlinear least-squares-parameter estimation algorithm (specifically: the "fminsearch" function in MATLAB) to satisfy the following objective function, F:

$$F = \sum_{i=1}^{5} \frac{1}{y_{ref,i}} \left(y_{\mathrm{m},i} - y_{ref,i} \right)^2 \tag{3.20}$$

where $y_{ref,i}$ is the i^{th} published healthy mean haemodynamic variables as listed in Table 3.3 and y_m is the i^{th} simulated healthy mean haemodynamic variables. If the optimised model parameters could not give satisfying range of reference mean haemodynamic variables, model parameters would be optimised manually using the outcome of the sensitivity analysis as guidance.

3.2.3 Simulation protocol

All model parameter values and the initial state values of the healthy heart scenario, heart-failure-pre-BiVAD-insertion scenario, and heart-failure-post-BiVAD-insertion scenario are listed in Tables A.2 in Appendix A. Healthy heart, heart-failure-pre-BiVAD-insertion, and heart-failure-post-BiVAD-insertion were simulated in the state-space model. The effects of preload, afterload, left pump speed, and right pump speed on steady-state mean haemodynamic variables of heart-failure-post-BiVAD-insertion were

simulated and the model-simulated results were compared with the published results (Nadeem et al., 2015).

3.3 Results

The results section includes the HQ fitting of the simplified hydraulic model of HVAD pumps as well as the comparison of the haemodynamic variable responses to changes in PVR, SVR, LVAD speed, and RVAD speed between the simplified model and the results published in the literature (Stevens, Wilson, Bradley, Fraser, & Timms,, 2014; Nadeem et al., 2015).

3.3.1 Hydraulic model of HVAD pump

Table 3.2 shows the model parameters of HVAD pump (HeartWare International Inc, Framingham, MA) fitted with experimental data.

Table 3.2: Model parameters of HVAD pump.

	a_{HVAD} (mmHg·s^2/mL^2)	b_{HVAD} (mmHg·s/mL)	c_{HVAD} (mmHg)
Values	-0.18	-0.0017	1.5×10^{-5}

Figure 3.2 depicts the graphical comparison between the modelled and experimental extracted HQ relationships of the HVAD pump. The HQ curves of the HVAD pump model fitted at a coefficient of determination (R^2) of 0.97 as shown in Figure 3.3. Although offsets were observed, the HQ curvature and the total pressure drop with respect to the changes in pump flow rate (from minimum to maximum) of the modelled results were comparable to the experimental data. Negative pump differential pressure would not occur in a VAD patient, as this requires the left atrial pressure (near to pump inlet

pressure) to be greater than systemic arterial pressure (near to pump output pressure). Therefore, although the HQ relationship of the pump (simplified model) shows that negative pressure occurred at very high pump flow rate and low pump speed, this operating region is not within our interest as it does not occur in a VAD patient.

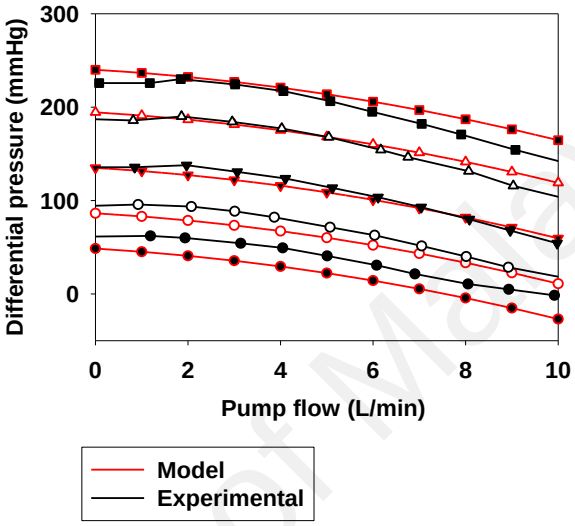

Figure 3.2: Comparison of the modelled and the experimental differential pressure-flow (HQ) relationship of HVAD pump. Round-filled, 1800 rpm; round-empty, 2400 rpm; triangle-filled, 3000 rpm; triangle-empty, 3600 rpm; square-filled, 4000 rpm. Model: The simulated results using Eq. (3.7), Experimental: published data.

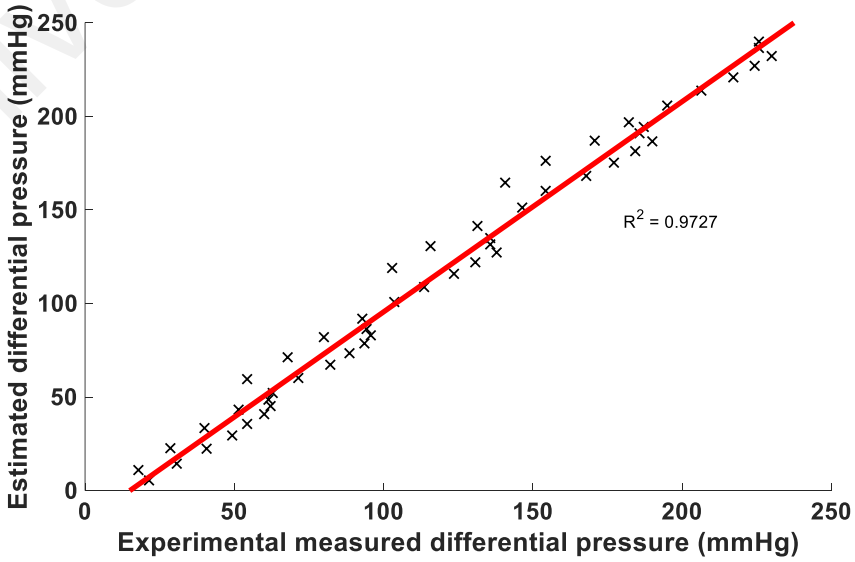

Figure 3.3: Comparison between the estimated differential pressure and the experimental measured differential pressure of HVAD pump.

3.3.2 Steady-state hemodynamic analysis

When LVAD speed was set to be equal to RVAD speed at 2400 rpm, the total mean outflow rate for both the systemic and pulmonary circulations were 5.2 L/min. When LVAD was operated at 2400 rpm, total support was given to left ventricle; aortic valve flow rate was zero. On the other hand, when RVAD was operated at 2400 rpm, partial assist was given to right ventricle; the mean pulmonary valve flow rate was 0.57 L/min. The reason that RVAD was not providing a full assist to the right ventricular was due to small banding diameter at the outflow cannula that limited the outflow rate through RVAD. Increasing the banding diameter or increasing the RVAD speed above 2400 rpm or both can provide a full assist to the right ventricle.

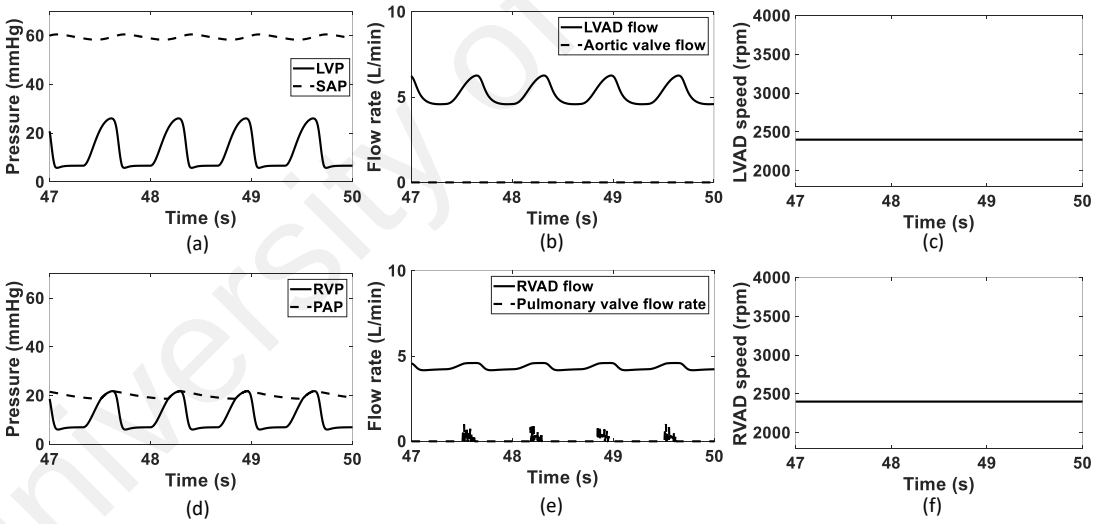

Figure 3.4: Steady-state hemodynamic variables at constant LVAD and RVAD speed setting. LVAD: left ventricular assist device, RVAD: right ventricular assist device, LVP: left ventricular pressure, SAP: systemic arterial pressure, RVP: right ventricular pressure, PAP: pulmonary arterial pressure.

3.3.3 Model comparison

The simulated baseline mean haemodynamic variables for the healthy heart were within the range of results recorded in the literature (listed in Table 3.3). Simulated mean CO, LAP, SAP, PAP, and RAP were at 5.6 L/min, 12.0 mmHg, 81.6 mmHg, 17.6 mmHg,

and 5.4 mmHg, respectively. In the heart-failure-pre-BiVAD-insertion scenario, the simulated mean CO, LAP, SAP, PAP, RAP, SVR, and PVR were at 3.7 L/min, 17.4 mmHg, 68.0 mmHg, 26.7 mmHg, and 10.3 mmHg, respectively. Like the published results, when comparing the heart-failure-pre-BiVAD-insertion scenario to the healthy heart, mean CO and SAP were lower in the heart failure scenario whereas LAP, RAP, and PAP were higher in the heart failure scenario. CO is lower in heart failure as compared to healthy heart due to the reduced cardiac contractility. SAP also decreased with decreasing CO. LAP and RAP increased because of the reduced cardiac contractility – blood built up in the heart chambers. To simulate pulmonary congestion, which is commonly occurred in heart failure patients, PVR was increased. Increasing PVR led to an increase in PAP.

Table 3.3: Model-Simulated haemodynamic variables for healthy heart and heart-failure pre-BiVAD-insertion scenario.

Mean haemodynamic variables	**Healthy heart**		**Heart-failure-pre-BiVAD-insertion**	
	Simplified model	Literature (Wolks et al., 2016, Kovacs et al., 2009, Guyton & Hall, 2006)	Simplified model	Literature (Nadeem et al., 2015)
LAP (mmHg)	12.0	7-13	17.4	21.9
SAP (mmHg)	81.6	80-85	68.0	72
PAP (mmHg)	17.6	12-19	26.7	31.1
RAP (mmHg)	5.4	4-6	10.3	15.7
CO (L/min)	5.6	4.2-6	3.7	3.6
SVR (dynes s/cm^{-5})	1100	1200-1300	1238	

PVR (dynes s/cm^{-5})	80	80-100	200

LAP, left atrial pressure; SAP, systemic arterial pressure; PAP, pulmonary arterial pressure; RAP, right atrial pressure; CO, cardiac output; LVAD, left ventricular assist device; RVAD, right ventricular assist device; BiVAD, biventricular assist device; SVR, systemic vascular resistance; PVR, pulmonary vascular resistance.

Table 3.4 compares the simulated mean haemodynamic variables of heart-failure-post-BiVAD-insertion in two scenarios: with and without right outflow diameter banding at 5 mm with three studies from the literature (*in silico*, *in vitro*, and *in vivo*). With the rightoutflow cannula banded, simulated mean CO, mean SAP, mean PAP, and mean LAP were lower when compared with the scenario where right outflow cannula was not banded. Conversely, mean RAP was higher when the right outflow cannula was banded when compared with the scenario where the right outflow cannula was not banded. The addition of banding on the right outflow cannula restricted the RVAD flow rate, thus mean CO was reduced. This subsequently led to the reduction in mean PAP and SAP. Apart from that, a more balanced left-right atrial pressure (i.e. smaller left-right atrial pressure difference) was observed when banding was added on the right outflow cannula. The difference between the model-simulated results with and without right outflow cannula banded was comparable to the results shown in the *in vitro* experimental results (Stevens, Wilson, Bradley, Fraser, & Timms,, 2014), as well as the complex numerical model (Nadeem et al., 2015). The model-simulated results (with right outflow cannula banded) also closely matched the *in vivo* experimental results (with right outflow cannula banded).

Table 3.4: Model-Simulated haemodynamic variables of heart-failure-post-BiVAD-insertion scenario. The pumps were operated at the constant speed mode, with LVAD and RVAD operated at the same speed in two scenarios: 1) with and 2) without RVAD outflow banding.

Mean haemodynamic variables	**Simulation**		**Literature**					
	Simplified model		*In silico* (Nadeem et al., 2015)		*In vitro* (Stevens, Wilson, Bradley, Fraser, & Timms,, 2014)		*In vivo* (Stevens, Wilson, Bradley, Fraser, & Timms,, 2014)	
	Without banding	Banding	Without banding	Banding	Without banding	Banding	Without banding	Banding
LAP (mmHg)	21.8	9.2	31.2	13.0	48.9	18.2	9	8
SAP (mmHg)	96.7	73.4	95.2	89.3	111.9	104.9	83	81
PAP (mmHg)	37.3	20.0	46.7	26.7	N/A	N/A	18	17
RAP (mmHg)	1.2	6.3	0.5	5.9	N/A	N/A	N/A	N/A
CO (L/min)	6.2	4.3	6.1	5.4	6.7	6	6	6
LVAD speed (rpm)	2400	2400	2400	2400	2400	2400	2300	2300
RVAD speed (rpm)	2400	2400	2400	2400	2400	2400	2300	2300
Banding diameter (mm)	-	5	-	5	-	6.5	-	8.1

SVR (dynes s cm^{-5})	1237.5	1237.5	1200	Not provided
PVR (dynes s cm^{-5})	200	200	100	514

LAP, left atrial pressure; SAP, systemic arterial pressure; PAP, pulmonary arterial pressure; RAP, right atrial pressure; CO, cardiac output; LVAD, left ventricular assist device; RVAD, right ventricular assist device; BiVAD, biventricular assist device; SVR, systemic vascular resistance; PVR, pulmonary vascular resistance.

Figure 3.5 shows that increasing PVR decreased total right outflow rate (pulmonary valve flow rate and RVAD flow rate), which in turn decreased LAP, SAP, and CO. On the other hand, RAP was increased because of the decreased total right outflow rate. PAP increased with increasing PVR. Figures 3.5(a)-3.5(c) show that the trends of SAP (gradient: -0.01 mmHg dynes^{-1} s^{-1} cm^{-5}), PAP (gradient: 0.03 mmHg dynes^{-1} s^{-1} cm^{-5}), and CO (gradient: -0.001 L min^{-1} dynes^{-1} s^{-1} cm^{-5}) of the model-simulated results were comparable to the literature (Nadeem et al., 2015). The model-simulated SAP, PAP, and CO had an average offset of -20 mmHg, -5.5 mmHg, and -0.8 L/min respectively, from the literature. Figures 3.5(d) and 3.5(e) show that there was a small difference between the trend of model-simulated LAP and RAP from the literature; the difference in LAP and RAP gradients were -0.02 mmHg dynes^{-1} s^{-1} cm^{-5} and 6×10^{-3} mmHg dynes^{-1} s^{-1} cm^{-5}, respectively.

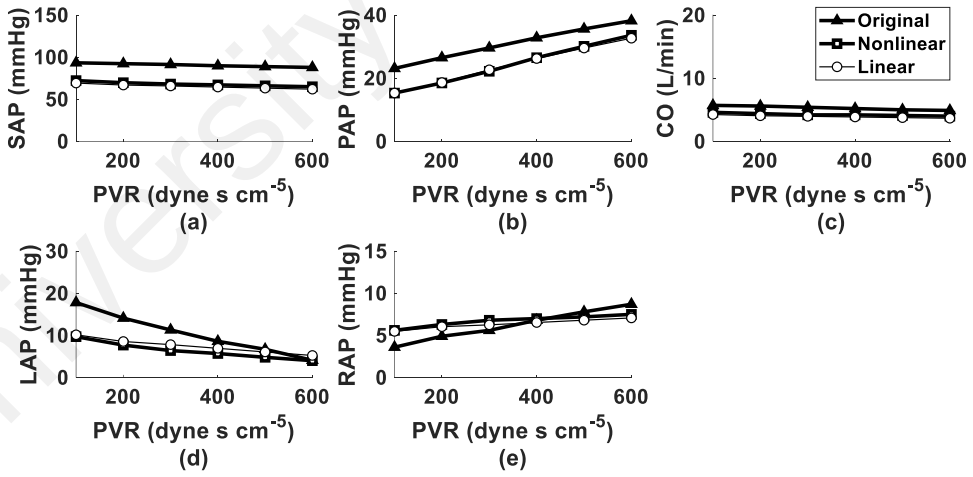

Figure 3.5: Comparison of simulated mean hemodynamic variables with *in silico* published data (Nadeem et al., 2015) at various PVR levels. PVR, pulmonary vascular resistance; SAP, systemic arterial pressure; PAP, pulmonary arterial pressure; CO, cardiac output; LAP, left atrial pressure; RAP, right atrial pressure. The diameter of the right outflow cannula was restricted to 5 mm in both the simplified models and the original model.

Figure 3.6 shows that increasing SVR decreased total left outflow rate (aortic valve flow rate and LVAD flow rate), which in turn decreased RAP and CO. On the other hand,

LAP was increased because of the decreased total left outflow rate. Both SAP and PAP increased with increasing SVR. Figures 3.6(a), (c) and (e) show that the trend of SAP (gradient: 0.03 mmHg dynes^{-1} s^{-1} cm^{-5}), CO (gradient: 0.001 L min^{-1} dynes^{-1} s^{-1} cm^{-5}), and RAP (gradient: -4×10^{-3} mmHg dynes^{-1} s^{-1} cm^{-5}) between the model-simulated results and the literature were the same. The model-simulated SAP, CO, and RAP had an average offset of -16 mmHg, -0.8 L/min, and -0.5 mmHg, respectively, from the literature. Figures 3.4(b) and 3.4(d) show that there was a knee-point (i.e. change in gradient of slope) in the slope of the model-simulated PAP and LAP curves at SVR=1200 dynes s cm^{-5}, but there was no knee-point observed in the literature. The knee-point in the slope indicates that there was partial assist of LVAD at SVR lower than 1200dynes s cm^{-5} and full assist of LVAD at SVR greater than 1200 dynes s cm^{-5}. In partial assist mode, total flow rate is contributed by valve flow rate and pump flow rate, whereas, in full assist mode, total flow rate is contributed by pump flow rate only. During partial assist of a BiVAD, the trend of PAP (gradient: 4×10^{-4} mmHg dynes^{-1} s^{-1} cm^{-5}) and LAP (gradient: 4×10^{-3} mmHg dynes^{-1} s^{-1} cm^{-5}) between the model-simulated results and literature were the same. During full assist of a BiVAD, the slope in PAP (gradient: 0.01 mmHg dynes^{-1} s^{-1} cm^{-5}) and LAP (gradient: 0.01 mmHg dynes^{-1} s^{-1} cm^{-5}) became steeper than during aortic-valve-opening in the model-simulated results.

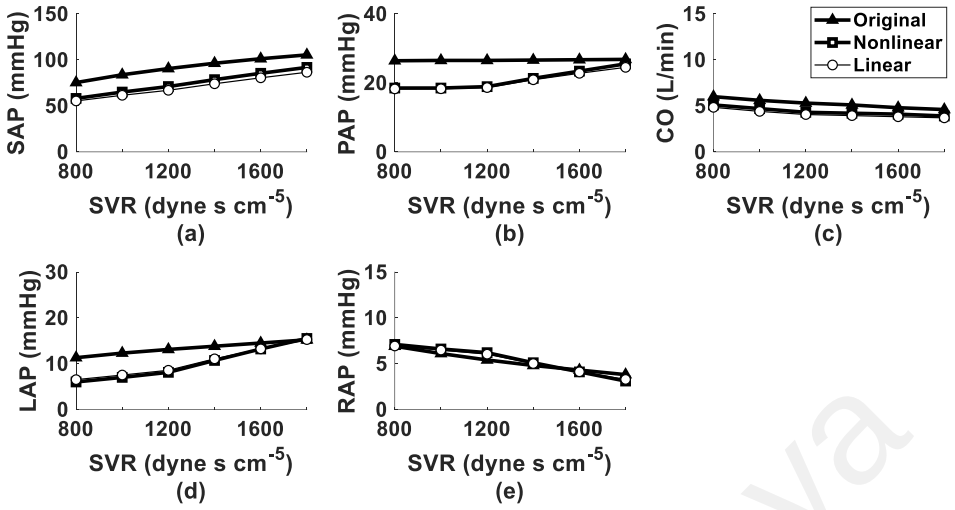

Figure 3.6: Comparison of simulated mean hemodynamic variables with *in silico* published data (Nadeem et al., 2015) at various SVR levels. SVR, systemic vascular resistance; SAP, systemic arterial pressure; PAP, pulmonary arterial pressure; CO, cardiac output; LAP, left atrial pressure; RAP, right atrial pressure. The diameter of the right outflow cannula was restricted to 5 mm in both the simplified models and the original model.

Figure 3.7 shows that increasing LVAD speed increased LVAD flow rate, which in turn increased CO and RAP. On the other hand, LAP decreased because of the increased mean LVAD flow rate. PAP also decreased with decreasing LAP as Figures 3.7(a) and (c) show similar trends. RVAD flow was increased indirectly because of the decrease in right pump differential pressure (i.e. difference between PAP and RAP). Figures 3.7(a) and (c) show that the cut-off speed between the partial assist and the full assist of LVAD was recorded at 2400 rpm in the simplified model. There was no defining knee-point in the changes in LAP and PAP with increasing LVAD speed recorded in the literature.

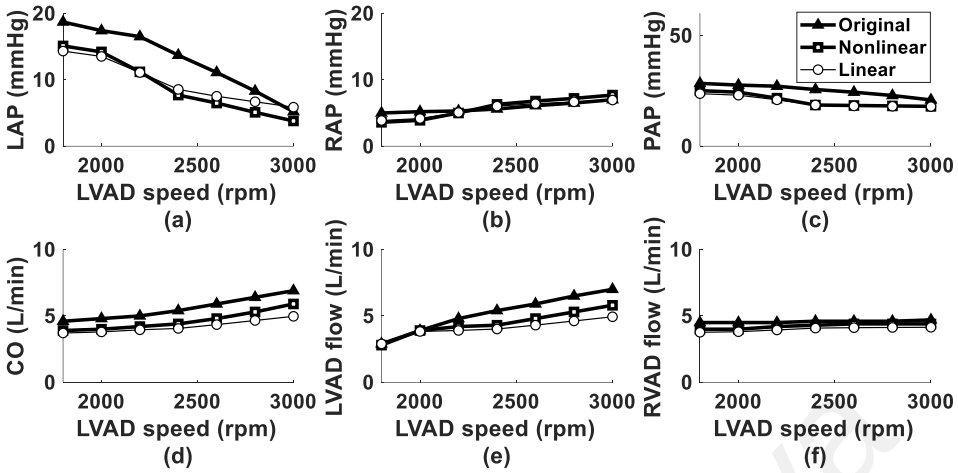

Figure 3.7: Comparison of simulated mean hemodynamic variables with *in silico* published data (Nadeem et al., 2015) at various left ventricular assist device (LVAD) speeds. SAP, systemic arterial pressure; PAP, pulmonary arterial pressure; CO, cardiac output; LAP, left atrial pressure; RAP, right atrial pressure. The diameter of the right outflow cannula was restricted to 5 mm in both the simplified models and the original model.

Figure 3.8 shows that increasing RVAD speed increased mean RVAD flow rate, which in turn increased mean CO and mean LAP. On the other hand, mean RAP decreased because of the increased mean RVAD flow rate. Mean PAP also increased with increasing LAP as Figures 3.8(a) and (c) show similar trendline. LVAD flow was increased indirectly because of the decrease in left pump differential pressure (i.e. difference between SAP and LAP). The knee-point recorded in the simplified model Figures 3.8(a) and (c) show that RVAD speed at 2400 rpm was the cut-off speed between the partial assist and the full assist of RVAD in the simplified model whereas the cut-off speed between the partial assist and the full assist of RVAD was identified at 2800 rpm in the literature.

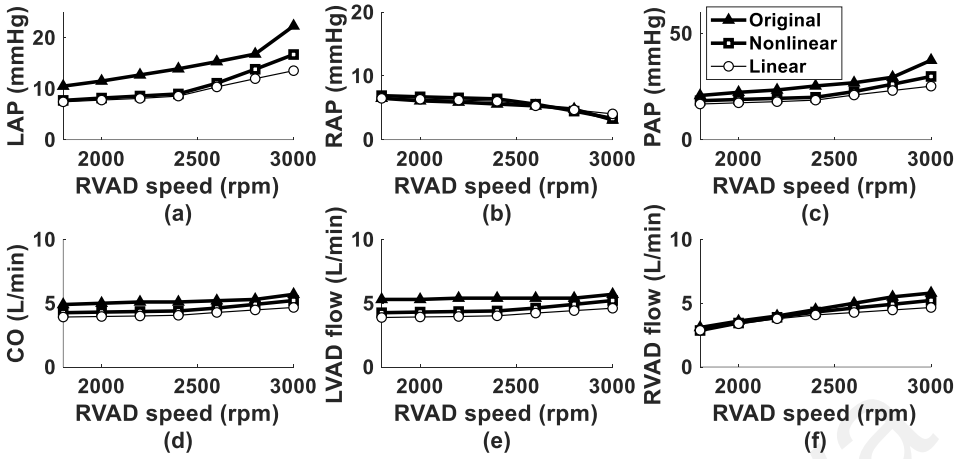

Figure 3.8: Comparison of simulated mean hemodynamic variables with *in silico* published data (Nadeem et al., 2015) at various right ventricular assist device (RVAD) speeds. SAP, systemic arterial pressure; PAP, pulmonary arterial pressure; CO, cardiac output; LAP, left atrial pressure; RAP, right atrial pressure. The diameter of the right outflow cannula was restricted to 5 mm in both linear simplified models and the original model.

3.4 Discussion

The present study presents the very first study on a simplified state-space form of the CVS-BiVAD interaction. The predecessor model of CVS-BiVAD interaction that was developed (Nadeem et al., 2015) is a highly complex model for it consists of multiple branches of vasculatures in the circulations (i.e. expanded arteries, capillaries, and veins), many time-varying terms (i.e. the elastance functions of atria and ventricles) and several non-linear terms (i.e. valve flow rate, banding resistance, suction resistance, etc.). Herein, the complex CVS-BiVAD has been simplified into a state-space model that is fit-for-purpose for the development of a model-based control scheme. As model simplification often comes at a cost of reduced model fidelity, careful selection of model parameters, accompanied by multiple routines of cross-comparison with the published data provided by clinical studies or textbook (Guyton & Hall, 2006), *in vivo* studies (Stevens, Wilson, Bradley, Fraser, & Timms,, 2014), *in vitro* studies (Stevens, Wilson, Bradley, Fraser, &

Timms,, 2014), as well as the original complex model (Nadeem et al., 2015), were conducted.

Similar model simplification and comparison methods were used by (Simaan et al., 2009) for the development of a physiological control of an LVAD. In the study, the complex CVS model was simplified to focus only on the interaction of an LVAD with the left heart and the systemic circulation; the right heart and pulmonary circulation were assumed to be healthy and therefore their effects on LVAD could be neglected. Similarly, in our simplified model, the effects of the extended vasculatures in both systemic and pulmonary circulations of the complex model on BiVAD were neglected. Model comparison was performed by superimposing the model-simulated results with available experimental results. While Simaan's simplified model has contributed to the development of an LVAD control, the simplified model of CVS-BiVAD model will also contribute to the development of a BiVAD control in the next chapters.

In the present study, RVAD speed was set at the same value as LVAD speed in the constant speed mode, with the option of a banded RVAD outflow cannula and non-banded RVAD outflow cannula, as was the pump operating modes of dual LVADs as a BiVAD used in previous studies (Stevens, Wilson, Bradley, Fraser, & Timms,, 2014; Strueber et al., 2010). The first option is to operate the RVAD at a lower speed than the LVAD. The second option is to operate both LVAD and RVAD at the same speed. The third option is to operate both the LVAD and the RVAD at the same speed, with RVAD outflow cannula banded. The second and third options were evaluated in the simplified state-space model. As PVR is much lower than SVR, operating the RVAD at the same pump speed as the LVAD would result in over-pumping of the RVAD, which subsequently led to risk of right ventricular suction (i.e. mean atrial pressure < 3 mmHg) and pulmonary congestion (i.e. mean atrial pressure > 20 mmHg). The safety limit of

mean atrial pressure was chosen between 3-20 mmHg in accordance with a suggestion given by Adj. Clin. Assoc. Prof. Robert Salamonsen, The Alfred Hospital, Melbourne. All model-simulated mean haemodynamic variables were all within acceptably safe limits at moderate values of PVR, SVR, LVAD speed and RVAD speed. To overcome risks of over-pumping of the RVAD for different patient scenarios, we could either fix the pump speeds and adjust the right outflow banding diameter or fix the right outflow banding diameter and adjust both pump speeds accordingly. The former option was used in the *in vitro* and *in vivo* experimental studies listed in Table 3.4, where appropriate banding diameter was selected to meet the healthy haemodynamic variables (Guyton & Hall, 2006). Adjusting banding diameter requires reoperation unless a restriction adjustable device, such as the FlowWatch PAB (Corno et al., 2004), was used. The latter option was evaluated in the complex numerical model (Nadeem et al., 2015). The 5 mm banding diameter was chosen so that both pumps could operate at the mid-range speed, to provide enough leeway for the alteration of both pump speeds, especially when an automatic physiological control system was to be implemented for dual LVADs. In addition, the 5 mm right outflow cannula banding diameter was also recommended in previous clinical cases (Hetzer, Krabatsch, Stepanenko, Hennig, & Potapov, 2010; Loforte, Montalto, Monica, Contento, & Musumeci, 2010). In the present simplified model, results showed that the model could reproduce steady-state mean haemodynamic variables at the evaluated pump operating modes.

The knee point indicates the transition from partial assist to full assist. There was no cutoff speed in varying SVR in the literature because the pumps were operated in full assist across all SVR ranges. The reason that there is difference in knee point between the simplified model and the literature data is that the two are not identical models. The difference in the cardiac elastance function, vascular compliance, and the complexity and

the simplicity of the models contributed to the difference in knee points. Nonetheless, the ability to simulate the presence of knee point that indicates the transition of partial assist and full assist shows that the simplified model has successfully characterised the behaviour of CVS-BiVAD interaction. The potential implication of this difference may affect the control performance of CMO-MPC due to the model mismatch. However, this problem can be resolved by updating the model-mismatch error in each iteration of the computation of the CMO-MPC algorithm.

Although the deviation (i.e. the offset between the simplified model and the original model as well as the literature) is more than 20% for some variables (e.g. PAP), the overall trend of the changes in all hemodynamic variables with changes in PVR, SVR, LVAD speed, RVAD speed were comparable between the simplified model and the original model (Figures 3.5 – 3.8). Human cardiovascular system is a highly complicated system (from the heart to the small vessel branches with different material properties) and vary from individuals to individuals due to differences in cardiac contractility, systemic vascular resistance, total blood volume, heart rate, etc. As a result, there is no one perfect model which could capture the entire system accurately. To date, all models were created for its designated purpose. For example, the LAP may vary from 6 mmHg in a VAD patient to 25 mmHg in another. Due to the invasive nature of pressure/flow measurements, to date, there are very limited studies which reported hemodynamic measurements in actual patients or in vivo (animal experiments). Therefore, the values presented in Table 3.4 were from the very limited data published in the literature. Careful validation of the results presented in this work (both original and simplified model) were done throughout the PhD study, by regular discussions with Dr Robert Salamonsen (an experienced anaesthelogist from The Alfred Hospidal, Melbourne, who has over 30 years of experience with VAD patients). For the purpose of a simplified model to be used in

MPC, it is more important that the model could accurately capture the trend of hemodynamic variables changes with changes in the physiological conditions (e.g. PVR, SVR) and pump speeds. All results in Chapter 3 were benchmarked against the original model (Table 3.3. and Figures 3.5 – 3.8). The results in the following Chapters 4 and 5 verified that the model is good enough. If the CMO-MPC could successfully meet the control objectives without steady-state error, then the simplified model was considered fit-for-purpose. There are two ways to improve the model prediction: 1) to increase the number of elements to describe more of the characteristics of the CVS-BiVAD interactions but it requires more computational power as the model complexity increases and 2) to constantly update the model-mismatch error to the CMO-MPC algorithm.

Perturbation of PVR, SVR, LVAD speed, and RVAD speed was evaluated in the simplified state-space model to confirm its validity over a wide range of clinical scenarios as well as pump operating regions. Simulation results show that the simplified model can reproduce the trend of mean haemodynamic response with respect to changes in PVR, SVR, LVAD speed, and RVAD speed, although there was some offset that could not be further reduced due to the limitations of the number of model parameters available for optimisation. Model simplification and model accuracy are two competing factors in the development of any model. As the current model was developed for use as the internal model of the CMO-MPC for BiVAD, it did not have a baroreflex control mechanism that contributed to the regulation of heart rate, SVR, vessel compliance, during variation in physical activities. Furthermore, the nonlinearities of the vascular pressure-volume (PV) relationship were replaced with linear approximations.

3.5 Conclusion

In conclusion, the simplified model presented in this chapter demonstrated that the mean haemodynamic variables of the simplified model are comparable to the literature in different patient scenarios such as biventricular failure before and after BiVAD insertion. Furthermore, the simplified model demonstrated haemodynamic responses with respect to changes in PVR, SVR, LVAD speed, and RVAD speed that compared closely to the literature. Although there were offsets between the haemodynamic responses of the simplified model and the literature results, the ranges of haemodynamic variables remain bounded within the acceptable range – the limits of LAP, SAP, PAP, RAP, and CO are 3-20 mmHg, 65-105 mmHg, <40 mmHg, 3-20 mmHg, and > 4 L/min, respectively (personal correspondence with Adj. Clin. Assoc. Prof. Robert Salamonsen, The Alfred Hospital, Melbourne). The control performance of MPC relies on the internal model accuracy. Therefore, if the MPC ill-performs, improvements in internal model accuracy will be required and this might involve additional model parameters and components to the current simplified model. The next chapter describes how this simplified model was used in an MPC.

CHAPTER 4: A CENTRALISED MULTI-OBJECTIVE MODEL PREDICTIVE CONTROL FOR A BIVENTRICULAR ASSIST DEVICE: AN *IN SILICO* EVALUATION

The aim of this chapter was to develop a CMO-MPC for BiVAD that adjusted pump flow rate according to changes in metabolic demands while minimising risks of ventricular suction and vascular congestion. To meet the aim of the chapter, several objectives were devised as follows:

- To evaluate the process interactions between the feedback loops of left and right preloads as well as the feedback loops of left and right pump flow rate.
- To formulate three control objectives: i) to adjust pump flow rate according to FS mechanism, ii) to avoid ventricular suction, and iii) to avoid vascular congestion for the physiological control of BiVAD.
- To benchmark the control performance of the CMO-MPC against the CS controller and the PI-FS controller in both exercise and postural change scenarios in a numerical model.

4.1 Introduction

In Chapter 2, Gaddum et al. (2012) speculated the existence of process interactions between the feedback loops of several dual independent control of BiVAD. The presence of process interactions between feedback loops may lead to control instability. Therefore, the CMO-MPC has been proposed for BiVAD control because it can handle process interactions while two separate PI controllers cannot. In the beginning of this Chapter, the Bristol's Relative Gain Array (RGA) was performed to quantify the degree of process interaction between feedback loops, to verify the existence of process interaction between the feedback loops of BiVAD control. Next, the CMO-MPC algorithm was designed

using the simplified state-space model of CVS-BiVAD system that was developed in Chapter 3 as the internal model. Before the Chapter ends, the CMO-MPC was benchmarked against the PI-FS controller and the CS controller in exercise and postural change scenarios designed in the original model.

Part of the work completed in this chapter was published as the original article Koh, V. C. A., Ho, Y. K., Stevens, M. C., Ng, B. C., Salamonsen, R. F., Lovell, N. H., & Lim, E. (2019). A centralized multi-objective model predictive control for a biventricular assist device: An in silico evaluation. *Biomedical Signal Processing and Control, 49*, 137-148. The descriptions of methods, results, and discussion were directly adopted from the submitted original article, however the pump models were changed from HeartMate II (Abbott, Thoratec, Pleasanton, CA, USA) to HeartWare HVAD (Medtronic, HeartWare International, Inc., Framingham, MA). The HeartMate II pump was an axial flow pump whereas the HVAD pump was a centrifugal flow pump.

4.2 Methods

The methods section includes the process interaction analysis of the closed-loop CVS-BiVAD system, the description of the CMO-MPC algorithm, and the simulation protocol used for the control performance evaluation.

4.2.1 Process interaction analysis

For simplicity, the magnitudes of interactions in the CVS–BiVAD system were examined as separate two-input-two-output (TITO) systems (i.e. the pump speed–pump flow system and the pump speed–preload system). To study the degree of interactions of a TITO system, the RGA method was employed. Given the open loop gain between the output y_j and input u_i is $K_{ij} = \Delta y_j / \Delta u_i$, the RGA matrix is written as:

$$\mathbf{\Lambda} = \begin{bmatrix} \lambda & 1-\lambda \\ 1-\lambda & \lambda \end{bmatrix} \tag{4.1}$$

where $\lambda = K_{LL}\left[1 - K_{RL}K_{LR}/\left(K_{LL}K_{RR}\right)\right]$ with L and R referring to the left and right circulations, respectively. For a TITO system, λ can be interpreted as follows. If $0 < \lambda < 1$, the process interaction is the largest at $\lambda = 0.5$ (Seborg et al., 2010). If λ=1, there is no process interaction. If $\lambda > 1$, the intensity of the process interactions increases with λ.

The left and right pump speeds were the manipulated variables of the CVS-BiVAD system. The controlled variables could vary, depending on the control strategy. The process interactions between the feedback loops of left and right preloads, as well as the process interactions between the feedback loops of left and right pump flow rates were tested, as they were the common controlled variables used in the control of dual LVAD systems (Gaddum et al., 2012; Stevens et al., 2014). Average values were used to refer to values of manipulated and controlled variables described in the present study.

To calculate the open loop gains required for the RGA analysis, the operating pump speeds were divided into nine different operating regions because the CVS-BiVAD interaction is a nonlinear system. In doing so, the changes in degree of process interactions in smaller pump operating regions could be analysed. Simulations were performed using the original model of the CVS-BiVAD system of which the effect of pump speeds on mean haemodynamic variables was validated *in vivo* (Lim et al., 2010). The model includes the dynamics of time-varying elastance function that drives the cardiac contraction, nonlinear valve interactions, characteristic of suction, and hydraulic characteristic of pump and cannula (Lim et al., 2010). During each simulation, while one pump was subjected to step changes associated with pump speed, the other remained at a

constant speed at 2400 rpm. This was repeated until all the open loop gains had been recorded.

4.2.2 Centralised multi-objective model predictive control (CMO-MPC)

Figure 4.1 shows a schematic diagram of the CMO-MPC. The CMO-MPC consists of five main components: 1) the time and state varying internal model, 2) the setpoint definition, 3) the multi-objective cost function optimiser, 4) tuning parameters, and 5) constraints. The tuning parameters and constraints are user-defined parameters.

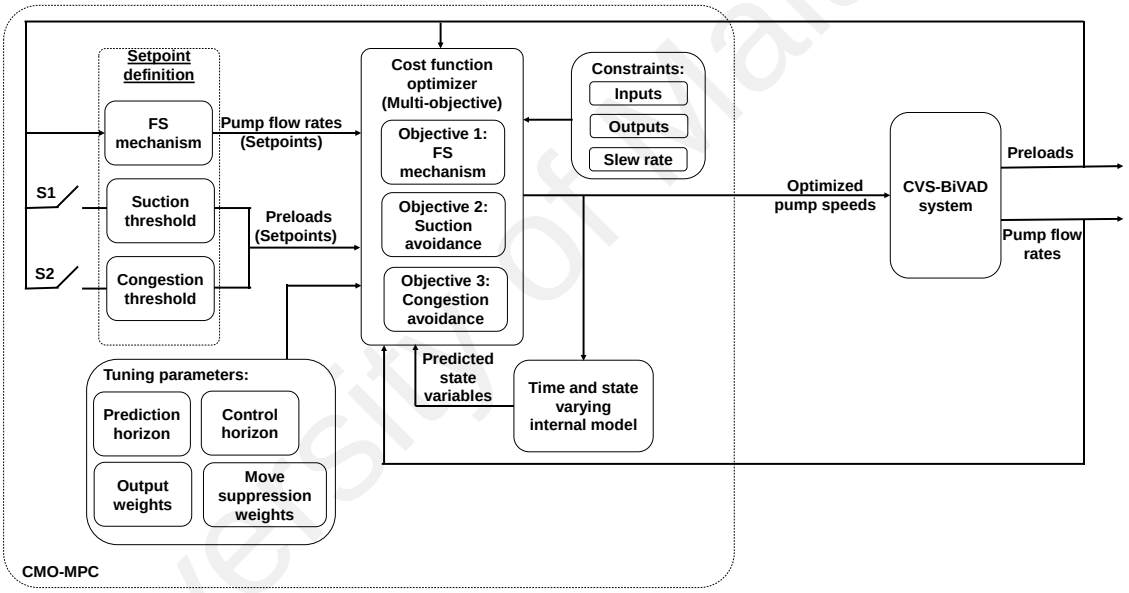

Figure 4.1: Schematic diagram of CMO-MPC. S1 turns on when preload falls below the suction threshold whereas S2 turns on when preload rises above congestion threshold. CMO-MPC, centralised multi-objective model predictive control; S1, switch 1; S2, switch 2.

4.2.2.1 General structure of the CMO-MPC algorithm

To employ the continuous time state-space model described in Chapter 3 as the internal model for the CMO-MPC, the model was discretised as follows:

$$
\begin{aligned}
x(k+1) &= A\big(k, x(k)\big)x(k) + Bu(k) \\
y(k) &= Cx(k)
\end{aligned}
\tag{4.2}
$$

where k is the current time step.

Having established the internal model for the CMO-MPC, here the general computation structure of the controller is presented. The main goal of the control algorithm is to compute the vector of optimised manipulated variables, $\boldsymbol{U}(k)$, that satisfies the pre-defined control objectives. Projecting Eq.(4.2) for several time steps ahead, the prediction equation is written as follows (Maciejowski, 2002):

$$
\begin{aligned}
&\hat{Y}(k+i) = \underbrace{\Psi(k)x(k) + \Upsilon(k)u(k-1)}_{past\ term\ (free\ response)} + \underbrace{\Theta(k)\Delta\hat{U}(k+j)}_{future\ term} \\
&for\ i = 1,\ 2, \ldots, H_p\ and\ j = 0,\ 1, \ldots, H_u - 1
\end{aligned}
\tag{4.3}
$$

where:

$$
\Psi(k) = \begin{bmatrix} A \\ \vdots \\ A^{H_u} \\ A^{H_u+1} \\ \vdots \\ A^{H_p} \end{bmatrix};\quad \Upsilon(k) \begin{bmatrix} B \\ \vdots \\ \sum_{i=0}^{H_u-1} A^i B \\ \sum_{i=0}^{H_u} A^i B \\ \vdots \\ \sum_{i=0}^{H_p-1} A^i B \end{bmatrix};\quad \Theta(k) = \begin{bmatrix} B & \cdots & 0 \\ \vdots & \cdots & 0 \\ \sum_{i=0}^{H_u-1} A^i B & \ddots & \vdots \\ \sum_{i=0}^{H_u} A^i B & \cdots & B \\ \vdots & \vdots & \vdots \\ \sum_{i=0}^{H_p-1} A^i B & \cdots & \sum_{i=0}^{H_p-H_u} A^i B \end{bmatrix}
\tag{4.4}
$$

Here, $\hat{Y}$, $\Delta\hat{U}$, and Θ are the vector of predicted controlled variables, vector of predicted slew rates, and the step response matrix, respectively. In addition, H_p and H_u are positive integers that represent the prediction horizon and control horizon, respectively. The sampling time used in the study is 0.1 s.

In the CMO-MPC, the foregoing prediction equation is used to formulate the cost function for the computation of the control law. Specifically, the control law accounts for the minimisation of tracking error (difference between the vector of predicted output and the vector of future reference trajectory) and slew rate in a quadratic weighted cost function:

$$J(k)=\sum_{i=1}^{H_p}\left\|\hat{Y}(k+i)-S(k+i)+e(k+i)\right\|_{Q_i}^2+\sum_{i=0}^{H_u-1}\left\|\Delta\hat{U}(k+i)\right\|_{R_i}^2 \qquad \textbf{(4.5)}$$

where ***S*** and ***e*** are the vector of future setpoints and the vector of plant-model mismatch, respectively, $Q_i = diag(q_1, q_2, q_3, ..., q_l)$ and $R_i = diag(r_1, r_2, r_3, ..., r_m)$ are the output weight matrix and the move suppression weight matrix, respectively. Here, *l* and *m* are the number of outputs and inputs, respectively.

To compute the optimised control moves with the consideration of the operating constraints, i.e. $y_{\min} < y < y_{\max}$, $u_{\min} < u < u_{\max}$, and $\Delta u_{\min} < \Delta u < \Delta u_{\max}$, a constrained minimisation of a modified cost function *J* is solved via the following quadratic programming (QP) problem:

$$\begin{aligned}&\min_{\Delta\hat{U}}\frac{1}{2}\Delta\hat{U}^T\Phi\Delta\hat{U}+\phi^T\Delta\hat{U}\\&subject\ to\\&\Omega\Delta\hat{U}\le\omega\end{aligned} \qquad \textbf{(4.6)}$$

where:

$$\Phi=\Theta^T Q\Theta+R \qquad \textbf{(4.7)}$$

$$\phi=-\Theta^T Q\left(S(k+i)-\left[\Psi x(k)+\Upsilon u(k-1)\right]-e(k+i)\right) \qquad \textbf{(4.8)}$$

Throughout this work, the manipulated variables (i.e pump speed) were constrained between 1500 and 4000 rpm, the slew rates were constrained within ±5 % of the operating range, the pump flow rates were constrained between 0 L/min and 10 L/min, the preloads were constrained between 3 mmHg and 18 mmHg. The other tuning parameters (i.e. $H_p = 10$, $H_u = 1$, and $R_i = \begin{bmatrix} 500 & 0 \\ 0 & 500 \end{bmatrix}$) were tuned empirically to give the best performance; the values remained constant throughout the evaluation. The best performance was chosen as the one that gave the fastest control responses at zero transient overshoot. Due to the receding horizon approach in predictive control, only the first move in the optimised solution is sent to the process, i.e. $U(k) = U(k-1) + \Delta\hat{U}(k)$. The full derivation of the generic MPC is presented in Appendix B.

4.2.2.2 Multi-objective control strategy

The general structure of the cost function in Eq. (4.5) was modified to accommodate multiple objectives. In the present study, four controlled variables, $Y(k) = [Q_{LVAD}; Q_{RVAD}; P_{la}; P_{ra}]$ and their corresponding future setpoints, $S(k) = [Q_{LVAD,ref}; Q_{RVAD,ref}; P_{la,ref}; P_{ra,ref}]$ were selected to satisfy three control objectives.

Objective 1: To maintain the Frank-Starling mechanism of the native heart

The first objective involves the control of the first two controlled variables (i.e. Q_{LVAD} and Q_{RVAD}). This objective was by default active, with unity weighting factors (i.e. q_1 and $q_2 = 1$). The future setpoints for the pump flow rates, $Q_{L/RVAD,ref}$, vary with the preloads, $P_{l/ra}$, according to the FS relationship defined in Eq. (4.9) as well as in Figure 4.2.

$$Q_{L/RVAD,ref} = \frac{K_1}{1+e^{-K_2(P_{l/ra}+K_3)}} \quad \textbf{(4.9)}$$

where K_1, K_2, and K_3 determine the upper limit, scaling, and shifting of the curves along the x-axis, respectively.

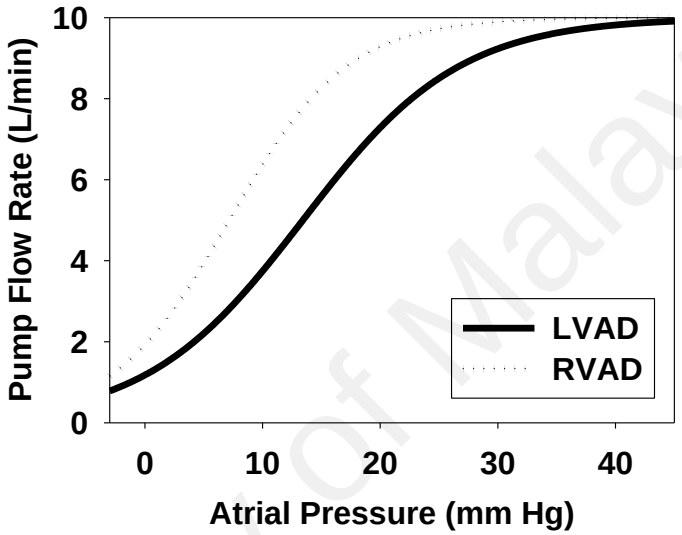

Figure 4.2: The Frank-Starling relationships that were used to define the setpoints for the flow rates of left ventricular assist device (LVAD) and right ventricular assist device (RVAD) according to their respective preloads.

Objective 2: To avoid ventricular suction

Mean atrial pressures (P_{la,suc_thres} and P_{ra,suc_thres}) were selected as the indicators for ventricular suction. The suction threshold was set at 3 mmHg. This was a marginal threshold used to prevent risk of ventricular suction from occurring. Real suction events may be anticipated if atrial pressure fell below 0 mmHg. Implementing this objective involved adjusting the weighting factors $q_{3/4}$, with the following logic Eq. (4.10)**.**

If $P_{l/ra} < P_{l/ra,suc\_threshold}$, then $q_{3/4} = q_{suc}\left|P_{l/ra,suc\_threshold} - P_{l/ra}\right|$. **(4.10)**

Here, q_{suc} is a tuning parameter that was empirically selected at 300.

Objective 3: To avoid pulmonary congestion

Mean atrial pressures ($P_{la,cong\_thres}$ and $P_{ra,cong\_thres}$) were selected as the indicators for vascular congestion. The congestion threshold was set at 18 mmHg. This was a marginal threshold used to prevent risks of vascular congestion from occurring. Real vascular congestion may be anticipated if mean atrial pressure rose above 20 mmHg. Implementing this objective involved adjusting the weighting factors $q_{3/4}$, with the following logic Eq. (4.11).

$$\text{If } P_{l/ra} > P_{l/ra,cong\_threshold}\text{, then } q_{3/4} = q_{cong}\left|P_{l/ra,cong\_threshold} - P_{l/ra}\right|. \quad \textbf{(4.11)}$$

Here, q_{cong} is a tuning parameter that was empirically selected at 300. If the suction and congestion thresholds were not violated, q_3 and q_4 were assigned as 0 to turn off the second and third control objectives.

4.2.3 Control performance evaluation

To benchmark the performance of the CMO-MPC against a PI-FS controller and the CS controller, a validated CVS-BiVAD model was selected as the evaluation platform (Lim et al., 2010; Nadeem et al., 2015). The numerical model had previously been used to evaluate the control performance of various control strategies for LVAD (Lim et al., 2015), and for dual LVADs (Ng et al., 2018). The PI-FS controller and the CMO-MPC used the same FS definition as given in Eq. (4.9). The control parameters of the PI-FS controller were tuned using the well-known internal model control (IMC) tuning rules to stiffly challenge the performance of the CMO-MPC (Hetzer et al., 2010).

Two simulation tests were performed: exercise and postural change from supine to upright position. Table 4.1 shows the changes in model parameters (i.e. SVR, PVR, systemic venous unstressed volume, $V_{sv,0}$, and HR) in two simulation tests. The transition from baseline to simulation tests occurred between t=150 s and t=160 s; and the reversed transition occurred between t=360 s and t=370 s. Changes in model parameters were set according to the expected baroreflex response in exercise and postural change scenarios in a previous study (Lim et al., 2015).

Table 4.1: Model parameters in different patient scenarios.

Model parameters	**SVR (dynes s cm^{-5})**	**PVR (dynes s cm^{-5})**	**$V_{sv,0}$ (mL)**	**HR (bpm)**
Baseline	1239	202	2200	90
Exercise	1045	78	1550	120
Postural change	1422	202	2798	90

SVR: systemic vascular resistance; PVR: pulmonary vascular resistance; $V_{sv,0}$: systemic venous unstress volume; HR: heart rate.

For a clearer comparison between the control performance of three different controllers in post processing, signals of pump speed, pump flow rate, and atrial pressure were forward and backward filtered with a second order Butterworth low pass filter with a cut-off frequency of 1 Hz to remove the pulsatility caused by the native heartbeat.

4.3 Results

The results section includes the process interaction analysis outcomes and the control performance outcomes in exercise and postural change scenarios.

4.3.1 Process interaction analysis

Figure 4.3 shows the degree of process interactions of pump speed-preload system and pump speed-pump flow system. The lambda of the pump speed-pump flow system was one across almost all speed ranges except the highest speed operating region (OR 10), indicating no process interaction between the control loops of pump speed-pump flow system across almost all speed ranges except the OR 10. Right ventricular suction was recorded in OR 10. The lambda of pump speed-preload system was neither zero nor one across all speed ranges, which indicated that process interactions existed between the control loops of pump speed-preload system. The lambda of pump speed-preload system increased by a small magnitude (from 1.36 to 2.31) between 1500 rpm and 3750 rpm but increased by a large magnitude (from 2.31 to 13.10) between 3750 rpm and 4000 rpm when right ventricular suction occurred between 3750 rpm and 4000 rpm. Since $\lambda = (\text{open loop gain})/(\text{closed loop gain})$, $\lambda > 1$ implies that the closed loop gain is much smaller than the open loop gain. This indicates that the left manipulated variable has less influence on the left controlled variable when the right loop is closed, and vice versa (Seborg et al., 2010).

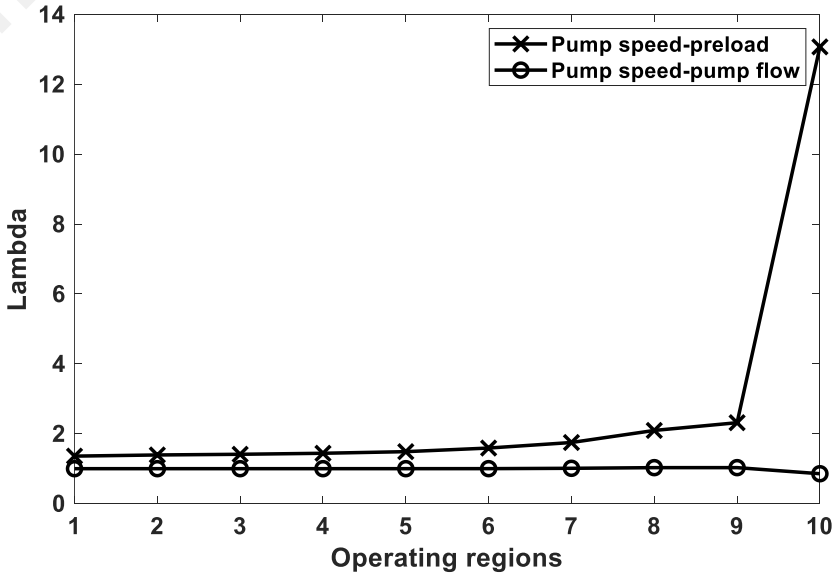

Figure 4.3: Plots of degree of process interaction (lambda) of pump speed-pump flow and pump speed-preload systems in various pump operating regions (OR). OR 1: 1500-1750 rpm; OR 2: 1750-2000 rpm; OR 3: 2000-2250 rpm; OR 4: 2250-2500 rpm; OR 5: 2500-2750 rpm; OR 6: 2750-3000 rpm; OR 7: 3000-3250 rpm; OR 8: 3250-3500 rpm; OR 9: 3500-3750 rpm; OR 10: 3750-4000 rpm.

4.3.2 Control performance

The control performance of the CS and the PI-FS controllers, as well as the CMO-MPC was evaluated in exercise and postural change tests.

4.3.2.1 Exercise test

Table 4.2 presents the simulated steady-state mean and instantaneous (min/max) haemodynamic variables at baseline and exercise scenarios. In the steady-state region of baseline and exercise scenarios, left and right total outflow rates were balanced (equal values) despite differences in flow distribution between the pump flow rate and valve flow rate. In exercise, preload and cardiac output increased because of the regulation by the central nervous system and local response of active muscles. Among the three controllers, the CMO-MPC recorded the highest mean left and right total outflow rates (7.1 L/min), followed by PI-FS controller (6.9 L/min), and CS controller (6.0 L/min). In exercise, the steady-state LVAD speed (3420 rpm) and RVAD speed (3950 rpm) controlled by PI-FS controller were lower than the LVAD speed (3510 rpm) and RVAD speed (4000 rpm) controlled by the CMO-MPC. The difference in speed regulation between the PI-FS controller and CMO-MPC resulted in a difference in left and right atrial pressure distribution. While the PI-FS controller (18.6 mmHg) and the CS controller (24.0 mmHg) failed to prevent mean LAP from exceeding beyond the predefined risk of pulmonary congestion (18 mmHg), the CMO-MPC (17.8 mmHg) successfully prevented mean LAP from exceeding beyond 18 mmHg. Mean SAP and PAP increased from

baseline to exercise in the case of PI-FS control and CMO-MPC control, because of increased total left and right outflow rate, despite a drop in SVR in the exercise scenario.

Table 4.2: Steady-state mean and instantaneous (min/max) haemodynamic variables in baseline and exercise scenarios.

Patient scenarios	**Baseline**	**Exercise**		
		CS control	**PI-FS control**	**CMO-MPC**
Systemic arterial pressure (mmHg)	83.8	88.6	100.4	103.3
Pulmonary arterial pressure (mmHg)	26.7	29.9	36.1	35.8
Left atrial pressure (mmHg)	13.9	24.0	18.6	17.8
Left ventricular pressure (mmHg)	8/81	15/91	11/83	10/80
Left ventricular volume (mL)	133/165	141/174	131/166	128/165
Right atrial pressure (mmHg)	5.5	10.3	11.0	11.1
Right ventricular pressure (mmHg)	4/30	8/35	8/38	8/38
Right ventricular volume (mL)	72/104	77/111	84/118	84/119
Total left outflow (L/min)	5.1	6.0	6.9	7.1
Total right outflow (L/min)	5.1	6.0	6.9	7.1
LVAD flow (L/min)	5.1	5.4	6.9	7.1
RVAD flow (L/min)	4.3	4.4	6.4	6.5

LVAD speed (rpm)	2880	2880	3420	3510
RVAD speed (rpm)	2860	2860	3950	4000

CS, constant speed; PI-FS, Frank-Starling-like-proportional-integral controller; LVAD, left ventricular assist device; RVAD, right ventricular assist device.

A sudden influx of blood to the left ventricle could result in pulmonary congestion if the pump speeds were not regulated in response to preload increase in the exercise scenario. Figure 4.4(a)-(b) show the speed updates controlled by the PI–FS controller and the CMO-MPC in response to risks of vascular congestion. The PI-FS controller and the CMO-MPC increased the right pump speed when the right preload was increased. When the LAP exceeded 18 mmHg, the third objective of the CMO-MPC was activated to reduce RVAD speed and increase LVAD speed, to reduce LAP to 18 mmHg. Figure 4.4(a)- (d) show that changes in pump flow rates were proportional to changes in pump speeds whereas Figure 4.4(e)-(h) show that changes in atrial pressures were proportional to changes in ventricular end diastolic pressure.

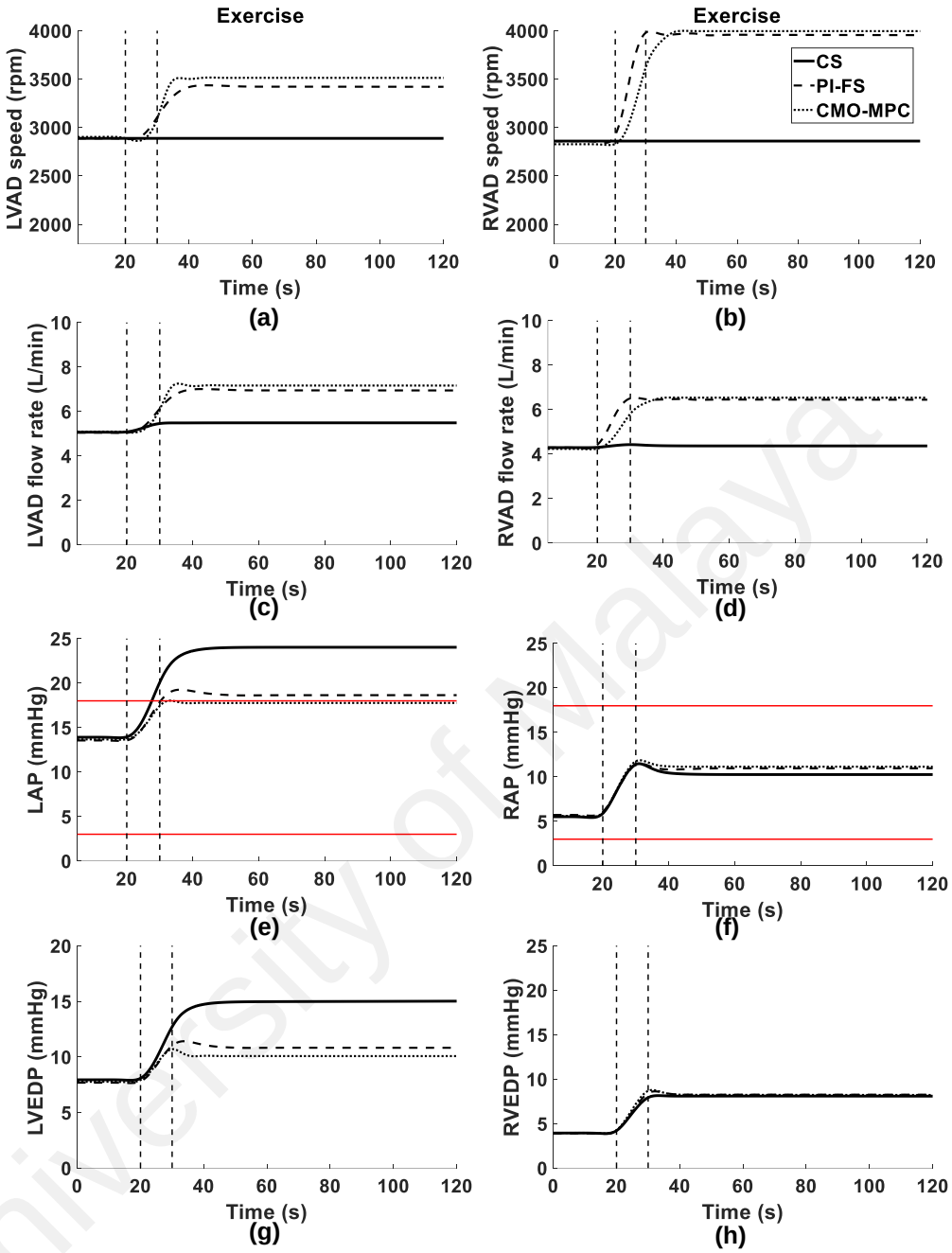

Figure 4.4: Transient changes in filtered hemodynamic variables between baseline (resting state) and exercise scenarios. LVAD, left ventricular assist device; RVAD, right ventricular assist device; LAP, left atrial pressure; RAP, right atrial pressure; LVEDP, left ventricular end diastolic pressure; RVEDP, right ventricular end diastolic pressure; CS, constant speed control; PI-FS, Frank-Starling like control using a proportional-integral controller; CMO-MPC, centralised multi-objective model predictive control. LVAD, left ventricular assist device and RVAD, right ventricular assist device. The vertical dashed lines indicate the duration where gradual changes in model parameters

occurred. The red solid horizontal line at 3 mmHg and 18 mmHg in subplot (e) and (f) mark the user-defined thresholds for suction and congestion.

4.3.2.2 Postural change from supine to upright position

Table 4.3 presents the simulated steady-state mean haemodynamic variables at baseline (supine position) and upright position. Postural change from supine to upright caused a drop in LAP and RAP, as well as left and right outflow rates. The total left and right outflow rates were equivalent to 4 L/min, under both the control of PI-FS controller and CMO-MPC. However, the flow distribution between pump flow rate and valve flow rate achieved by the two controllers were different. The difference between the steady-state mean LVAD speed (2460 rpm) and the steady-state mean RVAD speed (2170 rpm) in the region of upright position achieved by the PI-FS controller was 290 rpm, whereas the difference between the steady-state mean LVAD speed (2500 rpm) and mean RVAD speed (1740 rpm) in the region of upright position achieved by the CMO-MPC was 760 rpm. The different speed regulations by the PI-FS controller and the CMO-MPC resulted in different mean RAP in the upright posture. Mean RAP achieved by the CS controller, PI-FS controller and the CMO-MPC were 1.8 mmHg, 2.6 mmHg and 3.0 mmHg, respectively. Mean LAP achieved by the CS controller, PI-FS controller and CMO-MPC were 9.1 mmHg, 9.4 mmHg and 8.6 mmHg, respectively. Mean SAP and PAP decreased with decreasing pump flow rates despite the increase in SVR from supine to upright position. The minimum steady-state ventricular pressures in all three controllers were above 0 mmHg, indicating no suction events. However, the CMO-MPC managed to maintain minimum right ventricular pressure at 2 mmHg, which was 1 mmHg higher than the minimum right ventricular pressures recorded in both CS control and PI-FS control.

Table 4.3: Steady-state mean and instantaneous (min/max) haemodynamic variables in baseline (supine position) and upright position.

Patient scenarios	Baseline (supine position)	Upright position		
		CS control	PI-FS control	CMO-MPC
Systemic arterial pressure (mmHg)	83.8	85.7	72.8	72.4
Pulmonary arterial pressure (mmHg)	26.7	21.0	19.5	18.7
Left atrial pressure (mmHg)	13.9	9.1	9.4	8.6
Left ventricular pressure (mmHg)	8/81	4/74	5/76	5/74
Left ventricular volume (mL)	133/165	129/159	130/160	129/157
Right atrial pressure (mmHg)	5.5	1.8	2.6	3.0
Right ventricular pressure (mmHg)	4/30	1/23	1/24	2/25
Right ventricular volume (mL)	72/104	61/89	64/96	67/102
Total left outflow (L/min)	5.1	4.7	4.0	4.0
Total right outflow (L/min)	5.1	4.7	4.0	4.0
LVAD flow (L/min)	5.1	4.7	3.6	3.7
RVAD flow (L/min)	4.3	4.3	2.9	1.9
LVAD speed (rpm)	2880	2880	2460	2500
RVAD speed (rpm)	2860	2860	2170	1740

CS, constant speed; PI-FS, Frank-Starling-like-proportional-integral controller; LVAD, left ventricular assist device; RVAD, right ventricular assist device.

Figure 4.5(a) and (b) show the transient response of the LVAD and RVAD speeds regulated by the PI-FS controller and CMO-MPC during the postural change scenario. Both the PI-FS controller and CMO-MPC decreased the RVAD speed in the same manner as soon as the measured RAP was decreased, because both controllers applied the same FS relationship. When RAP fell below 3 mmHg, the suction avoidance objective of CMO-MPC was activated. The CMO-MPC firstly slightly increased the LVAD speed before decreasing the LVAD speed at a slower rate than the PI-FS controller, while further decreasing the RVAD speed until RAP returned to 3 mmHg. Figure 4.5(a)-(d) show that changes in pump flow rates were proportional to changes in pump speeds whereas Figure 4.5(e)-(h) show that changes in atrial pressures were proportional to changes in ventricular end diastolic pressure. In the CS control, right ventricular suction was recorded when RVEDP fell below 0 mmHg for 5 s.

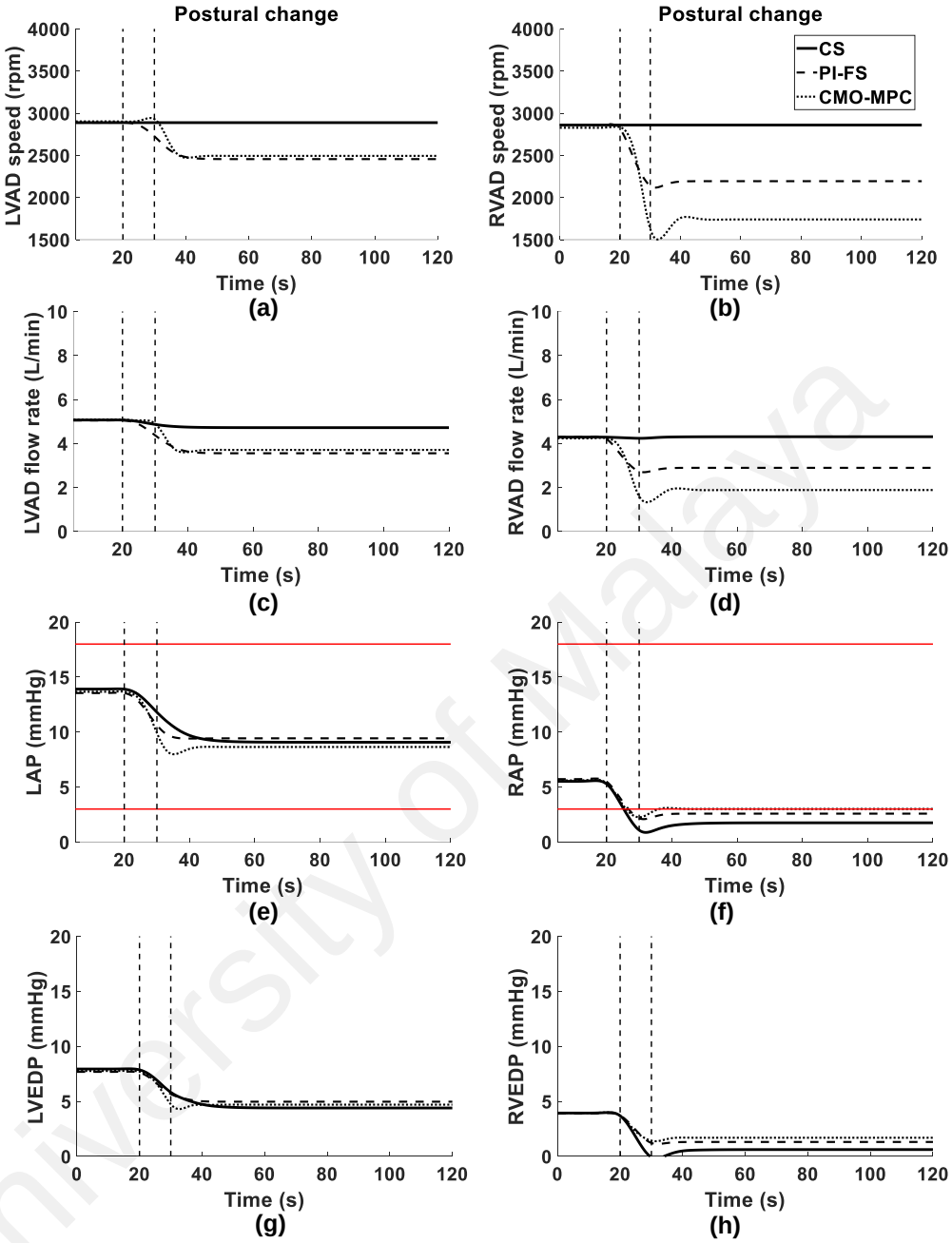

Figure 4.5: Transient changes in filtered haemodynamic variables between baseline (supine) and upright postures. LVAD, left ventricular assist device; RVAD, right ventricular assist device; LAP, left atrial pressure; RAP, right atrial pressure; LVEDP, left ventricular end diastolic pressure; RVEDP, right ventricular end diastolic pressure; CS, constant speed control; PI-FS, Frank-Starling like control using a proportional-integral controller; CMO-MPC, centralised multi-objective model predictive control. LVAD, left ventricular assist device and RVAD, right ventricular assist device. The vertical dashed lines indicate the duration where gradual changes in model parameters

occurred. The red solid horizontal line at 3 mmHg and 18 mmHg in subplot (e) and (f) mark the user-defined thresholds for suction and congestion.

4.3.3 Analysis of transient hemodynamic waveforms

The zoom-in plot in Figure 4.6(a) shows that the CMO-MPC had achieved the lowest diastolic LAP (18 mmHg) when compared to the PI-FS controller (19.7 mmHg) and the CS controller (23.4 mmHg). This is comparable to the results obtained in the mean LAP plot in Figure 4.4 because the diastolic portion of the LAP is larger than the systolic portion in a cardiac cycle therefore the mean hemodynamic plot could be an approximation of the diastolic characteristic of a hemodynamic variable. The diastole LAP is a good indicator for the risk of pulmonary congestion. Supposed there is a sudden increase in the diastolic LAP, the LVAD speed should be increased to unload the increased diastolic LAP. If the LVAD speed was not increased adequately to unload the left heart, diastolic LAP will increase in the subsequent cardiac cycles and this will lead to risks of pulmonary congestion as the overloaded LAP may result in backflow of blood to the pulmonary circulation. Figure 4.6(b) shows the CMO-MPC had prevented the systolic (or minimum) RAP from falling below 0 mmHg. Although all the controllers had prevented the mean RAP from falling below 0 mmHg, Figure 4.6(b) shows that the PI-FS and CS controllers had failed to prevent the systolic RAP from falling below 0 mmHg. Negative RAP was only used as a surrogate for the risk of ventricular suction as it correlates to the volume of blood within the heart chamber. The suction model used in the present study was only triggered when the free wall ventricular volume was below the suction threshold (40 mL). In the evaluated scenarios, there was no real episodes of suction reported.

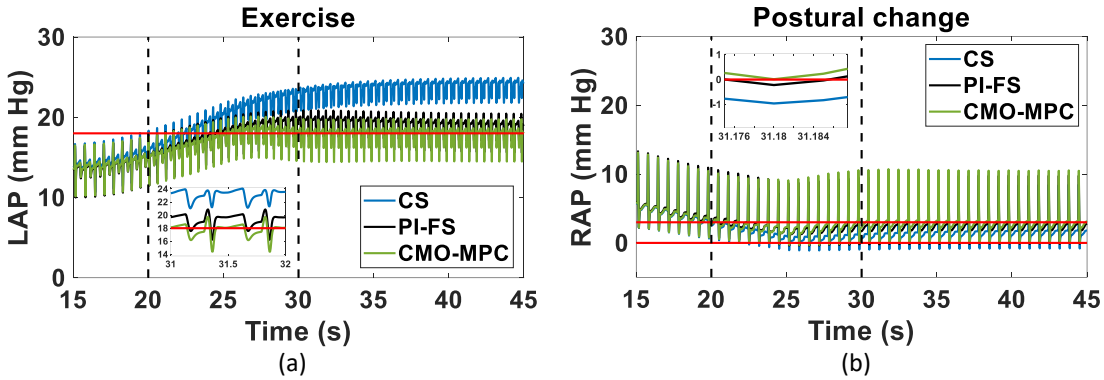

Figure 4.6: (a) Plots of LAP waveforms during the transition from rest to exercise and (b) RAP waveforms during the transition from supine to standing position. LAP: left atrial pressure, RAP: right atrial pressure, CS: constant speed, PI-FS: Frank-Starling-like=proportional-integral controller, CMO-MPC: centralised multi-objective model predictive control.

4.4 Discussion

The FS mechanism describes the relationship between preload and pump flow rate. In a healthy heart, myocardial contractility increases with the increase in preload to increase the cardiac output. Many investigators (Gregory et al., 2016; Ng et al., 2018; J. P. Pauls, Stevens, Schummy, et al., 2016; Stephens et al., 2017; Tchantchaleishvili et al., 2017) have revealed that the FS control has surpassed the control performance of other control strategies in VADs. Most of these FS controllers have only defined a single relationship between the pump flow rate and the preload, even though the FS relationship in a normal heart varies among patients and also varies over time according to the inotropic state of the heart. Therefore, the use of a single FS curve in BiVAD control (Gaddum et al., 2012; Stevens et al., 2014) is not physiological. To address this problem, an adaptive FS control (Chien & Fruehauf, 1990), and a multi-objective control (Ng et al., 2018) of dual LVADs have been proposed to reduce the risks of suction and congestion *in silico* and *in vitro*. However, both attempts incorporate non-centralised control schemes that fail to consider the process interaction of the CVS–BiVAD system.

Other investigators have proposed non-FS control strategies for BiVAD control. In recent years, Wang et al. extended the constant differential pressure (dP) control strategy they proposed earlier for LVAD (Giridharan & Skliar, 2003) to BiVAD (Wang et al., 2018a; Wang et al., 2018b). However, similar to the dual non-adaptive PI-FS control, the dual constant dP control of BiVAD (Wang et al., 2018b), could not explicitly prevent suction and congestion. Furthermore, the disadvantage of constant dP control strategy as compared to the FS control strategy is that it could not explicitly account for changes in preload and afterload, which may lead to higher risk of suction and congestion. Another argument against using dP control for BiVAD is that it was recently shown to be inferior in performance to FS control for LVADs, with respect to suction avoidance across a range of SVR and PVR changes (Jo P. Pauls, Stevens, et al., 2016b).

Prior to this study, the presence of process interactions in the CVS–BiVAD system that was suspected by Gaddum et al. in a previous study (Gaddum et al., 2012), had yet to be quantitatively studied. In this study, the RGA analysis reveals the presence of loop interactions between pump speeds and preloads. Since a centralised controller can handle process interactions while non-centralised control schemes cannot, the CMO-MPC for a dual-LVAD system has been proposed. The RGA analysis also shows negligible loop interaction in the pump speed-pump flow system. While the presence of negligible interaction for the pump speed-pump flow system might suggest the redundancy of a centralised controller, the proposed multi-objective control strategy that includes the interactive closed loops of preload may necessitate a centralised control scheme for control optimisation. This is because the pump speed-preload system has varying degree of process interactions across all pump operating regions as shown in Figure 4.3.

To evaluate the potential of the CMO-MPC to avoid congestion and suction, we simulated two patient scenarios (i.e. exercise and postural change). Pulmonary congestion

may occur in exercise when there is sudden increase in venous return, while ventricular suction may occur during postural change from supine to upright when there is sudden decrease in venous return, especially when the pumps are operated in CS control. Figures 4.4 and 4.5 demonstrate that the CMO-MPC is the most superior control scheme as it has successfully achieved the control objectives in avoiding events of suction and congestion by keeping mean atrial pressure within the safety boundary between 3 mmHg and 18 mmHg. During the exercise test, the CMO-MPC avoided events of pulmonary congestion with mean LAP less than 18 mmHg. In the postural change test, right ventricular suction occurred in the CS control. The CMO-MPC prevented RAP from falling below 3 mmHg because of the activation of control objective 2. In the PI-FS control, RAP fell to 2.6 mmHg, which was lower than the steady-state mean RAP recorded in the CMO-MPC. In a multi-objective control scheme, the computation of optimal control outputs accounts for all control objectives that are competing with one another according to the assigned weighting for each objective. Therefore, it is expected to have the control accuracy of each control objective compromised to satisfy the overall optimal cost function. For this reason, the margin defined in the safety boundary is necessary to prevent real events of suction and congestion from happening even if the control accuracy of the control objective is compromised.

In addition to the benefits of the multi-objective approach, the centralised control scheme of the CMO-MPC offers a second benefit in that it is relatively easy to tune as compared to two separate controllers that may face challenges in tuning control problems involving process interactions. Inappropriate tuning of two separate controllers may lead to control instability. Furthermore, the CMO-MPC can deal with the constraints of manipulated variables, slew rates, as well as controlled variables involved in the system.

In contrast, PI controllers can only deal with the constraints of the manipulated variables with the aid of the anti-windup algorithm.

In a previous study (Ng et al., 2018), a neural-network based MPC of a dual-LVAD system also showed better avoidance of ventricular suction and vascular congestion when benchmarked against the CS control and the PI-FS control. However, the use of a neural-network model is not favourable for practical implementation due to its empirical nature and the extensive computational time incurred for model training in different clinical scenarios. For this reason, we proposed a simpler approach using a first-principle state-space model, which will facilitate and motivate future development of the control of dual LVADs because it provides the knowledge of interactions within the CVS–BiVAD system. Identification of the model parameters in this case would also be relatively easier compared to the neural network model.

The CMO-MPC is dependent on the pump hydraulic models (i.e. axial flow and centrifugal flow). Although the control scheme is pump dependent, it can be easily modified to suit for axial flow pumps by updating the pump hydraulic model and constraints for speed and slew rate. The CMO-MPC has also been evaluated with axial flow pumps and the published results are comparable to the present study (Koh et al., 2019). Comparing to the PI controller of which tuning may be exhaustive for different pump models, only a slight tweak in tuning parameters of the CMO-MPC is required for different pump models. In the present study, the parameters of the internal state-space model were also not adaptive to physiological changes. Despite the model parameters being non-adaptive to physiological changes; the CMO-MPC was able to deal with plant-model mismatch, resulting in a robust control performance.

The present control scheme assumes that accurate preload and flow measurements are available. To date, there is no commercially available pressure sensor that is incorporated into LVAD due to potential sensor drifts that will lead to reduction in sensor accuracy. A few recent studies have shown improvements in the accuracy of pressure sensors (Hubbert et al., 2017; Troughton et al., 2011), which will support the future adoption of the current control scheme. Furthermore, there are flow sensors integrated into the HeartAssist5 LVAD (ReliantHeart Inc., Texas, U.S.) (Noon et al., 2001). In a recent study, Wang et al. (Wang et al., 2018b) utilised a VAD model to estimate differential pressure (dP) in their control strategy. The control strategy incorporated two gain scheduling PI controllers to control the left and right dP to meet adequate blood flow rate and two other gain scheduling PI controllers to control the left and right differential rotation per minute (dRPM) to prevent suction. Considering physiological sensors are not commercially available at this stage, the sensorless control strategy would be preferred over the sensor-based control strategy. Therefore, in the future, we may adopt the concept of this sensorless control strategy in the CMO-MPC. With the CMO-MPC, we could reduce the use of four gain scheduling PI controllers into a single controller, which could also effectively simplify the efforts of tuning.

The use of numerical model as the evaluation platform has offered the freedom to access all haemodynamic variables during the simulation study. Furthermore, the simulation protocol is also repeatable for a fair evaluation of different control strategies. However, the numerical model only serves as an approximate to the electrical and mechanical properties of the pumps as well as the biological properties of the cardiovascular system. Although the practical limitations of the pumps (i.e. maximum and minimum allowable pump speed and slew rate) can be included in the numerical evaluation study, the simulation results may differ from the *in vitro* and *in vivo* studies.

The baroreflex mechanism of the numerical model was also manually accounted in the tuning of model parameters in the simulation protocol to achieve the expected haemodynamic changes in exercise and postural change scenarios as observed in the literature (Brassard et al, 2011; Jacquet et al., 2011; Mancini et al., 1998; Muthiah et al., 2013; Markham et al., 2013). Although the numerical model that was used in the evaluation has attained experimental validation in previous studies (Lim et al., 2010; Lim et al., 2012), further *in vitro* and *in vivo* validations for the control performance of the CMO-MPC are still required in the future.

4.5 Conclusion

In this chapter, the process interactions between the feedback loops of pump speed-pump flow rate system and the pump speed-preload system have been analysed using the Bristol's RGA method. Process interactions existed between the feedback loops of pump speed-preload system but not the pump speed-pump flow rate system, which justified the need for a control methodology that could accommodate this process interaction. To adapt pump flow rate while ensuring no episodes of ventricular suction and vascular congestion, the CMO-MPC was developed for BiVAD. Three salient features of CMO-MPC are particularly attractive: a) the centralised scheme is for the optimisation of control problem that involves process interactions, b) the multi-objective scheme is to explicitly avoid suction and congestion while regulating the pump flow rate using a single FS mechanism, and c) predictive scheme is to provide pre-emptive control measures before real events of suction and congestion could occur. The study reveals the potential of the CMO-MPC to minimise risks of ventricular suction and vascular congestion within the predefined safety region (atrial pressure between 3 mmHg and 18 mmHg) while the CS controller and the PI-FS controller could not. The next chapter describes the *in vitro* validation of the CMO-MPC.

CHAPTER 5: A CENTRALISED MULTI-OBJECTIVE MODEL PREDICTIVE CONTROL FOR A BIVENTRICULAR ASSIST DEVICE: AN *IN VITRO* EVALUATION

The aim of the chapter was to validate the control performance of the CMO-MPC in the *in vitro* environment. To meet the aim of the study, several objectives were devised as follows:

- To design different patient scenarios in the *in vitro* environment (MCL) for control evaluation.
- To optimise the tuning parameters and FS control curves for the PI-FS controller and the CMO-MPC for the *in vitro* testing.

5.1 Introduction

In chapter 4, the control performance of the CMO-MPC had been benchmarked against the PI-FS controller and the CS controller in the *in silico* environment as the first stage control evaluation. However, the *in silico* environment does not represent the real CVS-BiVAD interaction. Therefore, in this chapter, the control performance of the CMO-MPC was benchmarked against the PI-FS controller and the CS controller in the *in vitro* environment. The work covered in this chapter has also been submitted to the journal of IEEE Transaction of Biomedical Engineering entitled "A centralised multi-objective model predictive control for a biventricular assist device: an in vitro evaluation."

5.2 Methods

The method section includes a description of an MCL, control strategies and the tuning parameters, and the control performance evaluated based on two aspects: 1) the control aspects and 2) the physiological aspects.

5.2.1 Mock circulation loop (MCL)

A physical five-element Windkessel MCL that included the systemic and pulmonary circulations (Figure 5.1) was used as the evaluation platform for this study. A more detailed description of the MCL was described by Timms et al..(Timms et al., 2011). In brief, a series of electropneumatic regulators (ITV2030-012BS5, SMC Corporation, Tokyo, Japan) and 3/2-way solenoid valves (VT325-035DLS, SMC Corporation) were used to provide passively filled heart chambers and variable contractility, heart rate, and systolic time for the control of ventricular systole. The baseline heart rate and systolic time were maintained at 80 beats per minute and 35%, respectively, throughout the study. Both left and right ventricular contractility were actively controlled by the electropneumatic regulator supply current, based on the ventricular preload, to replicate the Starling response introduced by Gregory, Stevens, Timms, & Pearcy (Gregory et al., 2011). Mechanical check valves were used to model the mitral, aortic, tricuspid, and pulmonary valves to ensure unidirectional flow throughout the circuit. Four independent Windkessel chambers were employed to simulate lumped systemic and pulmonary arterial and venous compliance. Socket valves (VMP025.03X.71, Alb. Klein Ohio, Plain City, OH, USA) enabled control of systemic and pulmonary vascular resistance. The working fluid was a water/glycerol mixture (60/40% by mass) that produced a viscosity (3.57 mPa/s at room temperature) within the normal range (3.5–4.5 mPa/s) of blood viscosity (Ramnarine et al., 1998).

Two HVAD pumps were used as a BiVAD. The inflow cannulation sites were the ventricles, while the outflow cannulation site was the aorta (for left pump) and pulmonary artery (for right pump). The outflow graft of the RVAD was banded to 5.5 mm equivalent banding diameter over a length of 30 mm, using a 3D-printed tubing connector (Objet24, Startasys, Edina, MN, USA). This enabled the RVAD speed to operate at almost the same

speed as the LVAD speed at normal pulmonary vascular resistance (PVR) and systemic vascular resistance (SVR), giving the two pumps the same allowance of speed adjustment.

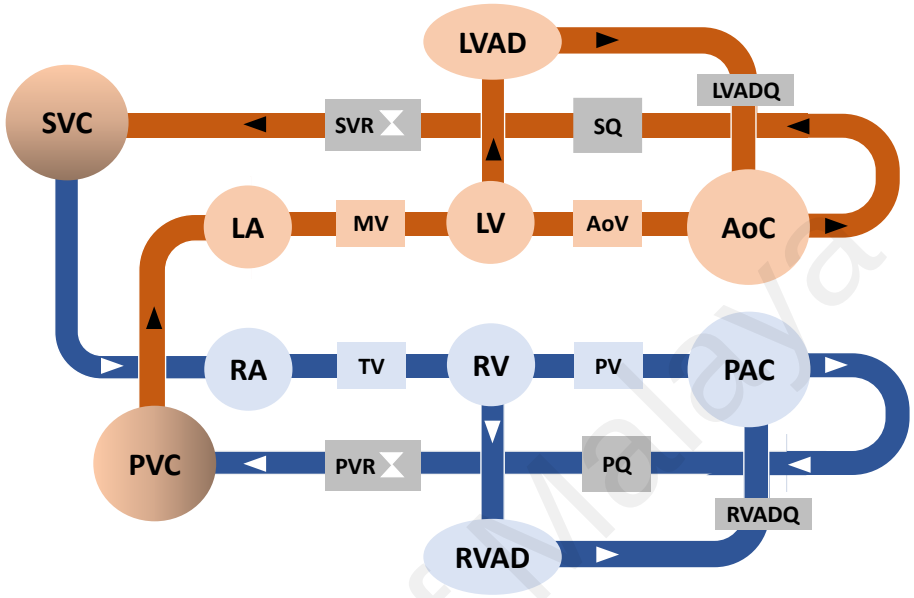

Figure 5.1: Schematic diagram of the mock circulation loop (MCL). SVC, systemic vascular compliance; PVC, pulmonary vascular compliance; LA, left atrium; RA, right atrium; MV, mitral valve; TV, tricuspid valve; LV, left ventricle; RV, right ventricle; AoV, aortic valve; PV, pulmonary valve; AOC, aortic compliance; PAC, pulmonary arterial compliance; SQ, systemic flow rate; PQ, pulmonary flow rate; LVADQ, left ventricular assist device flow rate; RVADQ, right ventricular assist device flow rate; LVAD, left ventricular assist device; RVAD, right ventricular assist device. Figure adapted from reference (Pauls et al., 2016b).

Left and right atrial and ventricular pressures, aortic pressure, pulmonary arterial pressure, and LVAD inlet/outlet pressures were monitored using silicon-based transducers (PX181B-015C5V, Omega Engineering, Stamford, CT, USA). Left and right ventricular volumes were recorded using magnetostrictive level sensors (IK1A, GEFRAN, Provaglio d'Iseo, Italy and Miran, MTL-4-550, Miran Technology, Co., Guangdong, China for left and right volumes respectively). Systemic flow rate was measured using a magnetic inductive flow meter (Optiflux 1010C/D, Krohne, Duisburg,

Germany), while pulmonary flow rate and VAD flow rates were measured using clamp-on ultrasonic flow sensors (TS410-20PXL, TS410-10PXL and TS410-10PXL respectively, Transonic Systems, Ithaca, NY, USA). All sensor readings were sampled into the model from a dSPACE 1103 (dSPACE GmbH, Paderborn, Germany) at a rate of 2 kHz and down sampled to 40 Hz for data postprocessing. The postprocessing involves a second order Butterworth low pass forward and backward filter with a cut-off frequency of 1 Hz to remove the pulsatility of the pump speeds, atrial pressure, and pump flow rate signals, that were caused by the native heartbeat to show a clearer comparison between the control performance of three different controllers.

5.2.2 Control strategies and tuning parameters

The elaborated design of control strategies for CMO-MPC and PI-FS control was described in section 4.2.2.2. The same FS control curves that were illustrated in Figure 4.2 and defined in Eq. (4.10) were tuned to set the baseline CO at 5 L/min. The K_1 and K_2 of Eq. (4.10) were the same as those used in chapter 4. The K_3 of left and right hearts were tuned manually by selecting the steady-state mean LAP and RAP that correspond to CO at 5 L/min at the CS control. The same IMC tuning method that was used in Chapter 4 was used to retune the PI-FS controller for the *in vitro* test. Optimal tuning parameters of CMO-MPC were selected empirically. Tables 5.1 and 5.2 show the tuning parameter values of PI-FS controller and CMO-MPC used in *in silico* and *in vitro* studies.

Table 5.1: Tuning parameters of PI-FS controller used in *in silico* and *in vitro* tests.

Tuning parameters	***In silico***		***In vitro***	
	Left	Right	Left	Right
K_p	8.75	253.8	391.58	391.58
K_i	0.01	0.01	1.45	1.45

K_p, proportional gain; K_i, integral gain. The tuning parameters are dimensionless as all control simulation performed in the thesis were normalised into dimensionless terms so that all variables share the same order of magnitude.

Table 5.2: Tuning of CMO-MPC used in *in silico* and *in vitro* tests.

Tuning parameters	*In silico*	*In vitro*
H_u	1	1
H_p	10	10
q_{suc}	300	500
q_{cong}	300	500
$\boldsymbol{R}$	$\begin{bmatrix} 500 & 0 \\ 0 & 500 \end{bmatrix}$	$\begin{bmatrix} 2000 & 0 \\ 0 & 2000 \end{bmatrix}$

H_u, control horizon; H_p, prediction horizon; q_{suc}, output weight for suction prevention; q_{cong}, output weight for congestion prevention; $\boldsymbol{R}$, move suppression weight matrix.

5.2.3 Control performance

The control performance evaluation of the CMO-MPC was divided into two sections: 1) control aspects and 2) physiological aspects. With respect to the control aspects, the time domain analysis was used to identify the rise time, settling time, and the integral of absolute error (IAE). Herein, the rise time was not referred to the standard rise time used in the open-loop system analysis (Seborg et al., 2010), but it refers to the closed-loop response time of manipulated variables, calculated between the 10% and 90% of the increase or decrease from the previous steady-state value to the new steady-state value. The same rise time was also used to depict changes in haemodynamic variables, *viz.* the atrial pressures and ventricular end diastolic pressure for the analysis of the physiological aspects in the results section. The PI-FS controller and the CMO-MPC used the same FS definition as given in Eq. (4.10). The control parameters of the PI-FS controller were tuned using the well-known IMC tuning rules (Hetzer et al., 2010). To demonstrate the competence of the CMO-MPC, the control performance of the CMO-MPC was

benchmarked with the conventional CS controller and the PI-FS controller based on the physiological aspects; the best physiological controller must adjust the pump flow rate according to metabolic demand while demonstrating the lowest risks of ventricular suction and vascular congestion.

5.2.3.1 Control aspects

To compare the differences in rise time, settling time, and IAE between the PI controller and the MPC, step changes in the target pump flow rate from 5 L/min to 7 L/min, and from 7 L/min to 6 L/min were applied to both controllers, with the baseline PVR, SVR, and HR, at t=20 s and t=120 s, respectively. The IAE was calculated using Eq. (5.1).

$$\text{IAE} = \int_{t_0}^{T} |e| \, dt \tag{5.1}$$

where t_0, T, and e are the initial time, the final time, and the error between the target and measured flow rate.

5.2.3.2 Physiological aspects

To demonstrate the physiological aspects, clinically relevant test beds such as the exercise test and the postural change (supine to upright position) test were designed for the study. Furthermore, the physiological control responses to a greater extent of preload and afterload changes were also evaluated. Table 5.3 shows the changes in model parameters (i.e. SVR, PVR, $V_{sv,0}$ and HR) in all evaluation tests. The transition from baseline to each evaluation test occurred between t=20 s and t=30 s. Changes of model parameters were determined to mimic the baroreflex response involved in exercise and postural change scenarios in a previous study (Lim et al., 2015) whereas changes of model

parameters in the preload and afterload tests were similar to other previous studies (J. P. Pauls, Stevens, Schummy, et al., 2016; Petrou et al., 2018).

Table 5.3: Model parameters in all evaluation tests.

Test	Baseline	Exercise	Upright posture	Changes in SVR		Increase in PVR
				Decrease	Increase	
SVR (dynes s cm^{-5})	1300	1000	1600	500	3000	-
PVR (dynes s cm^{-5})	120	80	120	120	120	500
HR (bpm)	80	95	80	80	80	-
Volume shift from the vascular compliant chamber to the reservoir (mL)	-	+1000	-500	-	-	-

SVR, systemic vascular resistance; PVR, pulmonary vascular resistance; HR, heart rate.

5.3 Results

The results section is divided into the control aspects and physiological aspects of the control performance. The control aspects include the time-domain specification such as the rise time and settling time as well as the IAE of the controllers. The physiological aspects examined the potential of the controllers to increase exercise capacity and prevent

events of ventricular suction and vascular congestion in all evaluated tests such as exercise, postural change, PVR variation, and SVR variation tests.

5.3.1 Control aspects

The closed-loop step responses of the PI controller and the MPC are shown in Figure. 5.2 and the calculated IAE values, rise time, and settling time for LVAD and RVAD pumps were listed in Table 5.4 and Table 5.5, respectively. The MPC had better control accuracy (smaller IAE), faster rise time and settling time as compared with the PI controller on LVAD. Conversely, the PI controller had better control accuracy, faster rise time and settling time on RVAD. Larger IAE and longer rise time and settling time were observed in two controllers when bigger step change in setpoints (5-7 L/min) were applied between t=20 s and t=120 s.

Table 5.4: Time domain analysis on the left pump flow rate.

		PI controller	MPC	Δ (PI-MPC)
IAE (L/min s)	20<t<120	34.2	24.2	10.0
	120<t<220	13.9	10.9	3.0
Rise time (s)	20<t<120	31.4	18.8	12.6
	120<t<220	25.9	15.5	10.4
Settling time (s)	20<t<120	59.3	39.5	19.8
	120<t<220	40.0	29.2	10.8

PI, proportional-integral controller; MPC, model predictive controller; Δ (PI-MPC): difference between control performance of PI controller and MPC; IAE, integral of absolute error.

Table 5.5: Time domain analysis on the right pump flow rate.

		PI controller	MPC	Δ (PI-MPC)
IAE (L/min s)	20<t<120	35.3	39.9	-4.6

	120<*t*<220	17.7	21.1	-3.4
Rise time (s)	20<*t*<120	35.9	37.0	-1.1
	120<*t*<220	34.6	36.5	-1.9
Settling time (s)	20<*t*<120	54.2	68.0	-13.8
	120<*t*<220	46.1	54.6	-8.5

PI, proportional-integral controller; MPC, model predictive controller; Δ (PI-MPC): difference between control performance of PI controller and MPC; IAE, integral of absolute error.

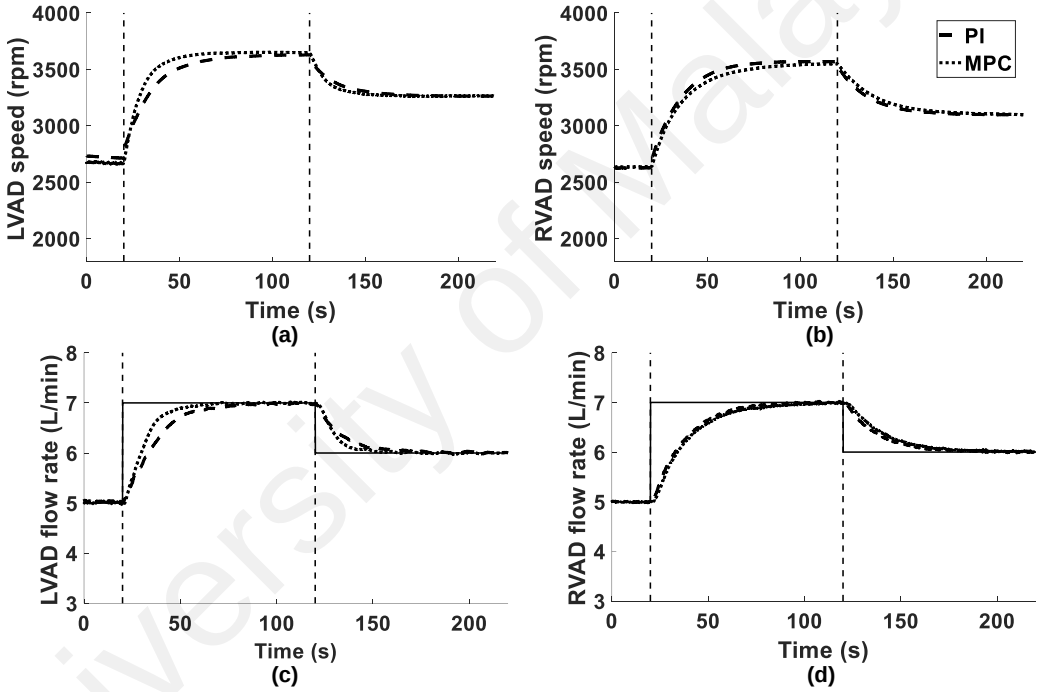

Figure 5.2: Time domain analysis on the speed and flow rate response during a step change in target pump flow rates. LVAD, left ventricular assist device; RVAD, right ventricular assist device; PI, proportional-integral controller; MPC, model predictive controller.

5.3.2 Physiological aspects

The controllers were evaluated based on the physiological aspects (i.e. capability to increase flow rate in exercise, capability to avoid ventricular suction, and capability to

avoid vascular congestion) in exercise, postural change, PVR variation and SVR variation tests.

5.3.2.1 Exercise

Table 5.6 shows that the steady-state mean arterial pressures, atrial pressures, and total flow rates increased from baseline to exercise in all three controllers. Among the three controllers, the CMO-MPC recorded the highest mean left and right total outflow rates (7.6 L/min), followed by the PI-FS controller (7.5 L/min), and the CS controller (6.0 L/min). With the speed adjustment by physiological controllers in exercise, the increase in pump flow rate was higher when compared with the CS controller (i.e. LVAD flow (L/min): 0.4 (CS), 2.3 (PI-FS), 2.3 (CMO-MPC); RVAD flow (L/min): 0.1 (CS), 2.4 (PI-FS), 2.4 (CMO-MPC)). Comparing the steady-state mean hemodynamic variables achieved by the PI-FS controller and the CMO-MPC, similar values were observed as recorded in Table 5.6.

Table 5.6: Steady-state mean haemodynamic variables in baseline and exercise scenarios.

Patient scenarios	**Baseline (rest)**	**Exercise**		
		CS control	**PI-FS control**	**CMO-MPC**
Systemic arterial pressure (mmHg)	88.4	89.0	106.7	107.7
Pulmonary arterial pressure (mmHg)	18.5	22.4	25.3	25.1
Left atrial pressure (mmHg)	11.3	16.4	18.3	17.9
Right atrial pressure (mmHg)	7.4	13.8	12.8	12.9

Total left outflow (L/min)	5.0	6.0	7.5	7.6
LVAD flow (L/min)	5.0	5.4	7.3	7.3
Total right outflow (L/min)	5.0	6.0	7.5	7.6
RVAD flow (L/min)	5.0	5.1	7.4	7.4
LVAD speed (rpm)	2508	2510	3067	3088
RVAD speed (rpm)	2670	2669	3792	3783

CS, constant speed; PI-FS, Frank-Starling-like-proportional-integral controller; LVAD, left ventricular assist device; RVAD, right ventricular assist device.

The rise time of LVAD speed (28.0 s), LVAD flow (37.0 s), and RAP (7.3 s) in the CMO-MPC was comparable to the PI-FS controller (Figure 5.3(a), (c), and (f)). The rise time of RVAD speed (CMO-MPC: 37.8 s; PI-FS: 28.0 s), RVAD flow (CMO-MPC: 39.2 s; PI-FS: 31.4 s), and LAP (CMO-MPC: 26.2 s; PI-FS: 21.2 s) was slower in the CMO-MPC compared with the PI-FS controller (Figure 5.3(b), (d), and (e)). The was no overshoot of LAP in the CS controller and CMO-MPC, however, an overshoot of 1 mmHg above the 18 mmHg threshold was observed in the PI-FS controller.

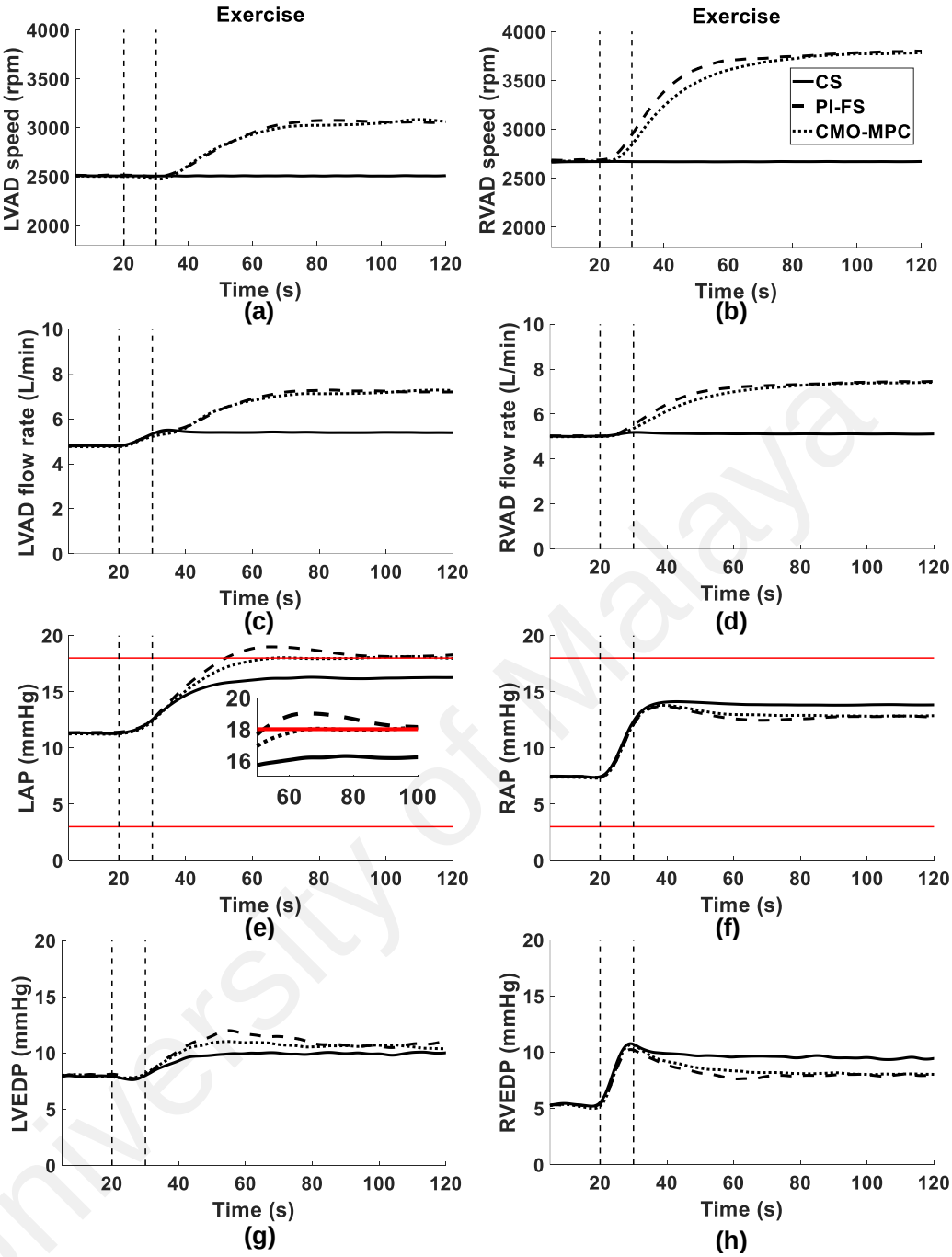

Figure 5.3: Plots of control and haemodynamic responses from rest to exercise. LVAD, left ventricular assist device; RVAD, right ventricular assist device; LAP, left atrial pressure; RAP, right atrial pressure; LVEDP, left ventricular end diastolic pressure; RVEDP, right ventricular end diastolic pressure. The vertical dashed lines indicate the duration where gradual changes in model parameters occurred. The red solid horizontal line at 3 mmHg and 18 mmHg in subplots (e)-(f) mark user-defined marginal threshold for the activation of objective 2 and 3.

5.3.2.2 Postural change

Table 5.7 shows that the right atrial pressure and the total outflow rates decreased during postural change from supine to upright in all three controllers. The lowest steady-state mean right atrial pressure observed when using the CS controller was 2.2 mmHg when compared with the PI-FS controller and the CMO-MPC that both recorded at 5.1 mmHg. On the other hand, the steady-state mean total outflow rates controlled by both physiological controllers (3.8 L/min) were lower than the CS controller (4.7 L/min). Like the exercise test, the steady-state mean hemodynamic variables achieved by the PI-FS controller were close to that of the CMO-MPC.

Figure 5.4(a) shows that the physiological controllers increased the LVAD speed during the postural change from supine to upright between t=25 s and t=40 s and decreased the LVAD speed after t=40 s till the system reached the steady-state. The CMO-MPC achieved a higher maximum LVAD speed (2771 rpm) than the PI-FS controller (2681 rpm). The start time to decrease RVAD speed in the CMO-MPC and the PI-FS controller was t=31.1 s and t=27.4 s, respectively (Figure 5.4(b)). The rise time of RVAD speed in both controllers was the same (19.0 s). The rise time of RAP (CMO-MPC: 9.4 s; PI-FS: 7.6 s) and RVEDP (CMO-MPC: 5.1 s; PI-FS: 2.7 s) was slower in the CMO-MPC as compared with the PI-FS controller (Figure 5.4(f)). The lowest minimum undershoot of RVEDP was recorded in the CS controller (0.1 mmHg), followed by the PI-FS controller (1.2 mmHg), and the CMO-MPC (2.0 mmHg). CO is lower in heart failure as compared to healthy heart due to the reduced cardiac contractility. SAP also decreased with decreasing CO. LAP and RAP increased because of the reduced cardiac contractility – blood built up in the heart chambers. To simulate pulmonary congestion, which is commonly occurred in heart failure patients, PVR was increased. Increasing PVR led to an increase in PAP.

Table 5.7: Steady-state mean haemodynamic variables in baseline (supine position) and upright position.

Patient scenarios	Baseline (supine position)	Upright position		
		CS control	PI-FS control	CMO-MPC
Systemic arterial pressure (mmHg)	88.4	96.3	81.0	81.7
Pulmonary arterial pressure (mmHg)	18.5	21.7	14.1	14.2
Left atrial pressure (mmHg)	11.3	14.8	8.5	8.5
Right atrial pressure (mmHg)	7.4	2.2	5.1	5.1
Total left outflow (L/min)	5.0	4.7	3.8	3.8
LVAD flow (L/min)	5.0	4.4	3.7	3.8
Total right outflow (L/min)	5.0	4.7	3.8	3.8
RVAD flow (L/min)	5.0	4.7	3.8	3.8
LVAD speed (krpm)	2507	2510	2335	2352
RVAD speed (krpm)	2669	2671	2117	2138

CS, constant speed; PI-FS, Frank-Starling-like-proportional-integral controller; LVAD, left ventricular assist device; RVAD, right ventricular assist device.

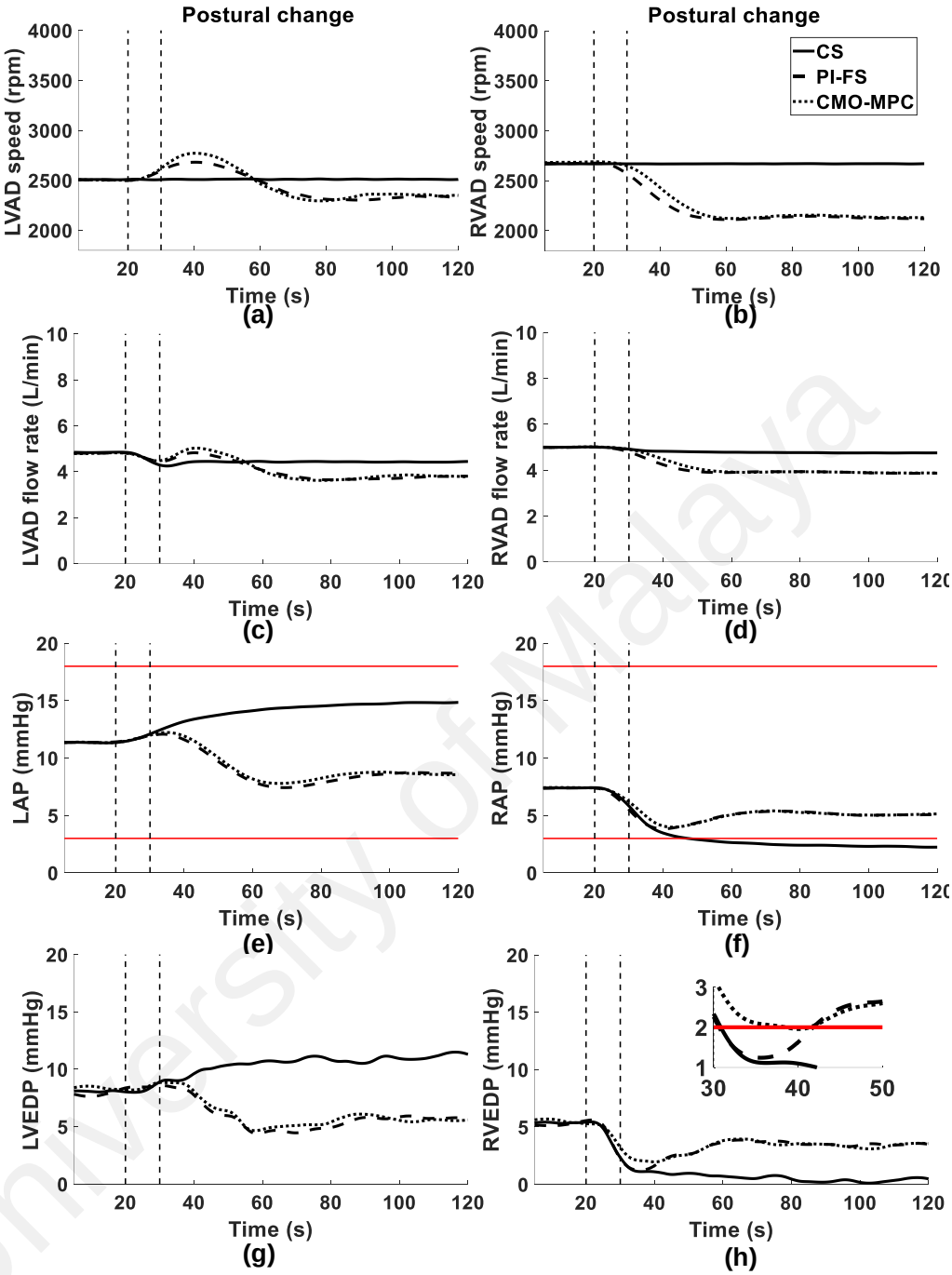

Figure 5.4: Plots of speed control and haemodynamic responses from supine position to upright position. LVAD, left ventricular assist device; RVAD, right ventricular assist device; LAP, left atrial pressure; RAP, right atrial pressure; LVEDP, left ventricular end diastolic pressure; RVEDP, right ventricular end diastolic pressure. The vertical dashed lines indicate the duration where gradual changes in model parameters occurred. The red solid horizontal line at 3 mmHg and 18 mmHg in subplots (e)-(f) mark user-defined marginal threshold for the activation of objective 2 and 3.

5.3.2.3 SVR changes

Figure 5.5(a) and 5.5(b) show that the physiological controllers decreased the LVAD speed and increased the RVAD speed when SVR was decreased, but opposite trends in the speed updates were observed when SVR was increased (as shown in Figure 5.6(a) and 5.6(b)). In the CS control, the LAP and LVEDP decreased with decreasing SVR till left ventricle suction occurred when LVEDP dropped below 0 mmHg. In the SVR increase test with the CS control, RAP and RVEDP decreased till right ventricular suction occurred when RVEDP dropped below 0 mmHg; LAP increased till it exceeded 20 mmHg (pulmonary congestion). The rise time of LVAD speed (CMO-MPC: 6.9 s; PI-FS: 10.9 s) was faster in the CMO-MPC than that of PI-FS controller in the SVR decrease test (Figure 5.5(a)). The rise time of LAP (CMO-MPC: 28.5 s; PI-FS: 25.7 s) was slower in the CMO-MPC than that of PI-FS controller in the SVR decrease test (Figure 5.5(e)). The undershoot of LVEDP in the CMO-MPC (4.0 mmHg) was smaller than that of PI-FS controller (3.6 mmHg) in the SVR decrease test (Figure 5.5(g)).

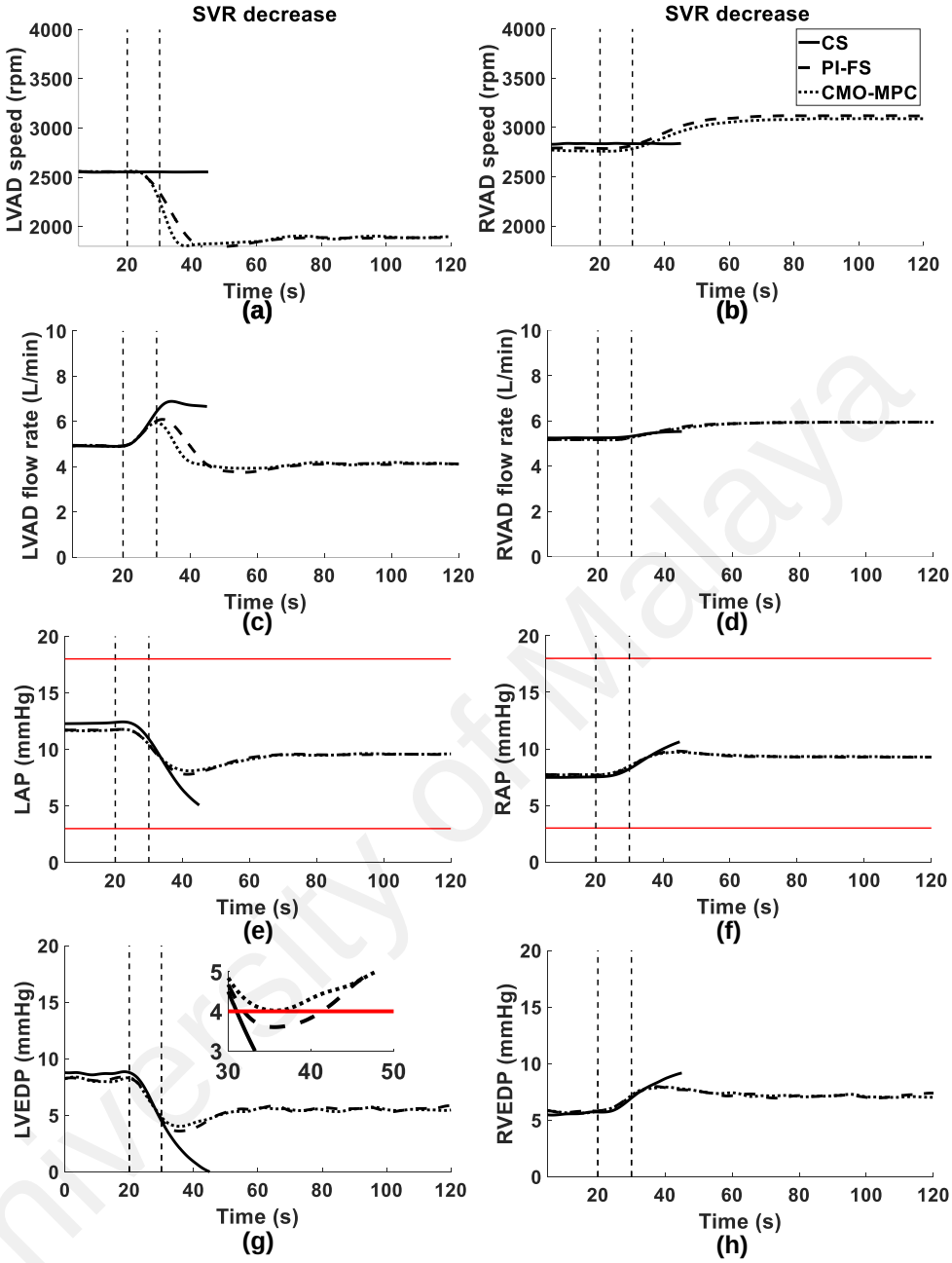

Figure 5.5: Plots of speed control and haemodynamic responses in an SVR decrease test. LVAD, left ventricular assist device; RVAD, right ventricular assist device; LAP, left atrial pressure; RAP, right atrial pressure; LVEDP, left ventricular end diastolic pressure; RVEDP, right ventricular end diastolic pressure. The vertical dashed lines indicate the duration where gradual changes in model parameters occurred. The red solid horizontal line at 3 mmHg and 18 mmHg in subplots (e)-(f) mark user-defined marginal threshold for the activation of objective 2 and 3.

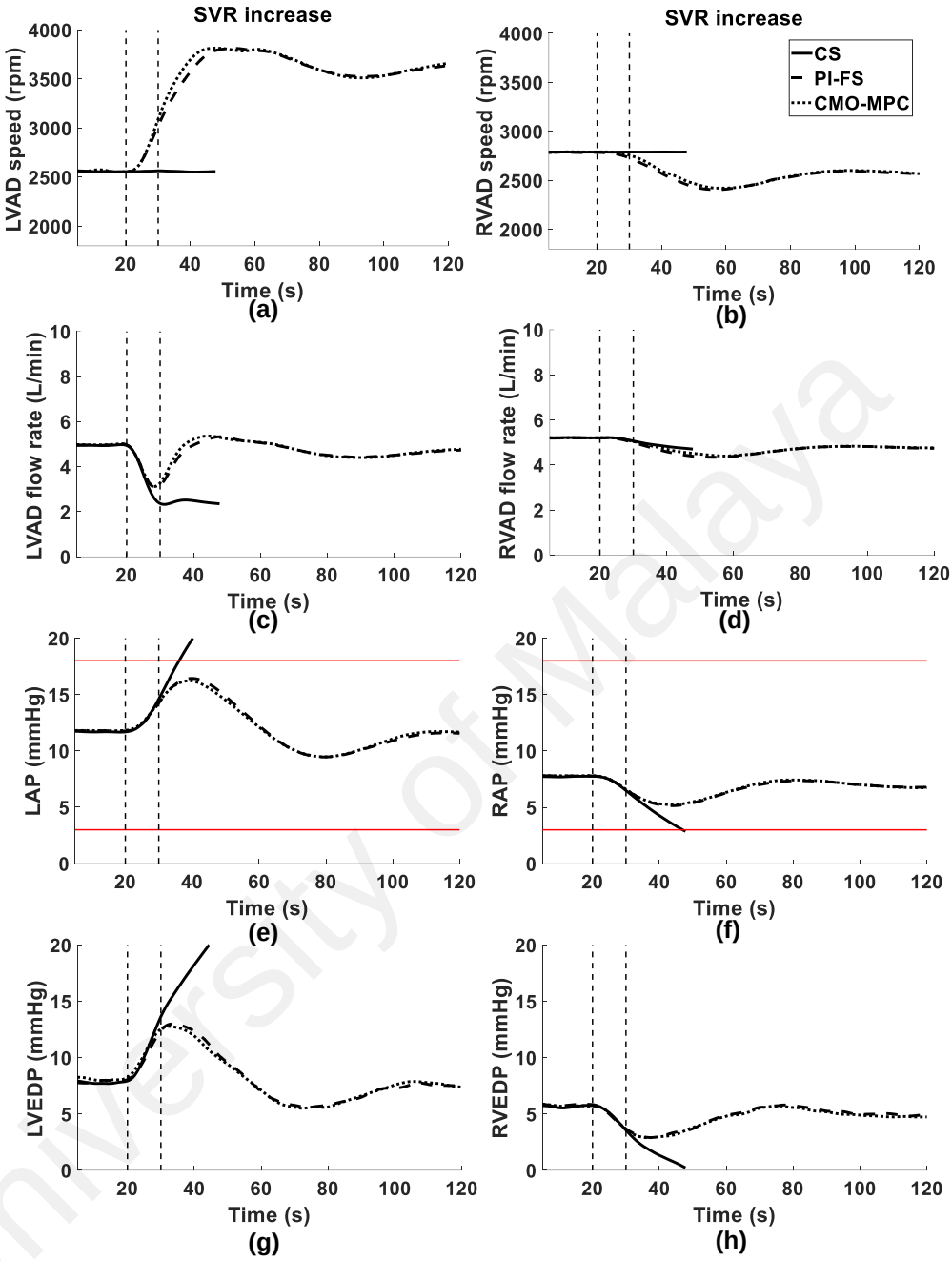

Figure 5.6: Plots of speed control and haemodynamic responses in an SVR increase tests\. LVAD, left ventricular assist device; RVAD, right ventricular assist device; LAP, left atrial pressure; RAP, right atrial pressure; LVEDP, left ventricular end diastolic pressure; RVEDP, right ventricular end diastolic pressure. The vertical dashed lines indicate the duration where gradual changes in model parameters occurred. The red solid horizontal line at 3 mmHg and 18 mmHg in subplots (e)-(f) mark user-defined marginal threshold for the activation of objective 2 and 3.

5.3.2.4 PVR changes

Figure 5.7(a) and 5.7(b) show that the physiological controllers decreased the LVAD speed and increased the RVAD speed when PVR was increased. Between t=20 s and t=40 s, the LAP and LVEDP decreased with increasing PVR in all three controllers. After t=40 s, the LAP and LVEDP was increased as attributed by the increase in RVAD speed and RVAD flow by both the PI-FS controller and the CMO-MPC. The rise time of LVAD speed (4.5 s) and RVAD speed (16.3 s) were the same for both the PI-FS controller and the CMO-MPC.

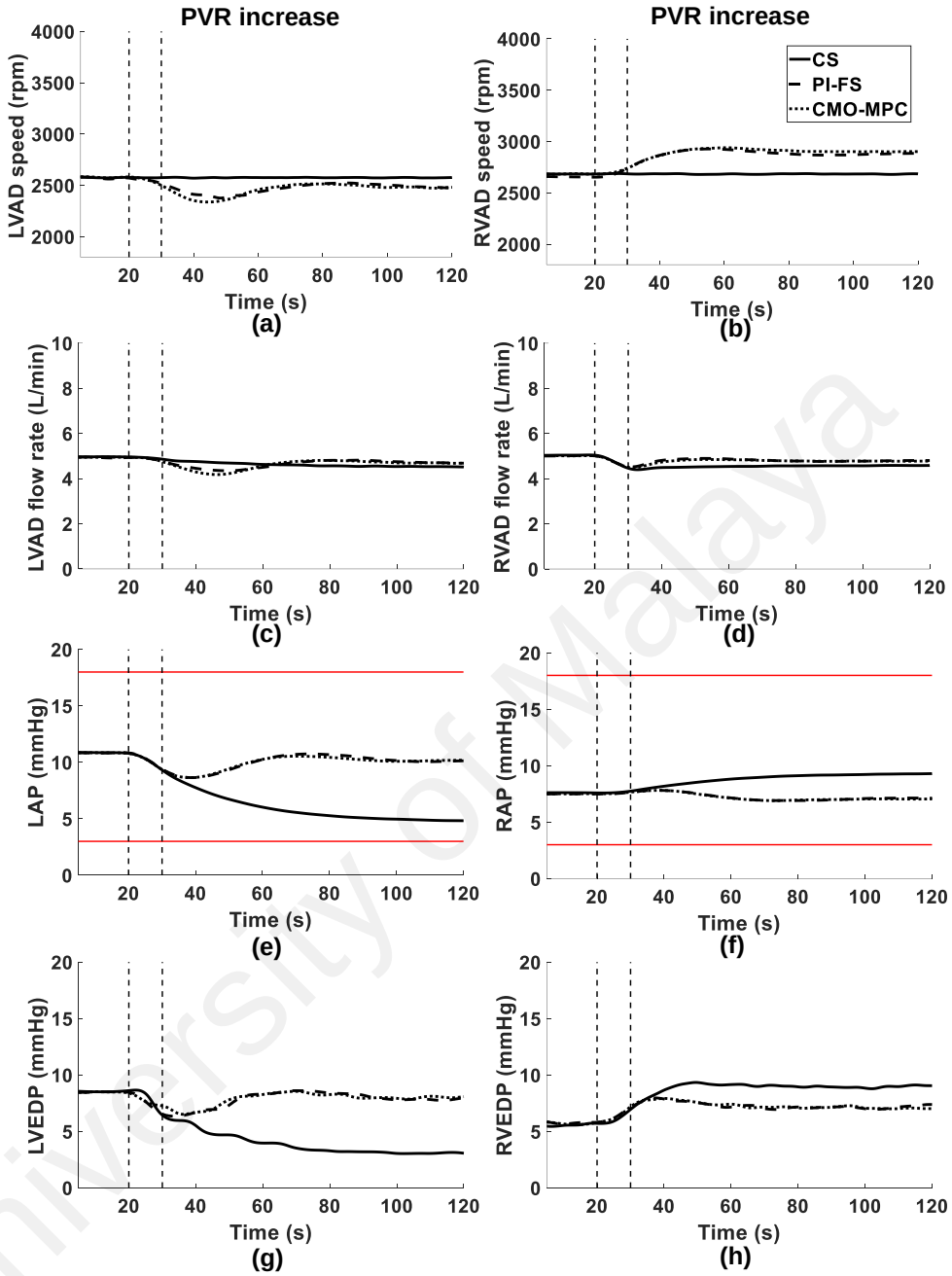

Figure 5.7: Plots of speed control and haemodynamic responses in an PVR increase test. LVAD, left ventricular assist device; RVAD, right ventricular assist device; LAP, left atrial pressure; RAP, right atrial pressure; LVEDP, left ventricular end diastolic pressure; RVEDP, right ventricular end diastolic pressure. The vertical dashed lines indicate the duration where gradual changes in model parameters occurred. The red solid horizontal line at 3 mmHg and 18 mmHg in subplots (e)-(f) mark user-defined marginal threshold for the activation of objective 2 and 3.

5.3.2.5 Analysis of transient hemodynamic waveforms

Comparing Figure 5.8(a) to Figure 5.3(e) and Figure 5.8(b) Figure 5.4(f), changes in the mean LAP and RAP can be used as a clearer approximate of the trend of changes in the LAP and RAP waveforms for the comparison of the control performance.

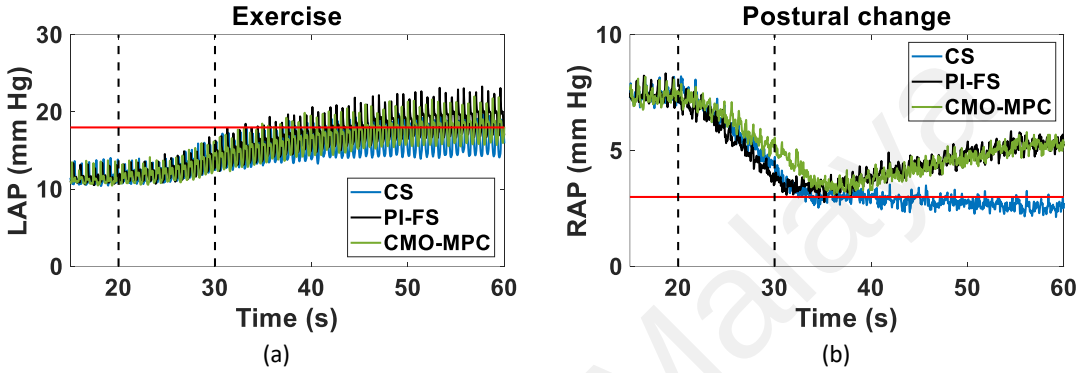

Figure 5.8: (a) Plots of LAP waveforms during the transition from rest to exercise and (b) RAP waveforms during the transition from supine to standing position. LAP: left atrial pressure, RAP: right atrial pressure, CS: constant speed, PI-FS: Frank-Starling-like=proportional-integral controller, CMO-MPC: centralised multi-objective model predictive control.

5.4 Discussion

The move suppression weights for the left and right pumps were set to be the same in the CMO-MPC. This is to limit the changes in pump speeds in each time step. The pulsatility of LVAD speed and RVAD speed are affected by left and right ventricular contractilities; the pulsatility of LVAD speed is larger than the pulsatility of RVAD speed due to the larger left ventricular contractility when compared with right ventricle, As a result, there was an "over-suppression" on the RVAD speed indicated by a larger rise time to reach the target as observed in Table 5.5 and Figure 5.2.

In the control evaluation in different clinical scenarios (e.g. exercise, postural change, and changes in SVR and PVR), the difference in rise time between the CMO-MPC and PI-FS controller was contributed by the changes in reference flow rate adjusted according

to the FS mechanism. Therefore, it is difficult to evaluate the control performance based on rise time. To identify which controller is performing better than another, we only evaluated based on its capability to achieve the three main control objectives as a physiological control of BiVAD: 1) to increase pump flow rate with increasing metabolic demand in exercise, 2) to minimise risks of ventricular suction, and 3) to minimise risks of vascular congestion.

As reported in the earlier studies (Gregory et al., 2016; Ng et al., 2018; J. P. Pauls, Stevens, Schummy, et al., 2016; Stephens et al., 2017; Tchantchaleishvili et al., 2017) the CS control of BiVAD limits the increase in cardiac output in exercise and imposes risks of ventricular suction and vascular congestion when there are changes in preload and afterload levels. The results shown in the present study agree with the previous findings: 1) the CS control contributed the lowest increment in cardiac output in exercise when compared with the physiological controllers (Figure 5.3), 2) events of ventricular suction occurred at high and low SVR levels (Figure 5.5(g) and Figure 5.6(h)), and 3) an event of pulmonary congestion occurred at a high SVR level (Figure 5.5(e)). Clearly, the physiological controllers are more desirable than the CS controller.

Physiological controllers that employ fixed FS control curves for BiVAD may lead to risks of ventricular suction and congestion because the FS relationship of the native heart varies with preload, afterload, and cardiac contractility. In the exercise test, although no real pulmonary congestion was reported in all three controllers, the PI-FS controller had the highest mean LAP in the transient region, indicating the highest risk of pulmonary congestion. With the activation of the control objective that avoids pulmonary congestion in the CMO-MPC, mean LAP was controlled at or below the 18 mmHg. This clearly shows the benefits of the multi-objective control scheme in avoiding pulmonary congestion in exercise, which also agrees with the advantages of multi-objective control

demonstrated in the previous studies (Koh et al., 2019; Ng et al., 2018; Petrou et al., 2017; Vollkron et al., 2005).

In all simulation tests, objective 2 of the CMO-MPC was not activated because the user-defined suction threshold was not violated in the FS control strategy. Without the activation of objective 2 and 3 in the CMO-MPC, the steady-state haemodynamic responses in CMO-MPC and the PI-FS would be similar because same FS control curves were used in both physiological controllers (Table 5.5). However, the haemodynamic responses between the CMO-MPC and the PI-FS controller were different in the transient region of the postural change test and SVR decrease test because the cost function design in the MPC (without the additional control objectives) is different from the PI controller. The cost function of the MPC accounts for the tracking error (up to the defined prediction horizon), slew rate (up to the defined control horizon), and the input and output operating constraints on the left and right hearts to decide the optimal LVAD and RVAD speeds at each time step whereas the PI controller only accounts for the tracking error on each side of the pump. With the additional consideration of predicted outputs, slew rate, and operating constraints, smoother haemodynamic responses resulted in the CMO-MPC as evidently observed by the smaller undershoots in LVEDP (Figure 5.4(h)) and RVEDP (Figure 5.5(g)) as compared to the PI-FS controller.

In the SVR change tests, results in the present study agreed with the previous findings that showed the potential of the fixed FS control strategy in achieving flow balancing in extreme SVR regions (J. P. Pauls, Stevens, Schummy, et al., 2016; Stephens et al., 2017). Extreme PVR regions were also evaluated in the present study, however, there was no event of ventricular suction and vascular congestion recorded even at the CS control. In the exercise and postural change tests, results in the present study also show agreement with other previous findings that demonstrate the potential of the adaptive FS control and

multi-objective FS control in minimising risks of ventricular suction and vascular congestion over the fixed FS control strategy (Ng et al., 2018; Ng et al., 2016).

The CMO-MPC is versatile to different devices as verified by the excellent control performance in the dual HeartMate II pumps in the *in silico* study (Koh et al., 2019) and the dual HVAD pumps in the present study. Apart from the suction prevention controller introduced by Wang et al. (Wang et al., 2018a), no other controllers in literature have been shown to work with different pump models for BiVAD. The suction prevention controller employs a gain scheduled differential pressure (dP) controller and another gain scheduled differential speed (dRPM) controller for the speed control of each side. Altogether, four PI controllers are needed, which requires exhaustive tuning efforts for the total of eight tuning parameters. In addition, the dRPM control may not be suitable for patients with minimal cardiac contractility as the dRPM diminishes with reduced cardiac contractility. Although the addition of dRPM controller to the dP control has prevented the event of constant suction, the strategy does not support the prevention of vascular congestion (Wang et al., 2018a). It has also been reported in another study that the suction prevention controller failed to avoid suction when the cardiac contractility was increased and the SVR level was decreased (Petrou et al., 2018).

Comparing the *in vitro* evaluation to the *in silico* evaluation that has been done in previous chapter, the *in vitro* evaluation provides a more realistic evaluation environment as the physical pump devices are involved in the experiments. In addition, the *in vitro* simulation protocol is also reproducible. However, similar to the *in silico* study, the autoregulatory mechanisms were absent in exercise and postural change tests and manual tuning of model parameters were used to mimic the autoregulatory mechanisms *in vitro*. There was no suction model in the MCL, thus the ventricular collapse was not observed during ventricular suction. The CMO-MPC requires two pump flow sensors and two

pressure sensors. To date, there are no commercially available pressure sensors that are incorporated into LVADs due to potential sensor drifts and compatibility issues. Improvements in the accuracy of pressure sensors in several studies have increased the hope of future adoption of the current control scheme (Hubbert et al., 2017; Troughton et al., 2011). Furthermore, flow sensors have also been integrated into the HeartAssist5 LVAD (ReliantHeart Inc., Texas, U.S.) (Noon et al., 2001). Alternatively, the development of reliable and accurate estimation algorithms (A. Arndt et al., 2010; Granegger et al., 2012; Reyes et al., 2016; Wang et al., 2018b) for flow and pressure signals that substitute the need of implantable sensors may also be integrated to the CMO-MPC in the future. The present FS control used LAP and RAP as preloads instead of LVEDP and RVEDP. Although LVEDP and RVEDP might be better indicators for ventricular suction, measurements and estimations of LAP and RAP may be easier than the LVEDP and RVEDP. Moreover, LAP and RAP were proportional to LVEDP and RVEDP in the present study. Finally, to increase the confidence of the CMO-MPC for BiVAD control, *in vivo* validation should be performed.

5.5 Conclusion

This chapter shows that the *in silico* control performance of the CMO-MPC that was reported in chapter 4 has been successfully validated *in vitro*. The CMO-MPC, having considered the tracking error, slew rate, operating constraints in the cost function optimiser, and process interactions between control loops, delivered a smoother transient response (smaller undershoots in the LVEDP and RVEDP) as compared to the PI-FS controller. This has effectively minimised the risk of ventricular suction and vascular congestion. The additional control objectives that prevent events of ventricular suction and vascular congestion allow the LVAD and RVAD speed to be adjusted within the safety region, provided the suction and congestion thresholds have been set accurately by

clinicians. Although the CMO-MPC has demonstrated excellent control performance in the evaluated scenarios, it requires pressure and flow measurements. As there are no commercially implantable sensors, future work should focus on the development and improvements of implantable pressure and flow sensors or reliable estimation algorithms for pressure and flow readings.

CHAPTER 6: CONCLUSIONS, CONTRIBUTIONS AND RECOMMENDATIONS

6.1 Conclusions and contributions

The main contribution of the thesis is the development of a centralised control system (i.e. the CMO-MPC) for the physiological control of a BiVAD. This has reduced the need for two controllers for the left and right pump speeds to a single controller. This has also reduced the number of tuning parameters involved in the control of a BiVAD. Prior to the development of the CMO-MPC, a simplified model of CVS-BiVAD interaction was acquired. This simplified model was the first and to date only simplified CVS-BiVAD model developed for control purposes.

To conclude the thesis, the highlights of each chapter are recapitulated as follows:

1. The first objective was to develop a simplified state-space model for the CVS-BiVAD system for used in the CMO-MPC. As model simplicity and model accuracy are trade-off factors, the simplified model was carefully evaluated and compared with literature in various PVR, SVR, LVAD speed, and RVAD speed. If the differences of the model behaviour between the simplified model and literature were too large, manual tuning of model parameters were performed to narrow the differences. The simplified model of CVS-BiVAD system demonstrated comparable haemodynamic trends as compared to the literature in all tested scenarios even after the number of state variables had been reduced from its predecessor complex numerical model.
2. The second objective was to derive the CMO-MPC algorithm. A generic MPC algorithm was first derived from the simplified state-space model of the CVS-BiVAD system. The multi-objective control strategies that adjusted pump flow

rate according to the FS mechanism and explicitly prevent ventricular suction and vascular congestion (suction and congestion threshold could be defined by clinical experts) were added to the generic MPC algorithm, formulating the CMO-MPC algorithm. For preliminary evaluation of the new control strategy, the CMO-MPC was benchmarked against the PI-FS control and the CS control in a valid *in silico* environment. In the *in silico* evaluation, the CMO-MPC demonstrated the benefits of additional control objectives that prevent ventricular suction and vascular congestion by ensuring the haemodynamic variables were within the assumed safety boundaries (i.e. atrial pressures within 3 mmHg and 18 mmHg) in exercise and postural change tests. On the other hand, although PI-FS control had demonstrated increased exercise capacity (same outcome as CMO-MPC) as compared to CS control in the exercise test, mean LAP exceeded 18 mmHg. In the postural change test, mean RAP fell below 3 mmHg for both the PI-FS and CS controllers.

3. The third objective aimed to validate the control performance of CMO-MPC in an *in vitro* environment. Similar exercise and postural change tests that were used in the *in silico* test were designed in an MCL. In agreement with the *in silico* evaluation, CMO-MPC prevented mean LAP from exceeding 18 mmHg in exercise while the PI-FS controller failed to. In the postural change test, although both CMO-MPC and PI-FS controller did not cause mean RAP to fall below 3 mmHg, a smaller undershoot in RVEDP was observed in CMO-MPC as compared with PI-FS controller, suggesting that lower risks of transient right ventricular suction was found in CMO-MPC as compared with the PI-FS controller.

6.2 Limitations

The limitations of the project can be summarised as follows:

1. The project assumed that measurements of pressure and flow were available however there is no reliable pressure and flow sensor that can be chronically implanted in the spatient's body.
2. Although the evaluation models used in this study are reasonable approximations of the cardiovascular system and have been used throughout the literature for physiological control system validation, they fail to accurately replicate some aspects of cardiovascular physiology, such as the baroreflex mechanism and ventricular suction.

6.3 Recommendations

Therefore, several recommendations are suggested as extensions for future work of the study as follows:

1. Reliable pressure and flow sensors should be developed and improved for future implantations.
2. New methods of estimating pressure and flow should be explored. If not, the accuracy of existing estimation algorithms for pressure and flow should be improved to replace the need of sensor placements in human bodies.
3. Adaptive tuning algorithms for the tuning parameters and the internal model parameters of CMO-MPC should be developed to improve control performance.
4. The current CMO-MPC should be validated *in vivo* to increase the understanding of the performance of the control strategy.
5. The performance of CMO-MPC should also be evaluated in valsalva maneuvers and different recovery scenarios for the left and right ventricle.

REFERENCES

Arndt, A., Nüsser, P., Graichen, K., Müller, J., & Lampe, B. (2008). Physiological control of a rotary blood pump with selectable therapeutic options: control of pulsatility gradient. *Artif Organs, 32*(10), 761-771.

Arndt, A., Nusser, P., & Lampe, B. (2010). Fully autonomous preload-sensitive control of implantable rotary blood pumps. *Artif Organs, 34*(9), 726-735. doi:10.1111/j.1525-1594.2010.01092.x

Boston, J. R., Antaki, J. F., & Simaan, M. A. (2003). Hierarchical control of heart-assist devices. *IEEE Robotics & Automation Magazine, 10*(1), 54-64.

Bull, D. A., Reid, B. B., Selzman, C. H., Mesley, R., Drakos, S., Clayson, S., . . . Patel, A. N. (2010). The impact of bridge-to-transplant ventricular assist device support on survival after cardiac transplantation. *The Journal of Thoracic and Cardiovascular Surgery, 140*(1), 169-173. doi:https://doi.org/10.1016/j.jtcvs.2010.03.026

Bullister, E., Reich, S., & Sluetz, J. (2002). Physiologic control algorithms for rotary blood pumps using pressure sensor input. *Artif Organs, 26*(11), 931-938.

Casas, F., Ahmed, N., & Reeves, A. (2007). Minimal sensor count approach to fuzzy logic rotary blood pump flow control. *ASAIO Journal, 53*(2), 140-146. doi:10.1097/01.mat.0000250786.56697.f2

Chien, I. L., & Fruehauf, P. S. (1990). Consider IMC tuning to improve controller performance. *Chemistry Engineering Progress, 86*(10), 33-41.

Drakos, S. G., Janicki, L., Horne, B. D., Kfoury, A. G., Reid, B. B., Clayson, S., . . . Renlund, D. G. (2010). Risk factors predictive of right ventricular failure after left ventricular assist device implantation. *The American Journal of Cardiology, 105*(7), 1030-1035.

Drakos, S. G., Kfoury, A. G., Stehlik, J., Selzman, C. H., Reid, B. B., Terrovitis, J. V., . . . Li, D. Y. (2012). Bridge to recovery: understanding the disconnect between clinical and biological outcomes. *Circulation, 126*(2), 230-241. doi:10.1161/circulationaha.111.040261

Endo, G., Araki, K., Oshikawa, M., Kojima, K., Nakamura, K., Matsuzaki, Y., & Onitsuka, T. (2002). A safe automatic driving method for a continuous flow ventricular assist device based on motor current pulsatility: in vitro evaluation. *ASAIO Journal, 48*(1), 83-89.

Ferreira, A., Chen, S., Galati, D. G., Simaan, M. A., & Antaki, J. F. (2005). *A Dynamical State Space Representation and Performance Analysis of a Feedback Controlled Rotary Left Ventricular Assist Device.* Paper presented at the ASME International Mechanical Engineering Congress and Exposition.

Fukunaga, N., & Rao, V. (2018). Left ventricular assist device as destination therapy for end stage heart failure: the right time for the right patients. *Curr Opin Cardiol, 33*(2), 196-201. doi:10.1097/hco.0000000000000486

Gaddum, N. R., Stevens, M. C., Lim, E., Fraser, J., Lovell, N., Mason, D., . . . Salamonsen, R. (2014). Starling-Like flow control of a left ventricular assist device: in vitro validation. *Artif Organs, 38*(3), E46-E56.

Gaddum, N. R., Timms, D. L., Stevens, M., Mason, D., Lovell, N., & Fraser, J. F. (2012). Comparison of preload-sensitive pressure and flow controller strategies for a dual device biventricular support system. *Artif Organs, 36*(3), 256-265. doi:10.1111/j.1525-1594.2011.01344.x

George, C. L. S., Ameduri, R. K., Reed, R. C., Dummer, K. B., Overman, D. M., & St. Louis, J. D. (2013). Long-Term Use of Ventricular Assist Device as a Bridge to Recovery in Acute Fulminant Myocarditis. *Ann Thorac Surg, 95*(3), e59-e60. doi:10.1016/j.athoracsur.2012.09.036

Giridharan, G. A., & Skliar, M. (2003). Control strategy for maintaining physiological perfusion with rotary blood pumps. *Artif Organs, 27*(7), 639-648.

Giridharan, G. A., Skliar, M., Olsen, D. B., & Pantalos, G. M. (2002). Modeling and control of a brushless DC axial flow ventricular assist device. *ASAIO Journal, 48*(3), 272-289.

Granegger, M., Moscato, F., Casas, F., Wieselthaler, G., & Schima, H. (2012). Development of a pump flow estimator for rotary blood pumps to enhance monitoring of ventricular function. *Artif Organs, 36*(8), 691-699. doi:10.1111/j.1525-1594.2012.01503.x

Gregory, S. D., Pearcy, M. J., & Timms, D. (2012). Passive control of a biventricular assist device with compliant inflow cannulae. *Artif Organs, 36*(8), 683-690. doi:10.1111/j.1525-1594.2012.01504.x

Gregory, S. D., Schummy, E., Pearcy, M., Pauls, J. P., Tansley, G., Fraser, J. F., & Timms, D. (2015). A compliant, banded outflow cannula for decreased afterload sensitivity of rotary right ventricular assist devices. *Artif Organs, 39*(2), 102-109. doi:10.1111/aor.12338

Gregory, S. D., Stevens, M., Timms, D., & Pearcy, M. (2011). Replication of the Frank-Starling response in a mock circulation loop. *Conf Proc IEEE Eng Med Biol Soc, 2011*, 6825-6828. doi:10.1109/iembs.2011.6091683

Gregory, S. D., Stevens, M. C., Pauls, J. P., Schummy, E., Diab, S., Thomson, B., . . . Timms, D. (2016). In vivo evaluation of active and passive physiological control systems for rotary left and right ventricular assist devices. *Artif Organs, 40*(9), 894-903. doi:10.1111/aor.12654

Guyton, A. C., & Hall, J. E. (2006). *Textbook of Medical Physiology*: Elsevier Saunders.

Gwak, K. W., Ricci, M., Snyder, S., Paden, B. E., Boston, J. R., Simaan, M. A., & Antaki, J. F. (2005a). In vitro evaluation of multiobjective hemodynamic control of a heart-assist pump. *Asaio j, 51*(4), 329-335.

Gwak, K. W., Ricci, M., Snyder, S., Paden, B. E., Boston, J. R., Simaan, M. A., & Antaki, J. F. (2005b). In vitro evaluation of multiobjective hemodynamic control of a heart-assist pump. *Asaio j, 51*(4), 329-335.

Hetzer, R., Krabatsch, T., Stepanenko, A., Hennig, E., & Potapov, E. V. (2010). Long-term biventricular support with the heartware implantable continuous flow pump. *The Journal of Heart and Lung Transplantation, 29*(7), 822-824.

Holley, C. T., Harvey, L., & John, R. (2014). Left ventricular assist devices as a bridge to cardiac transplantation. *J Thorac Dis, 6*(8), 1110-1119. doi:10.3978/j.issn.2072-1439.2014.06.46

Hubbert, L., Baranowski, J., Delshad, B., & Ahn, H. (2017). Left atrial pressure monitoring with an implantable wireless pressure sensor after implantation of a left ventricular assist device. *Asaio j, 63*(5), e60-e65. doi:10.1097/mat.0000000000000451

Jakovljevic, D. G., Yacoub, M. H., Schueler, S., MacGowan, G. A., Velicki, L., Seferovic, P. M., . . . Tan, L.-B. (2017). Left Ventricular Assist Device as a Bridge to Recovery for Patients With Advanced Heart Failure. *Journal of the American College of Cardiology, 69*(15), 1924-1933. doi:10.1016/j.jacc.2017.02.018

Kirklin, J. K., Pagani, F. D., Kormos, R. L., Stevenson, L. W., Blume, E. D., Myers, S. L., . . . Naftel, D. C. (2017). Eighth annual INTERMACS report: Special focus on framing the impact of adverse events. *The Journal of Heart and Lung Transplantation, 36*(10), 1080-1086. doi:10.1016/j.healun.2017.07.005

Klotz, S., Stypmann, J., Welp, H., Schmid, C., Drees, G., Rukosujew, A., & Scheld, H. H. (2006). Does continuous flow left ventricular assist device technology have a positive impact on outcome pretransplant and posttransplant? *Ann Thorac Surg, 82*(5), 1774-1778. doi:10.1016/j.athoracsur.2006.05.079

Koh, V. C. A., Ho, Y. K., Stevens, M. C., Ng, B. C., Salamonsen, R. F., Lovell, N. H., & Lim, E. (2019). A centralized multi-objective model predictive control for a biventricular assist device: An in silico evaluation. *Biomedical Signal Processing and Control, 49*, 137-148. doi:https://doi.org/10.1016/j.bspc.2018.10.021

Lee, S., Kamdar, F., Madlon-Kay, R., Boyle, A., Colvin-Adams, M., Pritzker, M., & John, R. (2010). Effects of the HeartMate II continuous-flow left ventricular assist device on right ventricular function. *J Heart Lung Transplant, 29*(2), 209-215. doi:10.1016/j.healun.2009.11.599

Lietz, K., Long, J. W., Kfoury, A. G., Slaughter, M. S., Silver, M. A., Milano, C. A., . . . Miller, L. W. (2007). Outcomes of left ventricular assist device implantation as destination therapy in the post-REMATCH era: implications for patient selection. *Circulation, 116*(5), 497-505. doi:10.1161/circulationaha.107.691972

Lim, E., Dokos, S., Cloherty, S. L., Salamonsen, R. F., Mason, D. G., Reizes, J. A., & Lovell, N. H. (2010). Parameter-optimized model of cardiovascular-rotary blood pump interactions. *IEEE Trans Biomed Eng, 57*(2), 254-266. doi:10.1109/tbme.2009.2031629

Lim, E., Salamonsen, R. F., Mansouri, M., Gaddum, N., Mason, D. G., Timms, D. L., . . . Lovell, N. H. (2015). Hemodynamic response to exercise and head-up tilt of patients implanted with a rotary blood pump: a computational modeling study. *Artif Organs, 39*(2), E24-E35.

Maciejowski, J. M. (2002). *Predictive Control: with Constraints*: Pearson Education.

Mansouri, M., Gregory, S. D., Salamonsen, R. F., Lovell, N. H., Stevens, M. C., Pauls, J. P., . . . Lim, E. (2017). Preload-based Starling-like control of rotary blood pumps: An in-vitro evaluation. *PloS one, 12*(2), e0172393-e0172393. doi:10.1371/journal.pone.0172393

Mansouri, M., Salamonsen, R. F., Lim, E., Akmeliawati, R., & Lovell, N. H. (2015). Preload-based starling-like control for rotary blood pumps: numerical comparison with pulsatility control and constant speed operation. *PloS one, 10*(4), e0121413-e0121413. doi:10.1371/journal.pone.0121413

Moazami, N., Fukamachi, K., Kobayashi, M., Smedira, N. G., Hoercher, K. J., Massiello, A., . . . Starling, R. C. (2013). Axial and centrifugal continuous-flow rotary pumps: A translation from pump mechanics to clinical practice. *The Journal of Heart and Lung Transplantation, 32*(1), 1-11. doi:10.1016/j.healun.2012.10.001

Moscato, F., Arabia, M., Colacino, F. M., Naiyanetr, P., Danieli, G. A., & Schima, H. (2010). Left ventricle afterload impedance control by an axial flow ventricular assist device: a potential tool for ventricular recovery. *Artif Organs, 34*(9), 736-744.

Nadeem, K., Ng, B. C., Lim, E., Gregory, S. D., Salamonsen, R. F., Stevens, M. C., . . . Lovell, N. H. (2015). Numerical simulation of a biventricular assist device with fixed right outflow cannula banding during pulmonary hypertension. *Ann Biomed Eng, 44*(4), 1008-1018. doi:10.1007/s10439-015-1388-2

Ng, B. C., Salamonsen, R. F., Gregory, S. D., Stevens, M. C., Wu, Y., Mansouri, M., . . . Lim, E. (2018). Application of multiobjective neural predictive control to biventricular assistance using dual rotary blood pumps. *Biomedical Signal Processing and Control, 39*(Supplement C), 81-93. doi:https://doi.org/10.1016/j.bspc.2017.07.028

Ng, B. C., Smith, P. A., Nestler, F., Timms, D., Cohn, W. E., & Lim, E. (2016). Application of Adaptive Starling-Like Controller to Total Artificial Heart Using Dual Rotary Blood Pumps. *Ann Biomed Eng*. doi:10.1007/s10439-016-1706-3

Noon, G. P., Morley, D. L., Irwin, S., Abdelsayed, S. V., Benkowski, R. J., & Lynch, B. E. (2001). Clinical experience with the MicroMed DeBakey ventricular assist device. *Ann Thorac Surg, 71*(3, Supplement 1), S133-S138. doi:https://doi.org/10.1016/S0003-4975(00)02634-5

Ochsner, G., Amacher, R., Amstutz, A., Plass, A., Schmid Daners, M., Tevaearai, H., . . . Guzzella, L. (2013). A novel interface for hybrid mock circulations to evaluate ventricular assist devices. *IEEE Trans Biomed Eng, 60*(2), 507-516. doi:10.1109/tbme.2012.2230000

Ochsner, G., Amacher, R., Wilhelm, M. J., Vandenberghe, S., Tevaearai, H., Plass, A., . . . Schmid Daners, M. (2014). A physiological controller for turbodynamic ventricular assist devices based on a measurement of the left ventricular volume. *Artif Organs, 38*(7), 527-538. doi:10.1111/aor.12225

Ochsner, G., Wilhelm, M. J., Amacher, R., Petrou, A., Cesarovic, N., Staufert, S., . . . Schmid Daners, M. (2017). In Vivo Evaluation of Physiologic Control Algorithms for Left Ventricular Assist Devices Based on Left Ventricular Volume or Pressure. *Asaio j, 63*(5), 568-577. doi:10.1097/mat.0000000000000533

Pagani, F. D. (2008). Continuous-flow rotary left ventricular assist devices with "3rd generation" design. *Semin Thorac Cardiovasc Surg, 20*(3), 255-263. doi:10.1053/j.semtcvs.2008.08.002

Pantalos, G. M., Koenig, S. C., Gillars, K. J., Giridharan, G. A., & Ewert, D. L. (2004). Characterization of an adult mock circulation for testing cardiac support devices. *Asaio j, 50*(1), 37-46.

Pauls, J. P., Stevens, M. C., Bartnikowski, N., Fraser, J. F., Gregory, S. D., & Tansley, G. (2016a). Evaluation of Physiological Control Systems for Rotary Left Ventricular Assist Devices: An In-Vitro. *Annals of Biomedical Engineering, 44*(8), 2377-2387.

Pauls, J. P., Stevens, M. C., Bartnikowski, N., Fraser, J. F., Gregory, S. D., & Tansley, G. (2016b). Evaluation of Physiological Control Systems for Rotary Left Ventricular Assist Devices: An In-Vitro Study. *Annals of Biomedical Engineering, 44*(8), 2377-2387. doi:10.1007/s10439-016-1552-3

Pauls, J. P., Stevens, M. C., Schummy, E., Tansley, G., Fraser, J. F., Timms, D., & Gregory, S. D. (2016). In vitro comparison of active and passive physiological control systems for biventricular assist devices. *Ann Biomed Eng, 44*(5), 1370-1380. doi:10.1007/s10439-015-1425-1

Perri, G., Filippelli, S., Adorisio, R., Iacobelli, R., Iodice, F., Testa, G., . . . Amodeo, A. (2017). Left ventricular assist device as destination therapy in cardiac end-stage dystrophinopathies: Midterm results. *J Thorac Cardiovasc Surg, 153*(3), 669-674. doi:10.1016/j.jtcvs.2016.08.016

Petrou, A., Lee, J., Dual, S., Ochsner, G., Meboldt, M., & Schmid Daners, M. (2018). Standardized Comparison of Selected Physiological Controllers for Rotary Blood Pumps: In Vitro Study. *Artif Organs, 42*(3), E29-e42. doi:10.1111/aor.12999

Petrou, A., Monn, M., Meboldt, M., & Schmid Daners, M. (2017). A Novel Multi-objective Physiological Control System for Rotary Left Ventricular Assist Devices. *Ann Biomed Eng, 45*(12), 2899-2910. doi:10.1007/s10439-017-1919-0

Petrou, A., Ochsner, G., Amacher, R., Pergantis, P., Rebholz, M., Meboldt, M., & Schmid Daners, M. (2016). A Physiological Controller for Turbodynamic Ventricular Assist Devices Based on Left Ventricular Systolic Pressure. *Artif Organs, 40*(9), 842-855. doi:10.1111/aor.12820

Potapov, E. V., Loforte, A., Weng, Y., Jurmann, M., Pasic, M., Drews, T., . . . Koster, A. (2008). Experience with over 1000 implanted ventricular assist devices. *Journal of cardiac surgery, 23*(3), 185-194.

Ramnarine, K. V., Nassiri, D. K., Hoskins, P. R., & Lubbers, J. (1998). Validation of a new blood-mimicking fluid for use in Doppler flow test objects. *Ultrasound Med Biol, 24*(3), 451-459.

Reineke, D. C., & Mohacsi, P. J. (2017). New role of ventricular assist devices as bridge to transplantation: European perspective. *Current Opinion in Organ Transplantation, 22*(3), 225-230. doi:10.1097/mot.0000000000000412

Reyes, C., Voskoboynikov, N., Chorpenning, K., LaRose, J. A., Brown, M. C., Nunez, N. J., . . . Tamez, D. (2016). Accuracy of the HVAD Pump Flow Estimation Algorithm. *Asaio j, 62*(1), 15-19. doi:10.1097/mat.0000000000000295

Rogers, J. G., Pagani, F. D., Tatooles, A. J., Bhat, G., Slaughter, M. S., Birks, E. J., . . . Milano, C. A. (2017). Intrapericardial Left Ventricular Assist Device for Advanced Heart Failure. *New England Journal of Medicine, 376*(5), 451-460. doi:10.1056/NEJMoa1602954

Rossiter, J. A. (2003). *Model-based predictive control: a practical approach*: CRC press.

Salamonsen, R. F., Lim, E., Gaddum, N., AlOmari, A. H., Gregory, S. D., Stevens, M., . . . Lovell, N. H. (2012). Theoretical foundations of a Starling-like controller for rotary blood pumps. *Artif Organs, 36*(9), 787-796. doi:10.1111/j.1525-1594.2012.01457.x

Salamonsen, R. F., Mason, D. G., & Ayre, P. J. (2011). Response of rotary blood pumps to changes in preload and afterload at a fixed speed setting are unphysiological when compared with the natural heart. *Artif Organs, 35*(3), E47-E53. doi:10.1111/j.1525-1594.2010.01168.x

Schima, H., Honigschnabel, J., Trubel, W., & Thoma, H. (1990). Computer simulation of the circulatory system during support with a rotary blood pump. *ASAIO Trans, 36*(3), M252-254.

Schima, H., Vollkron, M., Jantsch, U., Crevenna, R., Roethy, W., Benkowski, R., . . . Wieselthaler, G. (2006). First clinical experience with an automatic control system for rotary blood pumps during ergometry and right-heart catheterization. *J Heart Lung Transplant, 25*(2), 167-173. doi:10.1016/j.healun.2005.09.008

Seborg, D. E., Mellichamp, D. A., Edgar, T. F., & Doyle III, F. J. (2010). *Process Dynamics and Control*: John Wiley & Sons.

Simaan, M. A., Ferreira, A., Chen, S., Antaki, J. F., & Galati, D. G. (2009). A dynamical state space representation and performance analysis of a feedback-controlled rotary left ventricular assist device. *IEEE Transactions on Control Systems Technology, 17*(1), 15-28.

Slaughter, M. S., Bartoli, C. R., Sobieski, M. A., Pantalos, G. M., Giridharan, G. A., Dowling, R. D., . . . Koenig, S. C. (2009). Intraoperative evaluation of the HeartMate II flow estimator. *J Heart Lung Transplant, 28*(1), 39-43. doi:10.1016/j.healun.2008.10.007

Slaughter, M. S., Pagani, F. D., Rogers, J. G., Miller, L. W., Sun, B., Russell, S. D., . . . Farrar, D. J. (2010). Clinical management of continuous-flow left ventricular assist devices in advanced heart failure. *J Heart Lung Transplant, 29*(4 Suppl), S1-S39. doi:10.1016/j.healun.2010.01.011

Slaughter, M. S., Rogers, J. G., Milano, C. A., Russell, S. D., Conte, J. V., Feldman, D., . . . Frazier, O. H. (2009). Advanced heart failure treated with continuous-flow left ventricular assist device. *New England Journal Medicine, 361*(23), 2241-2251. doi:10.1056/NEJMoa0909938

Stephens, A. F., Stevens, M. C., Gregory, S. D., Kleinheyer, M., & Salamonsen, R. F. (2017). In vitro evaluation of an immediate response starling-like controller for dual rotary blood pumps. *Artif Organs, 41*(10), 911-922. doi:10.1111/aor.12962

Stevens, M. C., Gaddum, N. R., Pearcy, M., Salamonsen, R. F., Timms, D. L., Mason, D. G., & Fraser, J. F. (2011). Frank-starling control of a left ventricular assist device. *Conf Proc IEEE Eng Med Biol Soc, 2011*, 1335-1338. doi:10.1109/iembs.2011.6090314

Stevens, M. C., Wilson, S., Bradley, A., Fraser, J., & Timms, D. (2014). Physiological control of dual rotary pumps as a biventricular assist device using a master/slave approach. *Artif Organs, 38*(9), 766-774. doi:10.1111/aor.12303

Tchantchaleishvili, V., Luc, J. G. Y., Cohan, C. M., Phan, K., Hübbert, L., Day, S. W., & Massey, H. T. (2017). Clinical implications of physiologic flow adjustment in continuous-flow left ventricular assist devices. *ASAIO Journal, 63*(3), 241-250.

Timms, D. L., Gregory, S. D., Greatrex, N. A., Pearcy, M. J., Fraser, J. F., & Steinseifer, U. (2011). A compact mock circulation loop for the in vitro testing of cardiovascular devices. *Artif Organs, 35*(4), 384-391.

Troughton, R. W., Ritzema, J., Eigler, N. L., Melton, I. C., Krum, H., Adamson, P. B., . . . Abraham, W. T. (2011). Direct left atrial pressure monitoring in severe heart failure: long-term sensor performance. *J Cardiovasc Transl Res, 4*(1), 3-13. doi:10.1007/s12265-010-9229-z

Vollkron, M., Schima, H., Huber, L., Benkowski, R., Morello, G., & Wieselthaler, G. (2005). Development of a reliable automatic speed control system for rotary blood pumps. *J Heart Lung Transplant, 24*(11), 1878-1885. doi:10.1016/j.healun.2005.02.004

Wang, Y., Koenig, S. C., Slaughter, M. S., & Giridharan, G. A. (2015). Rotary blood pump control strategy for preventing left ventricular suction. *Asaio j, 61*(1), 21-30. doi:10.1097/mat.0000000000000152

Wang, Y., Koenig, S. C., Wu, Z., Slaughter, M. S., & Giridharan, G. A. (2018a). Sensor-Based Physiologic Control Strategy for Biventricular Support with Rotary Blood Pumps. *ASAIO Journal, 64*(3), 338-350. doi:10.1097/mat.0000000000000671

Wang, Y., Koenig, S. C., Wu, Z. J., Slaughter, M. S., & Giridharan, G. A. (2018b). Sensorless Physiologic Control, Suction Prevention, and Flow Balancing Algorithm for Rotary Biventricular Assist Devices. *IEEE Transactions on Control Systems Technology*, 1-13. doi:10.1109/TCST.2017.2773518

Waters, T., Allaire, P., Tao, G., Adams, M., Bearnson, G., Wei, N., . . . Khanwilkar, P. (1999). Motor feedback physiological control for a continuous flow ventricular assist device. *ARTIFICIAL ORGANS-OHIO-, 23*, 480-486.

Wieselthaler, G. M., Schima, H., Hiesmayr, M., Pacher, R., Laufer, G., Noon, G. P., . . . Wolner, E. (2000). First clinical experience with the DeBakey VAD continuous-axial-flow pump for bridge to transplantation. *Circulation, 101*(4), 356-359.

Wu, Y. (2009). Adaptive physiological speed/flow control of rotary blood pumps in permanent implantation using intrinsic pump parameters. *ASAIO Journal, 55*(4), 335-339.

Wu, Y., Allaire, P., Tao, G., Wood, H., Olsen, D., & Tribble, C. (2003). An advanced physiological controller design for a left ventricular assist device to prevent left ventricular collapse. *Artif Organs, 27*(10), 926-930.

Wu, Y., Allaire, P. E., Tao, G., Adams, M., Liu, Y., Wood, H., & Olsen, D. B. (2004). A Bridge from Short-term to Long-term Left Ventricular Assist Device—Experimental Verification of a Physiological Controller. *Artif Organs, 28*(10), 927-932.

Wu, Y., Allaire, P. E., Tao, G., & Olsen, D. (2007). Modeling, estimation, and control of human circulatory system with a left ventricular assist device. *IEEE Transactions on Control Systems Technology, 15*(4), 754-767.

Ziegler, J. G., & Nichols, N. B. (1942). Optimum Settings for Automatic Controllers. . *Transactions of the ASME, 64*, 759-768.

LIST OF PUBLICATIONS AND PAPERS PRESENTED

Publications:

- **Koh, V. C. A.**, Pauls, J. P., Wu, E. L., Stevens, M. C., Ho, Y. K., Lovell, N. H., & Lim, E. (2020). A centralized multi-objective model predictive control for a biventricular assist device: An in vitro evaluation. *Biomedical Signal Processing and Control*, *59*, 101914. doi: https://doi.org/10.1016/j.bspc.2020.101914

- **Koh, V. C. A.**, Ho, Y. K., Stevens, M. C., Ng, B. C., Salamonsen, R. F., Lovell, N. H., & Lim, E. (2019). A centralized multi-objective model predictive control for a biventricular assist device: An in silico evaluation. *Biomedical Signal Processing and Control, 49*, 137-148. doi:https://doi.org/10.1016/j.bspc.2018.10.021

Conferences attended:

- **Koh, V. C. A.**, Ho, Y. K., Stevens, M. C., Salamonsen, R. F., Lovell, N. H., & Lim, E. (2017, July). Synergy of first principles modelling with predictive control for a biventricular assist device: In silico evaluation study. In *2017 39th Annual International Conference of the IEEE Engineering in Medicine and Biology Society (EMBC)* (pp. 1291-1294). IEEE.
- **Koh, V. C. A.**, Lim, E., Ng, B. C., Ho, Y. K., & Lovell, N. H. (2016, August). A simplified state-space model of biventricular assist device-cardiovascular system interaction. In *2016 38th Annual International Conference of the IEEE Engineering in Medicine and Biology Society (EMBC)* (pp. 4317-4320). IEEE.